Syntheses, Structures, and Characteristics of the Trifluoromethylated Porphycene and Metalloporphycene

2008

Kazuyuki Ito

Department of Applied Chemistry
Graduate School of Engineering
Osaka University

Syntheses, Structures, and Characteristics of the Trifluoromethylated Porphycene and Metalloporphycene

（トリフルオロメチル基を導入したポルフィセンと
ポルフィセン金属錯体の合成、構造、及び化学的性質）

2008

Kazuyuki Ito

Department of Applied Chemistry
Graduate School of Engineering
Osaka University

Contents

General Introduction

Porphyrin and Metalloporphyrin

Porphyrins, typical tetrapyrrole compounds, have been called "pigments of life" [1]. They have been found in the wide range of the nature and played important roles in the natural system. Porphyrin-containing proteins perform various essential roles and reactions on the biological processes. For example, heme (Figure 1) is an iron porphyrin complex and works as a reaction center of hemoproteins. Hemoproteins are widely distributed in organisms and show a variety of physiological functions: O_2 storage and transport (myoglobin and hemoglobin), catalysis of various oxidation (cytochrome P450 and peroxidases), as well as electron transfer in respiratory system (cytochrome *c*). Therefore, porphyrins and its metal complexes have received great attentions from chemical and biological aspects. Indeed, these chromophores have been intensely investigated and applied to catalysts and dyes in industry.

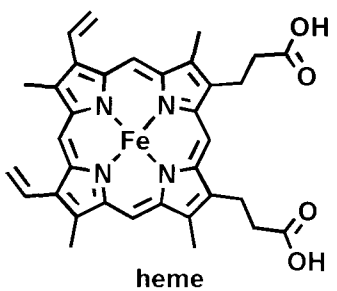

heme

Figure 1. Example of native iron porphyrin, "heme".

Porphyrin Isomers

A desire to understand and explore these characteristics has inspired a considerable interest in the preparation of new synthetic porphyrin isomers. Porphyrin isomers are the tetrapyrrolic macrocycles that consist of the $C_{20}H_{14}N_4$ skeleton with an 18π-congugated system. To date, the number of porphyrin isomers have been synthesized and the physicochemical properties of the isomers have been investigated (Figure 2) [2]. Interestingly, the change in the tetrapyrrolic arrangements in the framework significantly affects the chemical properties of the porphyrin isomers.

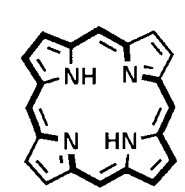

porphyrin

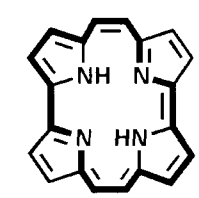

porphycene

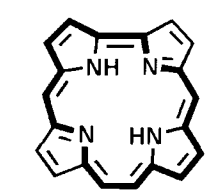

corrphycene

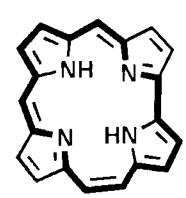

hemiporphycene

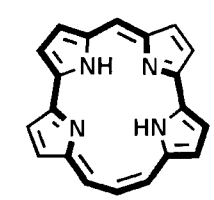

isoporphycene

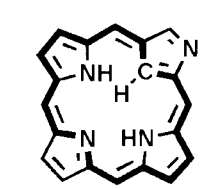

N-confused porphyrin

Figure 2. Porphyrin and selected porphyrin isomers.

Porphycene and Metalloporphycene

Porphycene is the first artificial porphyrin isomer reported by Vogel et al. in 1986 [3]. In case of porphyrin, [porphyrin-(1.1.1.1)], the four pyrroles are bridged with four *meso*-carbons between the pyrrole α-positions each other. In contrast, the porphycene skeleton has two bipyrroles directly bridged with two ethylenes, [porphyrin-(2.0.2.0)] (Figure 3). Because of the structural features, porphycene has the lower symmetry (D_{2h}) as compared to porphyrin (D_{4h}). The unsubstituted porphycene possesses poor solubility similar to the parent porphyrin against various solvents. Therefore, several porphycenes with alkyl groups in the periphery of the framework have been synthesized to improve solubility in organic solvents (Figure 4).

Porphyrins and porphycenes have some common physicochemical properties: they exhibit large electronic absorption in UV–vis region due to the highly conjugated macrocycles with 18π-electron system and are capable of forming a wide range of stable metal complexes [4]. On the other hand, porphycenes have many different chemical properties due to the lower symmetry. Especially, three important and attractive properties are described below.

1) HOMO–LUMO gap decreases, caused by significant stabilization of the LUMO energy level [5].
2) N4 core size and form are changed [3].
3) Metalloporphycene has strong Lewis acidity because of the lower symmetry and the smaller size of the porphycene cavity when compared to the porphyrin [6].

. Figure 5 shows the UV–vis spectra of free-base porphyrin and porphycene as etioporphyrin derivatives. These porphyrinoids exhibit an extraordinary large absorption in near-UV region (Soret band) and relatively small absorptions in visible region (Q-band). These absorptions are raised from π–π^* transitions of the macrocycle. The Q-band of porphycene exhibits much larger intensities and the red shifts than that of porphyrin. The red-shift of the Q-band indicates the decrease of HOMO–LUMO gaps. Furthermore, the HOMO–LUMO gaps electrochemically determined from the difference between the first reduction and oxidation potentials are shown in Figure 6. The gap for porphycene is clearly smaller than that observed in porphyrin. In addition, it is known that porphycene has the smallest HOMO–LUMO gap in a series of porphyrin isomers [7].

In spite of the fact that porphycene possesses a central cavity that is smaller than that of porphyrins, porphycene has indeed been found to form stable complexes with a wide range of metal cations (Figure 7) [7]. Therefore, a number of spectral, electrochemical and structural studies have been carried out on metalloporphycenes. Metalloporphycene will provide unique ligand environment and exhibit the strong Lewis acidity due to the different chemical and structural properties of porphycene. However, few functional studies on the use of metalloporphycene have been presented, although it has been estimated the different reactivities of metal complexes are due to the ligand environmental change.

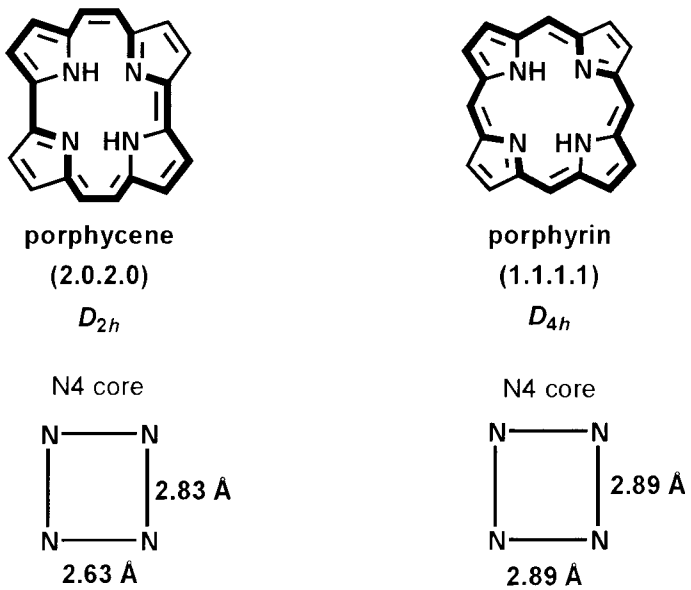

Figure 3. Structures of porphycene and porphyrin and geometries of N4 core with N—N distances.

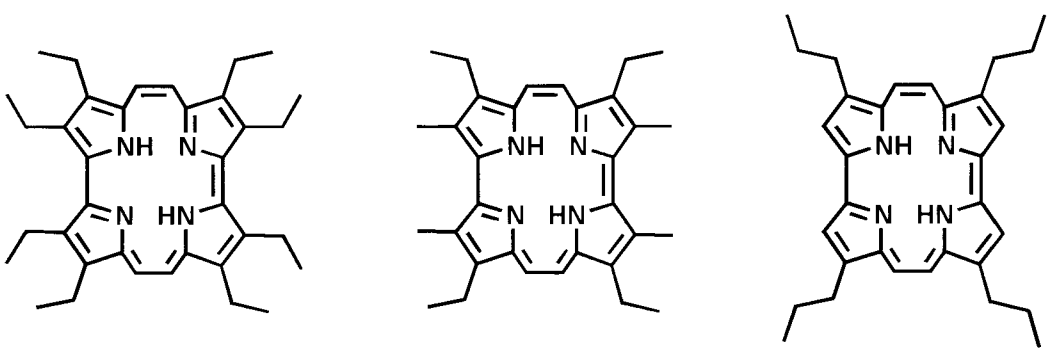

Figure 4. Examples of porphycenes with alkyl groups.

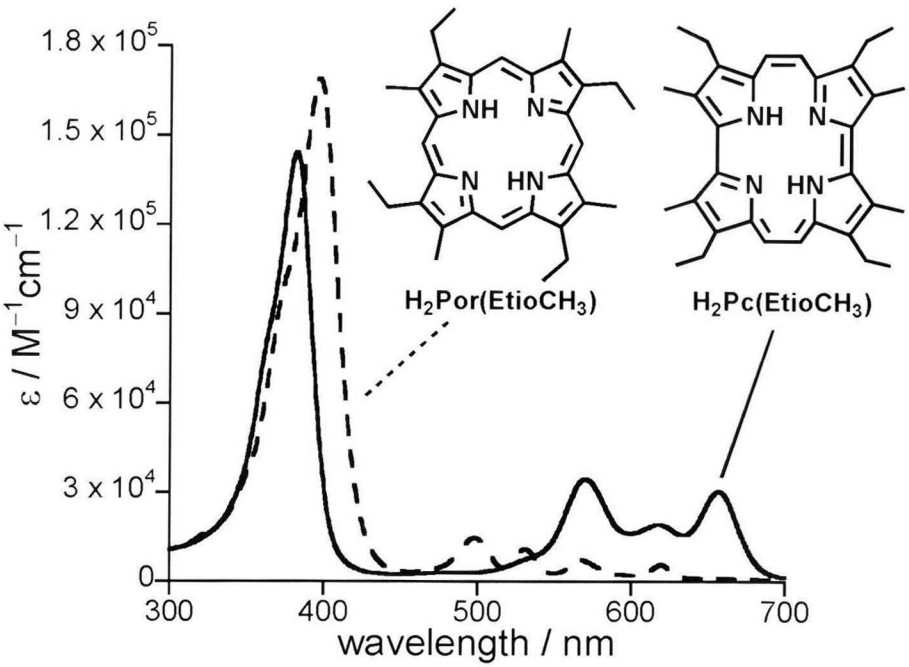

Figure 5. UV–vis spectra of porphyrin and porphycene in CH_2Cl_2.

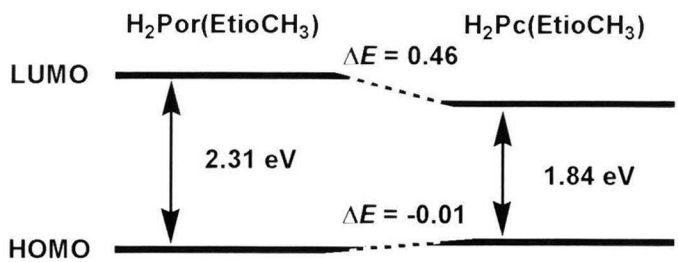

Figure 6. HOMO–LUMO gaps of porphyrin and porphycene.

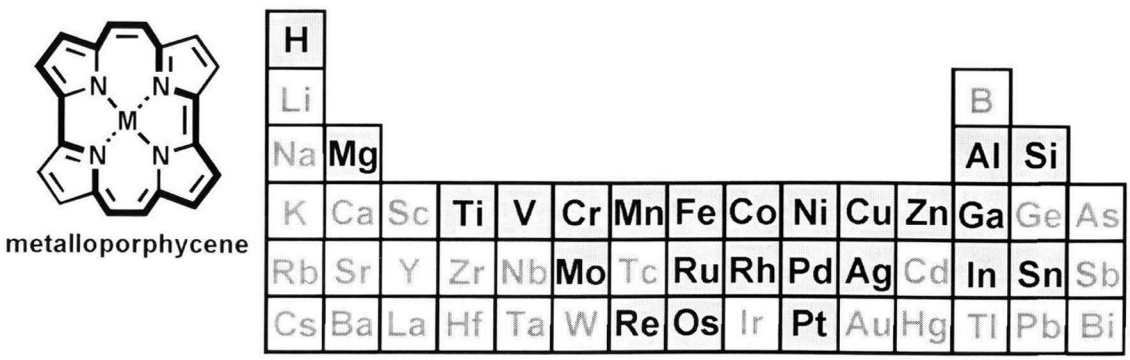

Figure 7. Periodic table of known metalloporphycenes [7].

Electron-Deficient Porphyrin

The π-conjugated system of porphyrin can be dramatically changed by alternating the porphyrin peripheral side chain. To study the effects of peripheral substituents in porphyrins, various types of porphyrins, e.g., *meso*-substituted porphyrins and β-pyrrole-substituted porphyrins, have been synthesized (Figure 8). The degree and mode of transmission of electron density from various points on the porphyrin ring through the σ and π orbitals of the four porphyrin nitrogens to the central metal ion have long been an interest of those who have investigated the physical properties and chemical reactions of metalloporphyrins. These studies revealed that electron-deficient porphyrins have some attractive properties and reactivities, e.g., the HOMO–LUMO gap of the porphyrin decreases by introducing electron-withdrawing groups on the framework [8] and the metal complex has strong Lewis acidity and produces remarkable improvements in oxidation reactions [9].

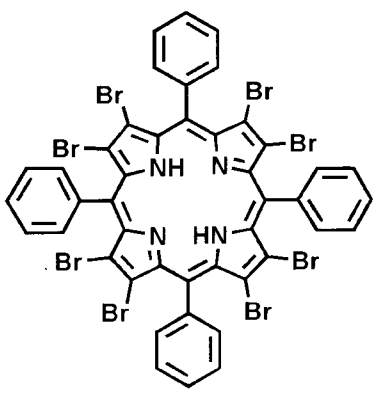

$(Br)_8TPP$, $[H_2Por(Br)_8(C_6H_5)_4]$
[8a]

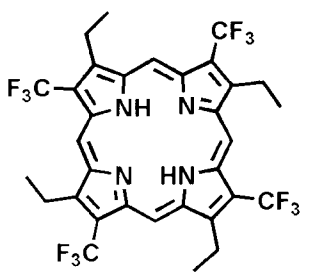

$H_2Por(EtioCF_3)$
[8b]

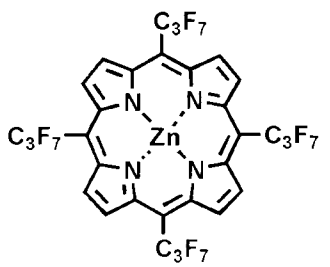

$ZnT(C_3F_7)P$, $[ZnPor(C_3F_7)_4]$
[8c]

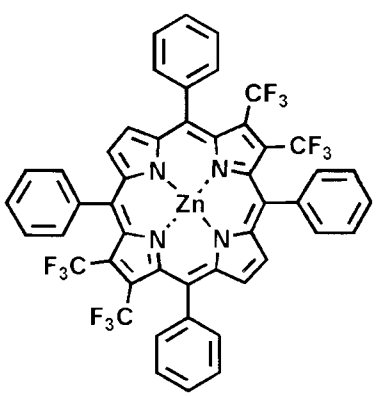

$[ZnPor(CF_3)_4(C_6H_5)_4]$
[8d]

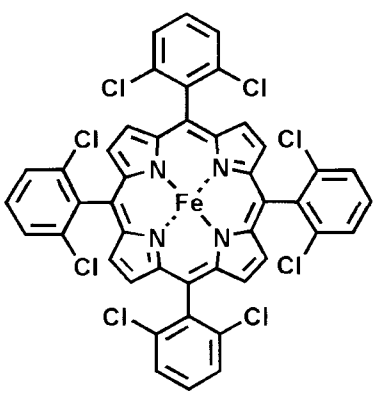

FeTDCPP, $[FePor(C_6Cl_2H_3)_4]$
[9a]

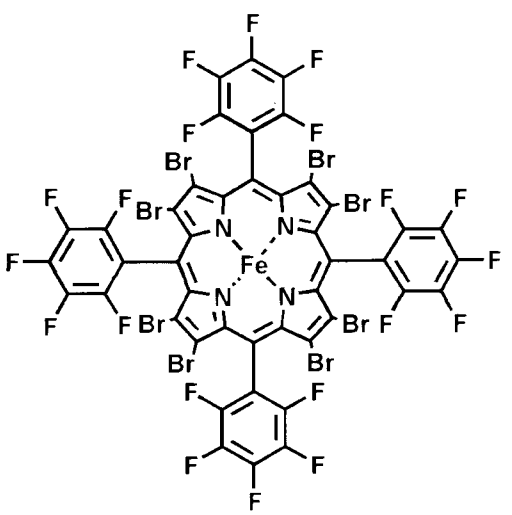

$Fe(Br)_8TFPP$, $[FePor(Br)_8(C_6F_5)_4]$
[9c]

Figure 8. Examples of electron-deficient porphyrins.

Myoglobin Reconstituted with Electron-Deficient Prosthetic Group

Myoglobin is an O_2-strage protein consisted with eight α-helices and a single heme as shown in Figure 9 [10]. The prosthetic group, heme, is ligated by the proximal His93 and retained in heme pocket with hydrophobic interaction between heme alkyl chains and nonpolar amino residues. Thus, the native heme can be easily replaced with an artificially created prosthetic group (Figure 10) [11]. The advantage of the reconstitutional technique using an artificial prosthetic group enables us to readily obtain a tailor-made protein having new functions.

Ogoshi et al. and Yamamoto et al. have independently reported the syntheses of artificial prosthetic groups with fluorine-contained substituents and the properties of myoglobins reconstituted with the electron-deficient heme (Figure 11) [12]. The reconstituted myoglobins are useful probes for the several researches on the properties of the myoglobins by use of ^{19}F NMR spectroscopy. Furthermore, the reconstituted myoglobins were investigated in the aspects of the ligand binding behaviors, electronic structure, spin state, rhombic perturbation to evaluate the influence of introducing the electron-deficient substituents.

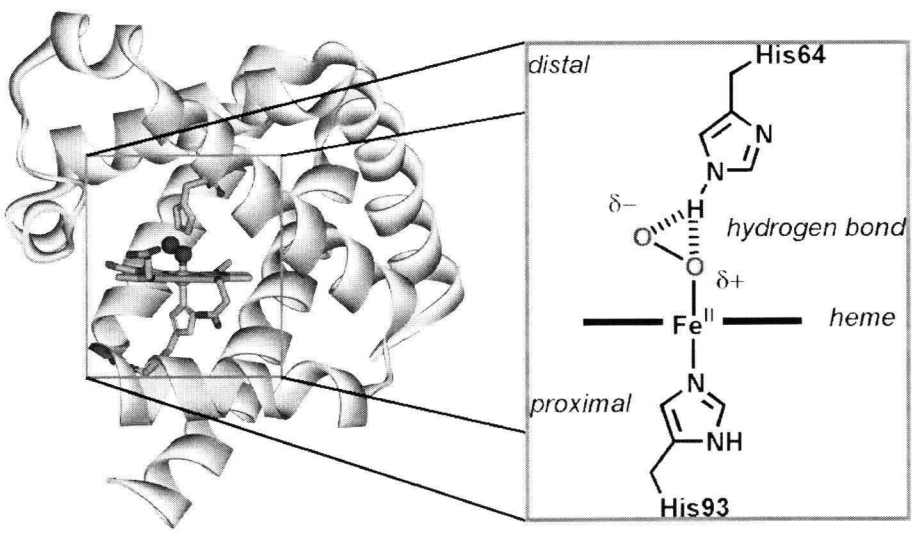

Figure 9. Crystal structure of oxy-Mb (PDB code: 1A6M) and schematic diagrams of the hydrogen bond in the O_2 binding site.

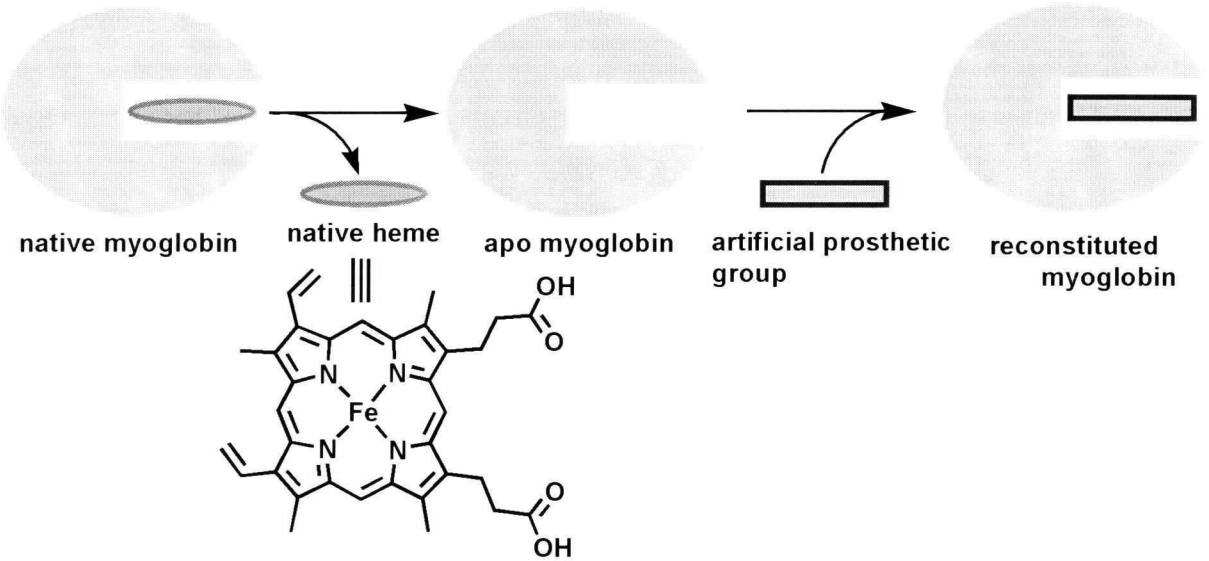

Figure 10. Strategy of reconstitutional technique of the prosthetic group in myoglobin.

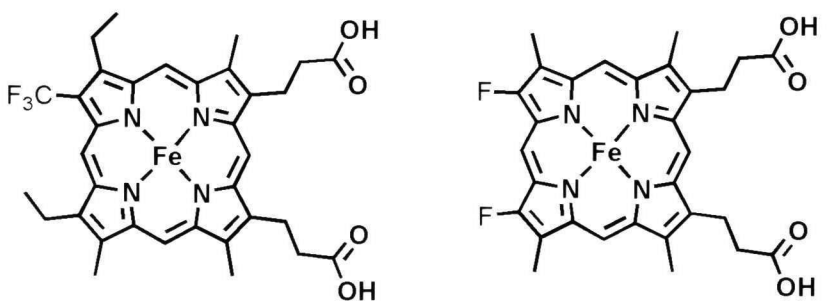

Figure 11. Examples of electron-deficient hemes [12].

Novel Electron-Deficient Porphycene Having Trifluoromethyl Groups

On the contrary to porphyrins, effects of peripheral substitution have been poorly established for porphycenes. Almost porphycenes have only simple alkyl groups, e.g., methyl, ethyl, and propyl groups as peripheral substituents [5], although it is thought that porphycene with electron-withdrawing groups has unique chemical properties. Thus, introducing electron-withdrawing groups onto the porphycene framework would give rise to inherent characteristics of porphycene. Brominated porphycene was only reported as an electron-deficient porphycene by Vogel et al., Chang et al., and Hisaeda et al [13]. Thus, the current interests are focused on producing the more electron-deficient porphycene and investigating the substituent effects on porphycene. It is thought that trifluoromethyl group is one of the suitable substituents to introduce on porphycene framework because trifluoromethyl group is a strong electron-withdrawing substituent. Trifluoromethyl group has large substituent constant as compare to bromine (Table 1) [14]. Furthermore, CF_3 group is chemically inert and useful as probe because ^{19}F NMR spectroscopy offers an excellent sensitivity and the spectra have wide chemical shift. To emphasize the substituent effect of CF_3 group, the author designed a novel trifluoromethylated porphycene, 2,7,12,17-tetraethyl-3,6,13,16-tetra(trifluoromethyl)porphycene, which has four CF_3 groups at β-pyrrolic carbon of the porphycene ring (Figure 12).

Meanwhile, it can be expected that the reconstitution approach is able to have an influence upon the inherent physiological property of myoglobin. Recently, we placed the native heme with 2,7-diethyl-3,6,12,17-tetramethyl-13,16-bis(2-methoxycarbonylethyl)porphycenatoiron(III) in sperm whale myoglobin. This reconstituted myoglobin with the iron porphycene showed extremely high oxygen affinity compared to the native myoglobin. On the basis of the result, to evaluate the influence of introducing trifluoromethyl group into the porphycene prosthetic group, the author designed a novel trifluoromethylated iron porphycene, 2,7-diethyl-3,6-bis(trifluoromethyl)-12,17-dimethyl-13,16-bis(2-methoxycarbonylethyl)porphycenatoiron(III).

In this thesis, the author demonstrates the structures and chemical properties of trifluoromethylated porphycene and its iron complex and the ligand binding behavior of myoglobin reconstituted with the iron porphycene having trifluoromethyl groups.

Table 1. Hammett Substituent Constants.

Substituents	σ_m	σ_p
CF_3	0.42	0.55
H	0.00	0.00
CH_3	−0.07	−0.17
CH_2CH_3	−0.07	−0.15
Br	0.39	0.23

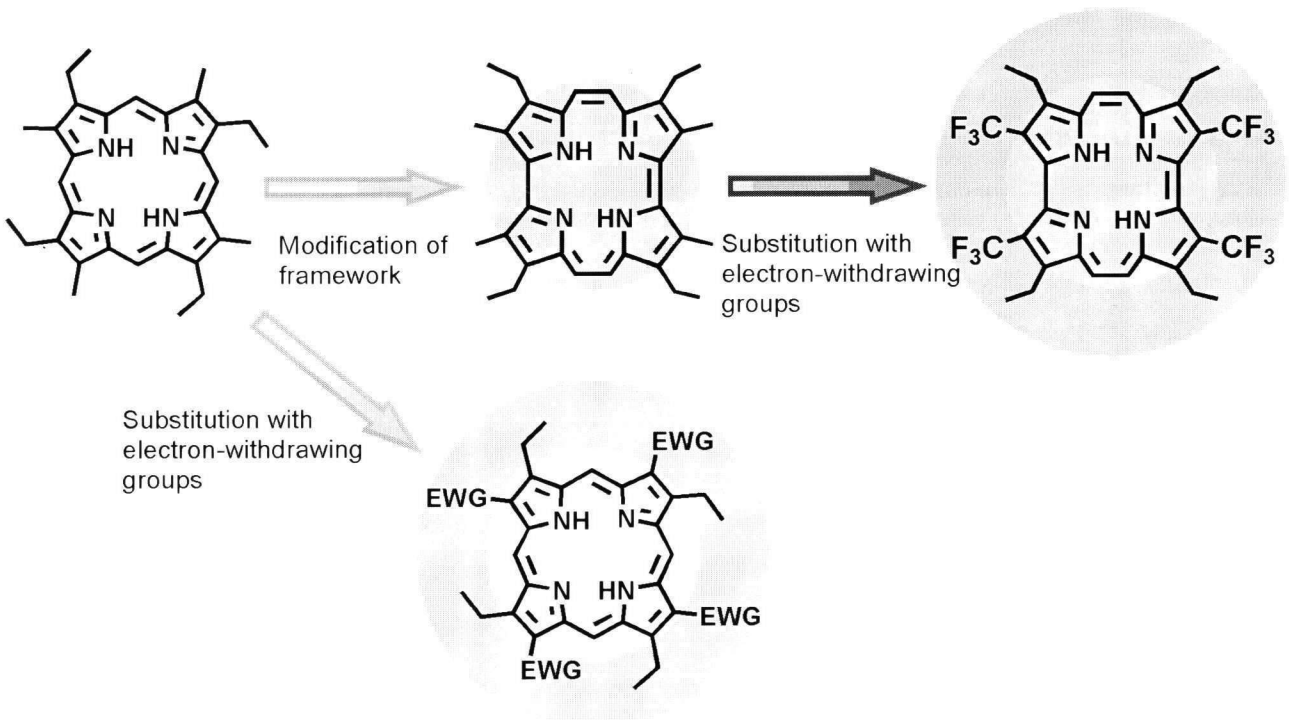

Figure 12. Combination of modification of framework and substitution with electron-withdrawing groups.

Outline of This Thesis

Chapter 1

Porphycene having trifluoromethyl groups was synthesized and characterized with spectroscopic measurements. The UV–vis measurements showed significant red-shifted spectrum when compared to porphycene having methyl groups instead of trifluoromethyl groups. The crystal structure of the porphycene was successfully determined and the framework was found to have a highly distort structure. From the electrochemical study, the redox potential of the porphycene shows anodic shift by the strong electron-withdrawing CF_3 groups. In this chapter, the chemical properties and the structure of free-base porphycene with CF_3 groups in comparison with those for porphycene without CF_3 groups are discussed.

Chapter 2

20π-conjugated porphycene was successfully isolated from the reduction products of the 18π-conjugated porphycene having CF_3 groups. The reaction to yield the 20π-conjugated porphycene required $2H^+$ and $2e^-$. The 20π-conjugated porphycene was fully characterized. These data show its nonaromatic character. The crystal structure of the 20π-conjugated porphycene was successfully obtained and the structure also supported its nonaromatic character. The ethylene bridge moieties in the 20π-conjugated framework displayed the olefinic characters. In this chapter, chemical properties, structures, oxidative stabilities, and reactively of the 20π-conjugated porphycene are discussed.

Chapter 3

Peripherally trifluoromethylated iron porphycenes, iron μ-oxo dimer and monomeric complex, were synthesized and the substituent effects were evaluated from UV–vis absorption, redox behavior. The structure of μ-oxo dimer was obtained, showing a severe saddled distortion of framework. The μ-oxo dimer is smoothly converted into the monomeric ferrous complex in pyridine. In addition, three structural analogs of the iron porphycene having CF_3 groups were prepared and investigated in the influence of the framework structure and/or peripheral substituents for the autoreduction in pyridine. In this chapter, property of the iron porphycenes and the kinetics of the autoreduction of iron porphycene are discussed.

Chapter4

Myoglobin reconstituted with the iron porphycene having CF_3 groups was prepared and the formation of the myoglobin reconstituted with the iron porphycene was confirmed by UV–vis and mass spectroscopic measurements. The prepared myoglobin shows the higher O_2 affinity than the native protein. However, the O_2 affinity of the reconstituted myoglobin is lower than that of the myoglobin having an iron porphycene without trifluoromethyl groups, which is mainly originated from the enhancement of the O_2 dissociation. The CO affinity of the myoglobin with the trifluoromethylated iron porphycene is similar to that observed for the reference

protein having the iron porphycene without trifluoromethyl groups, although their C–O stretching frequencies are significantly different. In this chapter, the relationship between the electronic states of the porphycene ring and the ligand bindings is discussed.

Reference

1. (a) Battersby, A. R.; Fookes, C. J. R.; Matcham, G. W. J.; McDonald, E. *Nature* **1980**, *285*, 17–21. (b) Kräutler, B. *Chimia* **1987**, *41*, 277–292.
2. Sessler, J. L.; Weghorn, S. J. In *Expanded, Contracted & Isomeric Porphyrins*, Pergamon: New York, 1997.
3. Vogel, E.; Köcher, M.; Schmickler, H.; Lex, J. *Angew. Chem., Int. Ed. Engl.* **1986**, *25*, 257–259.
4. Sessler, J. L.; Gebauer, A.; Vogel, E. In *The Porphyrin Handbook*; Kadish, K. M., Smith, K. M., Guilard, R., Eds.; Academic Press: San Diego, 2000; Vol. 2, Chapter 8 and reference therein.
5. (a) Bernard, C.; Gisselbrecht, J. P.; Gross, M.; Vogel, E.; Lausmann, M. *Inorg. Chem.* **1994**, *33*, 2393–2401. (b) Renner, M. W.; Forman, A.; Wu, W.; Chang, C. K.; Fajer, J. *J. Am. Chem. Soc.* **1989**, *111*, 8618–8621.
6. Bernard, C.; Le Mest, Y.; Gisselbrecht, J. P. *Inorg. Chem.* **1998**, *37*, 181–190.
7. Fowler, C. J.; Sessler, J. L.; Lynch, V. M.; Waluk, J.; Gebauer, A.; Lex, J.; Heger, A.; Zuniga-y-Rivero, F.; Vogel, E. *Chem. Eur. J.* **2002**, *8*, 3485–3496.
8. (a) D'Souza, F.; Zandler, M. E.; Tagliatesta, P.; Ou, Z.; Shao, J.; Van Caemelbecke, E.; Kadish, K. M. *Inorg. Chem.* **1998**, *37*, 4567–4572. (b) Homma, M.; Aoyagi, K.; Aoyama, Y.; Ogoshi, H. *Tetrahedron Lett.* **1983**, *24*, 4343–4346. (c) Goll, J. G.; Moore, K. T.; Ghosh, A.; Therien, M. J. *J. Am. Chem. Soc.* **1996**, *118*, 8344–8354. (d) Terazono, Y.; Patrick, B. O.; Dolphin, D. H. *Inorg. Chem.* **2002**, *41*, 6703–6710. (e) Terazono, Y.; Dolphin, D. H. *J. Org. Chem.* **2003**, *68*, 1892–1900. (f) Hodge, J. A.; Hill, M. G.; Gray, H. B. *Inorg. Chem.* **1995**, *34*, 809-812. (g) Woller, E. K.; DiMagno, S. G. *J. Org. Chem.* **1997**, *62*, 1588–1593.
9. (a) Traylor, P. S.; Dolphin, D.; Traylor, T. G. *J. Chem. Soc., Chem. Commun.* **1984**, 279–280. (b) Dolphin, D.; Traylor, T. G.; Xie, L. Y. *Acc. Chem. Res.* **1997**, *30*, 251–259. (c) Grinstaff, M. W.; Hill, M. G.; Birnbaum, E. R.; Schaefer, W. P.; Labinger, J. A.; Gray, H. B. *Inorg. Chem.* **1995**, *34*, 4896–4902.
10. (a) Philips, G. N., Jr. In *Handbook of metalloproteins*; Messerschmidt, A.; Huber, R., Poulos, T., Weighardt, K., Eds.; Wiley: 2001; Vol. 1, pp. 5–15. (b) Raven, E. L.; Mauk, A. G. In *Advances in Inorganic Chemistry*; Sykes, A. G. Ed.; Academic Press: 2000; Vol. 51, pp. 1–49.
11. Hayashi, T.; Hisada, Y. *Acc. Chem. Res.* **2002**, *35*, 35–43.
12. (a) Toi, H.; Homma, M.; Suzuki, A.; Ogoshi, H. *J. Chem. Soc., Chem. Commun.* **1985**, 1791–1792. (b) Suzuki, A.; Tomizawa, T.; Hayashi, T.; Mizutani, T.; Ogoshi, H. *Bull. Chem. Soc. Jpn.* **1996**, *69*, 2923–2933. (c) Yamamoto, Y.; Hirai, Y.; Suzuki, A. *J. Biol. Inorg. Chem.* **2000**, *5*, 455–462. (d) Hirai, Y.; Nagao, S.; Mita, H.; Suzuki, A.; Yamamoto, Y. *Bull. Chem. Soc. Jpn.* **2004**, *77*, 1485–1486. (e) Nagao, S.; Hirai, Y.; Suzuki, A.; Yamamoto, Y. *J. Am. Chem. Soc.* **2005**, *127*, 4146–4147.
13. (a) Will, S.; Rahbar, A.; Schmicker, H.; Lex, J.; Vogel, E. *Angew. Chem., Int. Ed. Engl.* **1990**, *29*, 1390–1393. (b) Oertling, W. A.; Wu, W.; Lopez-Garriga, J. J. ; Kim, Y.; Chang, C. K. *J. Am. Chem. Soc.* **1991**, *113*, 127–134. (c) Baba, T.; Shimakoshi, H.; Aritome, I.; Hisaeda, Y. *Chem. Lett.* **2004**, *33*, 906–907.
14. In *Hammett rules*; Inamoto, N. Ed., Maruzen: Tokyo, 1983.

Chapter 1.
Synthesis and Characterization of Trifluoromethylated Free-Base Porphycene

1-1. Preface

Over the last two decades, a variety of free bases and metal complexes of fluorinated porphyrins, perfluoroalkyl or perfluoroaryl porphyrins have been prepared, because the electron-deficient porphyrins have been very useful not only for understanding the physicochemical properties of tetrapyrrolic macrocycles but also for utilization as oxidation catalysts [1]. One of the interesting aspects of the fluorine containing porphyrins is that the oxidation and reduction potentials are relatively more positive than those of the corresponding usual porphyrins [2]. Furthermore, it has often been found that the structure of the electron-deficient porphyrins is highly distorted due to the steric and/or electronic effects of electron-withdrawing substituents [3]. Therefore, considerable effort has been devoted to studying unique porphyrins with strongly electron-withdrawing groups. In contrast, it is known that a porphycene, a structural isomer of porphyrin [4,5], reveals that the reduction potentials are also clearly shifted to a more positive value despite having no electron-withdrawing substituents bound at the porphycene framework [6,7], because of the lower symmetry of the porphycene compared to the geometry of the corresponding porphyrin [8]. Therefore, a modified porphycene incorporating a CF_3 or perfluoroalkyl group at the peripheral β-pyrrolic position will attract considerable interest as a highly electron-deficient tetrapyrrolic macrocycle, although, to the best of my knowledge, there is no report describing the preparation of a fluorine-containing porphycene [9]. Recently, the author and our group members have synthesized the first trifluoromethylated porphycene, 2,7,12,17-tetraethyl-3,6,13,16-tetra(trifluoromethyl)porphycene, $H_2Pc(EtioCF_3)$ (**1**), which seems to be an analogue of etioporphycene, 2,7,12,17-tetraethyl-3,6,13,16-tetramethylporphycene, $H_2Pc(EtioCH_3)$ (**2**) as shown in Scheme 1-1 [10]. In this chapter, the author reports the structure, electrochemical property and unique reactivity of **1**.

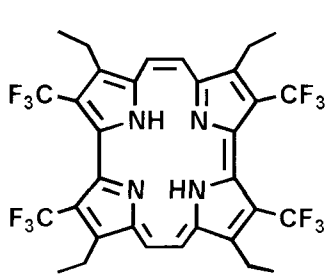

$H_2Pc(EtioCF_3)$ (1)

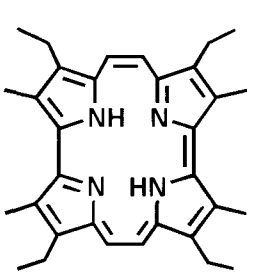

$H_2Pc(EtioCH_3)$ (2)

Chart 1-1.

1-2. Materials and Methods

1-2-1. Instruments

All NMR were recorded on Bruker Avance 500 instruments in $CDCl_3$ solvents at 25 °C; ^1H NMR and ^{19}F NMR chemical shifts were reported relative to residual $CHCl_3$ (7.24 ppm) and $CFCl_3$ (0 ppm), respectively. UV–vis spectra were measured on a Shimazu U-3500 double beam spectrophotometer equipped with a thermostated cell holder. FAB positive ion mass spectra were obtained from the NBA matrix on a JEOL JMS-SX10A high resolution mass spectrometer. MALDI-TOF mass spectra were performed on an Applied Biosystems Voyager Biospectrometry Workstation with a dithranol matrix. ESI-TOF and APCI-TOF mass spectra were performed on an Applied Biosystems Mariner API-TOF Workstation. Electrochemical studies were performed on Bioanalytical Systems CV-50W electrochemical workstations.

1-2-2. Materials

All reagents and chemicals were obtained from commercial sources and used as received unless stated otherwise. All solvents were dried and distilled prior to use under N_2.

1-2-3. Syntheses

2-Benzyloxycarbonyl-3-trifluoromethyl-4-ethyl-5-methylpyrrole (**3**) was synthesized by the reported procedure [11]. The trifluoromethylated porphycene was synthesized as described below (Scheme 1-2).

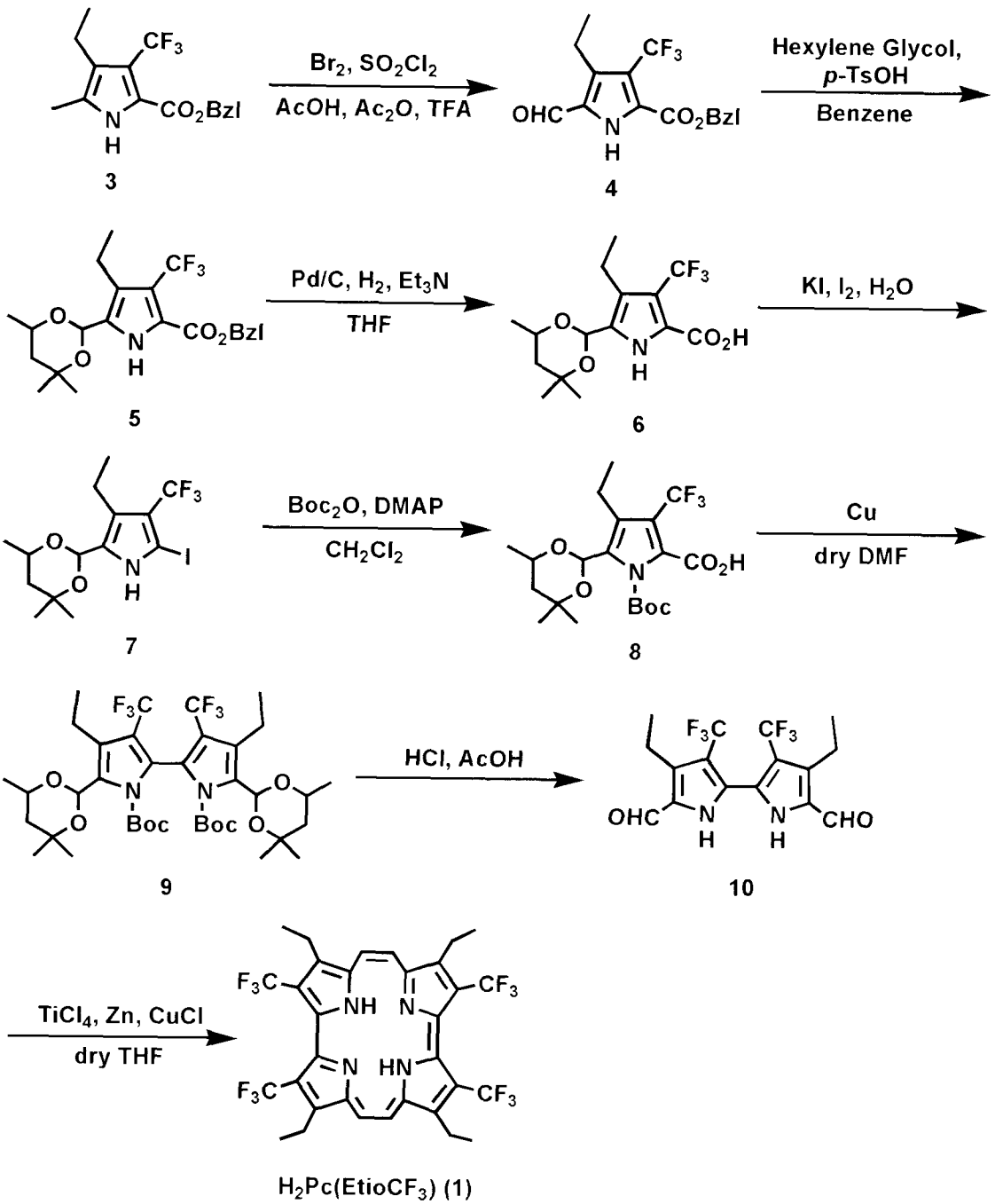
CF3
CO2Bzl
N
H
3
Br2, SO2Cl2
AcOH, Ac2O, TFA
OHC
4
Hexylene Glycol,
p-TsOH
Benzene
Pd/C, H2, Et3N
THF
5
CO2H
6
KI, I2, H2O
I
7
Boc2O, DMAP
CH2Cl2
Boc
8
Cu
dry DMF
F3C
9
HCl, AcOH
CHO
10
TiCl4, Zn, CuCl
dry THF
NH
HN
H2Pc(EtioCF3) (1)

Scheme 1-1.

2-Benzyloxycarbonyl-3-trifluoromethyl-4-ethyl-5-formylpyrrole (4):

To a mixture of acetic acid (90 mL), trifluoroacetic acid (45 mL) and anhydrous acetic acid (45 mL) was added 2-Benzyloxycarbonyl-3-trifluoromethyl-4-ethyl-5-methylpyrrole (**3**) (10.2 g, 31.3 mmol). After the mixture was cooled ice bath, Br_2 (5.20 g, 32.5 mmol) was added all at once, and the solution was stirred for 1 h. Furthermore, SO_2Cl_2 (13.2 g, 97.8 mmol) was added dropwise over 3 h to the solution. The solution was poured onto ice and stored overnight. The resulting precipitate was collected via filtration and washed with water to yield a white powder of **4** (8.89 g, 84%). ^{1}H NMR (500 MHz, $CDCl_3$): δ (ppm) = 10.04 (brs, 1H), 9.84 (s, 1H), 7.46–7.38 (m, 5H), 5.40 (s, 2H), 2.95 (q, J = 7.5 Hz, 2H), 1.29 (t, J = 7.5 Hz, 3H).

2-Benzyloxycarbonyl-3-trifluoromethyl-4-ethyl-5-(4',4',6'-trimethyl-1',3'-dioxane-2-yl)pyrrole (5):

In a round-bottomed flask with a Dean-Stark apparatus, a solution containing **4** (5.6 g, 15 mmol), *p*-toluene sulfonic acid (10 mg), and hexylene glycol (3.6 mL, 28.2 mmol) in benzene (50 mL) was refluxed for 1 h. After cooling to room temperature, the reaction mixture was poured into a saturated $NaHCO_3$ solution, and the combined organic layers were washed with water and dried over anhydrous $MgSO_4$. Removal of solvent by an evaporator afforded an orange oil of **5** (7.0 g, quant.). ^{1}H NMR (500 MHz, $CDCl_3$): δ (ppm) = 9.56 (brs, 1H), 7.44–7.28 (m, 5H), 5.83 (s, 1H), 5.36 (s, 2H), 4.12–4.06 (m, 1H), 2.61 (q, J = 7.4 Hz, 2H), 1.53 (d, J = 3.7 Hz, 2H), 1.41 (s, 3H), 1.32 (s, 3H), 1.27 (d, J = 6.0 Hz, 3H), 1.16 (t, J = 7.4 Hz, 3H).

2-Carboxy-3-trifluoromethy-4-ethyl-5-(4',4',6'-trimethyl-1',3'-dioxane-2-yl)pyrrole (6):

To a solution of **5** (11.5g, 27 mmol) in THF (100 mL) containing triethylamine (0.1 mL, 0.72 mmol) was added 10% palladium on charcoal (1.0 g). The mixture was stirred at room temperature over 20 h under hydrogen atmosphere. After filtration to removal Pd/C powder, the solvent was evaporated to yield an orange power of **6** (9.5 g, quant.). ^{1}H NMR (500 MHz, $CDCl_3$): δ (ppm) = 9.61 (brs, 1H), 5.72 (s, 1H), 4.14–4.07 (m, 1H), 2.66 (q, J = 7.3 Hz, 2H), 1.55 (d, J = 2.8 Hz, 2H), 1.44 (s, 3H), 1.35 (s, 3H), 1.30 (d, J = 7.4 Hz, 3H), 1.17 (t, J = 7.3 Hz, 3H). ^{19}F NMR (470 MHz, $CDCl_3$): δ (ppm) = −55.4. MS (ESI-TOF, negative mode) calculated for [M − H]$^-$ $C_{15}H_{19}F_3NO_4^-$, 334.127; found 334.180.

2-Iodo-3-trifluoromethy-4-ethyl-5-(4',4',6'-trimethyl-1',3'-dioxane-2-yl)pyrrole (7):

To a solution of water (150 mL) containing $NaHCO_3$ (10 g) was added **6** (9.4 g, 28 mmol), and then the solution was heated at 50 °C. An aqueous solution of I_2 (7.1 g, 28 mmol) and KI (11.6 g, 69.9 mmol) was added dropwise over 2 h, and the mixture was stirred for and additional 1h. After cooling to room temperature, aqueous $Na_2S_2O_3$ was added to the solution until the solution became to colorless, and the mixture was further stirred for 30 min. The resulting precipitate was collected by filtration and dried in vacuo to yield **7** (9.32 g, 80%). ^{1}H NMR (500 MHz, $CDCl_3$): δ (ppm) = 8.60 (brs, 1H), 5.80 (s, 1H), 4.11–4.05 (m, 1H), 2.59 (q, J = 7.5 Hz, 2H), 1.53 (d, J = 3.7 Hz, 2H), 1.41 (s, 3H), 1.33 (s, 3H), 1.28 (d, J = 6.1 Hz, 3H), 1.15 (t, J = 7.5 Hz, 3H). MS (ESI-TOF) calculated for [M + H]$^+$, $C_{14}H_{20}F_3INO_2^+$ 418.049; found 418.060.

***N*-*tert*-Butoxycarbonyl-2-iodo-3-trifluoromethyl-4-ethyl-5-(4',4',6'-trimethyl-1',3'-dioxane-2-yl)pyrrole (8):**

To a solution of CH_2Cl_2 (50 mL) containing **7** (4.81 g, 11.5 mmol) was added di-*tert*-butylcarbonate (3.01 g, 13.8 mmol), *N*,*N*-dimethylaminopyridine (110 mg, 0.90 mmol) and the solution was stirred at room temperature for 2 h. After removal of the solvent by an evaporator, the crude residue was purified by silica gel chromatography ($CHCl_3$) to afford an orange oil **8** (4.67 g, 79%). ^{1}H NMR (500 MHz, $CDCl_3$): δ (ppm) = 6.07 (s, 1H), 4.02 (m, 1H), 2.76 (m, 2H), 1.49 (d, J = 2.7 Hz, 2H), 1.41 (s, 3H), 1.26 (d, J = 6.1 Hz, 3H), 1.16 (t, J = 7.4 Hz, 3H).

***N*,*N*'-Di-*tert*-butoxycarbonyl-3,3'-di(trifluoromethyl)-4,4'-diethyl-5,5'-bis(4",4",6"-trimethyl-1",3"-dioxane-2"-yl)-2,2'-bipyrrole (9):**

To a 100 mL round-bottomed flask was added **8** (3.34 g, 6.5 mmol) and activated Cu power (4.03 g, 65 mmol) under N_2 atmosphere. After the addition of dry DMF (20 mL), the solution was stirred at room temperature for 18 h and then poured into water. The mixture was filtered over Celite, and the eluent was extracted with $CHCl_3$. The combined organic layers were washed with water, 20% of aqueous HNO_3, a saturated $NaHCO_3$ solution, and water and then dried over anhydrous $MgSO_4$. After evaporation, the resulting solid was washed with methanol and dried in vacuo to yield a white powder of **9** (1.61 g, 64%). mp 145.2–146.5 °C. ^{1}H NMR (500 MHz, $CDCl_3$): δ (ppm) = 6.48 (d, J = 2.5 Hz, 1H), 6.45 (d, J = 1.4 Hz, 1H), 4.05–3.98 (m, 2H), 2.98–2.90 (m, 2H), 1.50–1.15 (m, 44H). MS (FAB) calculated for $[M]^-$ $C_{38}H_{54}F_6N_2O_8^-$, 780.3784; found 780.3771. Anal. Calcd for $C_{38}H_{54}F_6N_2O_8$: C, 58.45; H, 6.97; N, 3.59. Found: C, 58.20; H, 6.97; N, 3.64.

3.3'-Di(trifluoromethyl)-4,4'-diethyl-5,5'-diformyl-2,2'-bipyrrole (10):

A solution of acetic acid (80 mL) containing **9** (2.0 g, 2.6 mmol) was heated at 50 °C, and then 20 mL of conc. HCl was added all at once to the solution. After stirring at 50 °C for 10 min, the mixture was poured into water and stored at room temperature overnight. The resulting precipitate was collected by filtration and recrystallized from hexane–$CHCl_3$ to yield a light green powder of **10** (702 mg, 71%). mp > 216 °C (dec). ^{1}H NMR (500 MHz, $CDCl_3$): δ (ppm) = 9.81 (s, 2H), 9.51 (brs, 2H), 2.96 (q, J = 7.5 Hz, 4H), 1.35 (t, J = 7.6 Hz, 6H). MS (FAB) calculated for $[M + H]^+$ $C_{16}H_{15}F_6N_2O_2^+$, 381.1037; found 381.1047. Anal. Calcd for $C_{16}H_{14}F_6N_2O_2$: C, 50.53; H, 3.71; N, 7.37. Found: C, 49.75; H, 3.66; N, 7.22.

2,7,12,17-Tetraethyl-3,6,13,16-tetra(trifluoromethyl)porphycene H_2Pc(EtioCF$_3$) (1):

To dry THF solution (200 mL) containing activated Zn (4.5 g, 68.8 mmol) and CuCl (684 mg, 6.9 mmol) was added $TiCl_4$ (3.7 mL, 33.7 mmol) at 0 °C over 1 h, and the mixture was refluxed for 3 h. After cooling to room temperature, dry THF solution (200 mL) containing **10** (260 mg, 0.68 mmol) was added dropwise to the mixture over 6 h. The solution was then refluxed for 30 min. After cooling to 0 °C, a solution of 1% aqueous Na_2CO_3 (70 mL) was added over 1 h. After filtration of the precipitate, the filtrate was extracted with CH_2Cl_2, washed with water and dried over anhydrous $MgSO_4$. The solvent was removed and the residue was dissolved in $CHCl_3$. To the mixture was added 2,3-dichloro-4,5-dicyano-p-benzoquinone (DDQ) (77 mg, 0.34 mmol) and then stirred at room temperature for 10 min. After the solvent was removed by an evaporator, the crude residue was purified by silica gel chromatography ($CHCl_3$) to afford a pure greenish blue precipitate of **1** (22 mg, 10%). mp > 250 °C (dec). ^{1}H NMR (500 MHz, $CDCl_3$): δ (ppm) = 9.38 (s, 4H), 3.86 (q, J = 7.4 Hz, 8H), 2.33 (brs, 2H), 1.59 (t, J =

7.4 Hz, 12H). ^{13}C NMR ($CDCl_3$, 125 MHz): δ (ppm) = 150.1, 143.4, 134.8, 124.5 (q, $^1J_{CF}$ = 270.8 Hz), 124.5 (br), 114.6, 20.8, 18.3. ^{19}F NMR (470 MHz, $CDCl_3$): δ (ppm) = −51.8 (s). MS (FAB) calculated for $[M + H]^+$ $C_{32}H_{27}N_4F_{12}^+$, 695.2044; found 695.2032. UV–vis λ_{max} (ε, $M^{-1}cm^{-1}$) in CH_2Cl_2; 376 (8.9×10^4), 623 (3.3×10^4), 670 (2.2×10^4), 720 (4.3×10^4) nm. Anal. Calcd for $C_{32}H_{26}F_{12}N_4$: C, 55.34, H, 3.77; N, 8.07. Found: C, 54.22; H, 3.86; N, 7.49.

1-2-4. X-ray Crystallography

Crystal of **1** suitable for X-ray crystal structure analysis was grown by slow evaporation from a CH_2Cl_2/*n*-octane mixture. X-ray diffusion data were measured on a Bruker SMART APEX CCD diffractometer with graphite monochromated Mo Kα radiation (λ = 0.71073 Å). Frames collected by a combination of ω and ϕ scans with frame widths of 0.30°. Data collection and cell refinement were handled with Bruker SMART 5.629 software. Frame integration were carried out using the SADABS program [12]. The structure was solved by direct methods and refined using all data (based on F^2) with Bruker SHELXTL 6.14 and local programs therein [13].

1-2-5. Cyclic Voltammetry

Cyclic voltammetry was carried out with a three-electrode system consist of a platinum button electrode as working, a platinum wire electrode as counter, and an Ag/AgCl electrode as reference. The reference electrode was separated from the bulk solution by a fritted-glass bridge filled with 0.1 M KCl aqueous solution.

1-3. Results and Discussion

1-3-1. Syntheses

As shown in Chart 1-1, the synthesis of **1** started from the preparation of trifluoromethylpyrrole [11]. Although an α-methyl group of the pyrrole ring is generally oxidized to a carboxyl group through halogenation of the methyl group by treatment with Br_2 and SO_2Cl_2 [14], α-formylpyrrole was obtained under similar conditions in quantitative yield, because the CF_3 group might reduce the reactivity of halogenation at the α-methyl group. After the formyl group was protected by hexylene glycol, deprotection of the benzyl ester and decarboxylative iodination led to an activated α-iodopyrrole. An α,α'-diformylbipyrrole, a precursor of **1**, was achieved by Ullmann coupling of the α-iodopyrrole and the following deprotection of acetal in 45% yield. The cyclization of two 5,5'-diformyl-2,2'-bipyrrole molecules in the presence of $TiCl_4$ via the reductive McMurry coupling gave a light-yellow oil as an initial condensation product that could be a dihydroporphycene species, although it has never been purified and characterized. After the addition of DDQ into the solution of the intermediate species, a greenish blue 18π-electron aromatic porphycene **1** was obtained in 10% yield. In the case of normal porphycene synthesis, the aromatization due to the autoxidation occurs spontaneously under ambient atmosphere after the McMurry cyclization. This finding suggests that an oxidant such as DDQ is required to prepare **1**, because the coupling intermediate is not readily oxidized [15].

The porphycene **1** was characterized by UV–vis, ^1H and ^{19}F NMR, and mass spectroscopy. The λ_{max} values of the Q-band in the UV–vis spectrum for **1** appeared at 622, 670, and 719 nm in CH_2Cl_2, which showed a 53–63 nm red shift with respect to those observed for **2** as shown in Figure 1-1. The significant Q-band shift, which is often seen in a series of porphyrins with bulky electron-withdrawing groups [16–20], indicates that the HOMO-LUMO energy gap decreases with respect to that for **2**. The ^1H NMR spectrum of **1** in $CDCl_3$ is comparable with that observed for **2** except for the internal NH proton resonance [10]. The NH proton of **1** was found to resonate at 2.33 ppm, which is 1.47 ppm lower than that for **2**. This result probably comes from the increase in the hydrogen bonding interaction of NH proton with the pyrrole imine nitrogen and/or the decrease in the aromatic ring current due to the distorted structure.

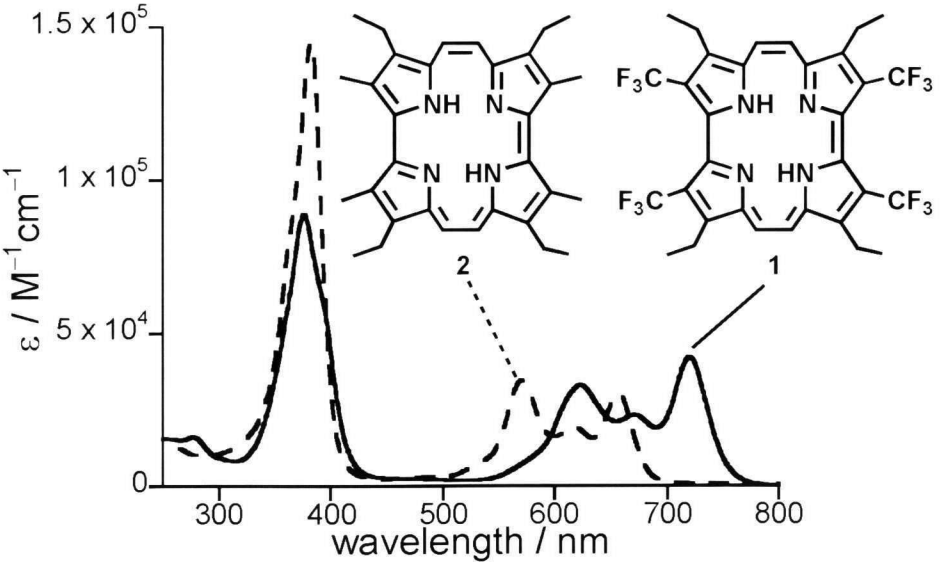

Figure 1-1. UV–vis spectra of **1** and **2**.

1-3-2. Crystal Structure

The molecular structure of **1** determined by X-ray crystallographic analysis is shown in Figure 1-2. Crystallographic data for **1** are summarized in Table 1-1. The framework of **1** is found to show a saddle-distorted structure that is not seen for the planar structure of normal porphycene such as **2** [10a]. Particularly, each bipyrrole is strongly twisted along the pyrrolic Cα–Cα' axis to reduce the steric and electronic repulsion of the two adjacent CF_3 groups; the average values of the pyrrole–pyrrole dihedral angles for **1** and **2** are 23.13 and 10.50°, respectively. Therefore, the displacement of the β-pyrrolic carbon from the average plane defined by the four pyrrole nitrogen atoms is determined to be a maximum of 0.976 Å for **1**, whereas the same value for **2** is 0.307 Å [10a]. These comparisons demonstrate that **1** reveals the most distorted structure among the known porphycene compounds [8].

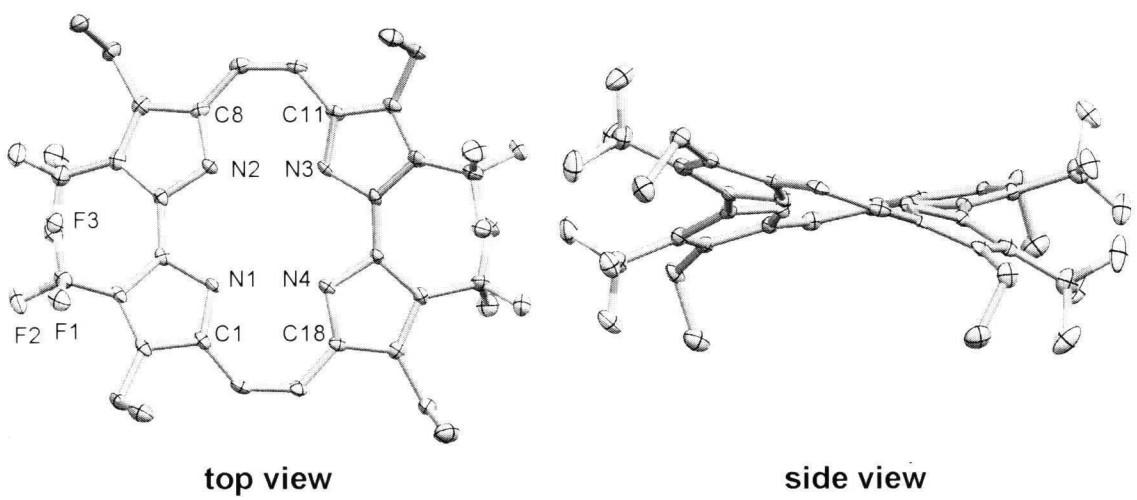

Figure 1-2. ORTEP diagram of **1** with 50% thermal probability elipsoilds. Hydrogen atoms are omitted for clarity.

Table 1-1. Crystallographic Data for **1**.

Empirical formula	$C_{32}H_{26}F_{12}N_4$
Formula weight	694.57
Temperature, K	100(2)
Crystal color	purple plate
Crystal size, mm^3	$0.20 \times 0.13 \times 0.02$
Crystal system	orthorhombic
Space group	*Pbca*
a, Å	22.732(2)
b, Å	9.6336(6)
c, Å	26.742(2)
α, deg	90
β, deg	90
γ, deg	90
V, $Å^3$	5856.3(7)
Z	8
D_{calcd}, g cm^{-1}	1.576
$F(000)$	2832
μ(Mo, Kα), mm^{-1}	0.148
Theta range for data collection	1.52 to 25.52
Reflections collected	33454
Independent reflections	5454
Parameters	437
Goodness-of-fit on F^2	1.196
$R1^{a)}$, $wR2^{b)}$ [$I > 2\sigma(I)$]	0.0723, 0.1424
Largest diff. peak and hole	0.486 and −0.270

a) $R1 = \Sigma||F_o|-|F_c||/\Sigma|F_o|$. b) $wR2 = [\Sigma w(F_o^2-F_c^2)^2/\Sigma w(F_o^2)^2]^{1/2}$.

1-3-3. Redox Behavior

The redox potentials of **1** and **2** were measured by cyclic voltammetry in PhCN. First and second reduction peaks were observed with each reversible one-electron-transfer separation ($E_{pa} - E_{pc}$ = 92 and 100 mV, respectively, for **1**) in PhCN, whereas the first and second oxidation potentials were determined by differential pulse voltammetry, because clear reversible peaks were not detected under the normal condition [7,21]. Table 1-2 summarizes the comparative oxidation and reduction potentials for the porphycenes and the corresponding porphyrins. In a manner similar to a series of free-base porphycenes, the first reduction of **2** occurs at a 0.46 V less negative potential than that for 2,7,12,17-tetramethyl-3,8,13,18-tetraethylporphyrin, H_2Por(EtioCH$_3$) (**11**), due to splitting of the π^* molecular orbitals with a decrease in the symmetry of the tetrapyrrolic macromolecule, whereas the first oxidation potential of **2** is comparable with that observed for **11** [6,7]. Interestingly, **1** is reduced at a potential of −0.14 V (vs. Ag/AgCl) in PhCN; this first reduction potential is 0.78 V more positive than that observed for **2**, indicating that a remarkable stabilization of the LUMO energy level results from the introduction of four strongly electron-withdrawing CF_3 substituents at the β-pyrrolic positions. In fact, a significant positive shift upon the introduction of electron-withdrawing groups has also been seen in porphyrin chemistry, e.g., the value of the first reduction potential for 1,3,5,7-tetra(trifluoromethyl)2,4,6,8-tetraethylporphyrin, H_2Por(EtioCF$_3$) (**12**) is ca. 0.5 V more positive compared to that of **11**. The first oxidation of **1** occurs at a potential of +1.30 V, which is 0.38 V higher than that observed for **2**. Therefore, the stabilization of the one-electron oxidation and reduction states does not occur to the same degree; the positive shift in the oxidation state for **1** is less than half that observed in the reduction potential. These results suggest that the HOMO energy level is destabilized due to the distortion of the porphycene structure of **1**, as shown in Figure 1-2 [18,23–25].

In addition, it is of interest to discuss the HOMO–LUMO energy gap electrochemically determined from the difference between the first reduction and oxidation potentials described above. As shown in Figure 1-3, the gap for **2** ($\Delta E = E_{ox1} - E_{red1}$ = 1.84 V) is clearly smaller than that observed in normal porphyrins (ΔE = 2.31 V for **11**) [7]. Furthermore, the dramatic HOMO–LUMO gap decrease to 1.44 V for **1** was observed due to the introduction of strongly electron-withdrawing groups on the porphycene framework. The significantly smaller HOMO – LUMO gap for **1** is clearly indicative of the large red-shifted Q-band in the optical spectrum. As seen in several electron-deficient porphyrins, it is concluded that the reduced gap value comes from the electronic effect of the strongly electron-withdrawing CF_3 groups and the distorted macrocycle structure [16,17,19,20,23].

Table 1-2. Comparative Oxidation and Reduction Potentials (V vs. Ag/AgCl) for Free-base Porphycenes and Porphyrins.[a)]

Compounds	2nd ox	1st ox	1st red	2nd red	solvent	reference
1	+1.51[b]	+1.30[b]	−0.14	−0.43	PhCN	this work
2	+1.26[b]	+0.92[b]	−0.92	−1.21	PhCN	this work
11	+1.38[b]	+0.93[b]	−1.38		PhCN	this work
12			−0.80	−1.19	PhCN	this work
	+1.22	+0.84			CH_2Cl_2	ref 22

a) 0.1 M TABP at 25 °C, Scan rate = 0.1 V/s. The ferrocene/ferrocenium redox couple (0.51 V vs. Ag/AgCl) was used as the internal standard. b) These oxidation potential were determined by a different pulse voltammetry technique.

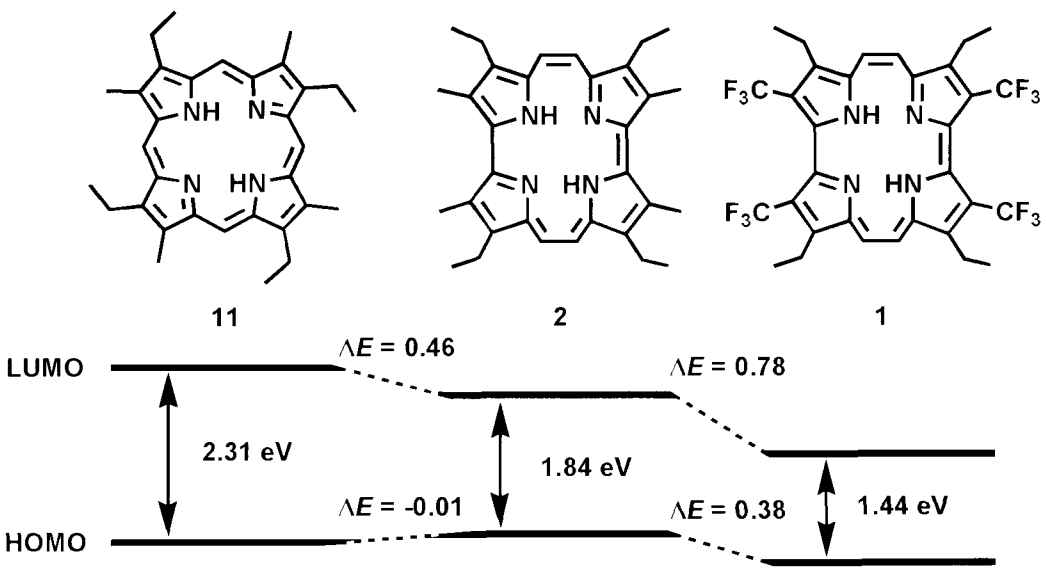

Figure 1-3. HOMO–LUMO gaps of free-base porphycenes and porphyrin.

1-3-4 p*K*a of Inner N–H Proton.

The electron-deficient property of the tetrapyrrolic ligand was also evaluated by monitoring the deprotonation of the inner N–H proton to yield a monoanion species upon the addition of a base such as 1,8-diazabicyclo-[5.4.0]-undec-7-ene (DBU) [18,20b]. The addition of an excess of DBU to a CH_2Cl_2 solution containing **2** ([DBU]/[H_2Pc(EtioCH$_3$)] > 10^4) caused no spectral changes in the Soret and Q-band regions under the conditions, indicating that the inner protons of **2** were much less acidic than the protonated DBU ($DBUH^+$). In contrast, drastic changes in the optical spectrum of **1** were observed upon the addition of DBU, and the color of the solution turned purple. The difference in p*K*a values between **1** and $DBUH^+$ was 1.2 ± 0.5 in CH_2Cl_2 [26]. Furthermore, the addition of triethylamine to CH_2Cl_2 solution containing **1** also led to the same spectral changes. These titrimetric measurements with DBU or triethylamine support the facts that the inner N–H of **1** is more acidic than that of **2** or **11**, indicating that the monoanion species of **1**, HPc(EtioCF$_3$)$^-$, is stabilized by the inductive effect of the σ-electron-withdrawing CF_3 substituents.

1-4. Summary

H_2Pc(EtioCF$_3$) (**1**) exhibits an extremely electrondeficient nature. Particularly, the substitution of CF_3 groups at the β-pyrrolic carbon effectively stabilizes the LUMO energy level by 1.24 V compared to general porphyrins such as H_2Por(EtioCH$_3$) (**11**). The present results indicate that the combination of the porphycene framework and the strongly electron-withdrawing substituents gives us a new family of highly electron-deficient tetrapyrrolic macrocycles.

Reference

1. (a) Dolphin, D.; Traylor, T. G.; Xie, Y. L.; *Acc. Chem. Res.* **1997**, *30*, 251–259. (b) Mansuy, D.; Battioni, P.; In *Bioinorganic Catalysis*, 2nd ed.; Reedijk, J.; Bouwman, E.; Eds.; Marcel Dekker: New York, 1999; Chapter 11. (c) Meunier, B. In *Biomimetic Oxidations Catalyzed by Tradition Metal Complexes*; Meunier, B. Ed.; Imperial College Press: 2000; Chapter 4. (d) Senge, M. O. In *The Porphyrin Handbook*; Kadish, K. M., Smith, K. M., Guilard R., Eds.; Academic Press: San Diego, 2000; Vol. 1, Chapter 6 and references therein.
2. Kadish, K. M.; Royal, G.; Gaemelbecke, E. V.; Gueletti, L. In *The Porphyrin Handbook*; Kadish, K. M., Smith, K. M., Guilard, R., Eds.; Academic Press: San Diego, 2000; Vol. 9, Chapter 59.
3. Kadish, K. M.; Van Caemelbecke, E.; Royal, G. In *The Porphyrin Handbook*; Kadish, K. M., Smith, K. M., Guilard, R., Eds.; Academic Press: San Diego, 2000; Vol. 8, Chapter 55 and reference therein.
4. Vogel, E.; Köcher, M.; Schmickler, H.; Lex, J. *Angew. Chem., Int. Ed. Engl.* **1986**, *25*, 257–259.
5. Sessler, J. L.; Weghorn, S. J. *Expanded, Contracted & Isomeric Porphyrins*, Pergamon: New York, 1997.
6. Renner, M. W.; Forman, A.; Wu, W.; Chang, C. K.; Fajer, J. *J. Am. Chem. Soc.* **1989**, *111*, 8618–8621.
7. (a) Gisselbrecht, J. P.; Gross, M.; Köcher, M.; Laumsmann, M.; Vogel, M. *Angew. Chem., Int. Ed. Engl.* **1990**, *112*, 8618–8620. (b) Bernard, C.; Cisselbrecht, J. P.; Gross, M.; Vogel, E.; Lausmann, M. *Inorg. Chem.* **1994**, *33*, 2393–2401.
8. Sessler, J. L.; Gebauer, A.; Vogel, E. In *The Porphyrin Handbook*; Kadish, K. M., Smith, K. M., Guilard, R., Eds.; Academic Press: San Diego, 2000; Vol. 2, Chapter 8.
9. As an example of electron-deficient porphycene, only a brominated porphycene where four bromines were introduced at the β-pyrrolic carbons has been reported in the literature. (a) Will, S.; Rahbar, A.; Schmicker, H.; Lex, J.; Vogel, E. *Angew. Chem., Int. Ed. Engl.* **1990**, *29*, 1390–1393. (b) Aritome, I.; Shimakoshi, H.; Hisaeda, Y. *Acta Crystallogr.* **2002**, *C58*, o563–o564.
10. (a) Vogel, E.; Koch, P.; Hou, X.-L.; Lex, J.; Lausmann, M.; Kisters, M. Aukauloo, M. A.; Richard, P.; Guilard, R. *Angew. Chem., Int. Ed. Engl.* **1993**, *32*, 1600–1604. (b) Guilard, R.; Aukauloo, M. A.; Tardieux, C.; Vogel, E. *Synthesis*, **1995**, 1480–1482.
11. Homma, M.; Aoyagi, K.; Aoyama, Y.; Ogoshi, H. *Tetrahedron Lett.* **1983**, *24*, 4343–4346.
12. G. Sheldrick, "SADABS", University of Göttingen, Germany, **1996**.
13. G. Sheldrick, "SHELXS97" and "SHELXL97", University of Göttingen, Germany, **1996**.
14. Richert, C.; Wessels, J. M.; Müller, M.; Kisters, M.; Benninghaus, T.; Goetz, A. E. *J. Med. Chem.* **1994**, *37*, 2797–2807.
15. (a) Vogel, E. *Pure Appl. Chem.* **1990**, *62*, 557–564. (b) Vogel, E. *Pure Appl. Chem.* **1993**, *65*, 143–152.
16. Hodge, J. A.; Hill, M. G.; Gray, H. B. *Inorg. Chem.* **1995**, *34*, 809–812.
17. Goll, J. G.; Moore, K. T.; Ghosh, A.; Therien, M. J. *J. Am. Chem. Soc.* **1996**, *118*, 8344–8354.
18. Woller, E. K.; DiMagno, S. G. *J. Org. Chem.* **1997**, *62*, 1588–1593.
19. D'Souza, F.; Zandler, M. E.; Tagliatesta, P.; Ou, Z.; Shao, J.; Van Caemelbecke, E.; Kadish, K. M. *Inorg. Chem.* **1998**, *37*, 4567- 4672.
20. (a) Terazono, Y.; Patrick, B. O.; Dolphin, D. *Inorg. Chem.* **2002**, *41*, 6703–6710. (b) Terazono, Y.; Dolphin, D. *J. Org. Chem.* **2003**, *68*, 1892–1900.

21. In the cyclic voltammetry experiment, E_{pa} peaks were clearly observed at 1.36 and 1.62 V for **1**.
22. Ono, N.; Kawamura, H.; Maruyama, K. *Bull. Chem. Soc. Jpn.* **1989**, *62*, 3386–3388.
23. Kadish, K. M.; D'Souza, F.; Villard, A.; Autret, M.; Van Caemelbecke, E.; Bianco, P.; Antonini, A.; Tagliatesta, P. *Inorg. Chem.* **1994**, *33*, 5169–5170.
24. Ochsenbeim, P.; Ayougou, K.; Mandon, D.; Fischer, J.; Weiss, R.; Austin, R. N.; Jayaraj, K.; Gold, A.; Terner, J.; Fajer, J. *Angew. Chem., Int. Ed. Engl.* **1994**, *33*, 348–350.
25. Birnbaum, E. R.; Hodge, J. A.; Grinstaff, M. W.; Schaefer, W. P.; Henling, L.; Labinger, J. A.; Bercaw, J. E.; Gray, H. B. *Inorg. Chem.* **1995**, *34*, 3625–3632.
26. Decomposition of deprotonated species was partially observed at the final stage of the titrimetric measurement upon the addition of DBU, although the experiment was performed under the normal anaerobic and anhydrous conditions. Thus, it was difficult to reduce the error in the ΔpKa value.

Chapter 2.
Synthesis, Structure, and Reactivity of 20π-Conjugated Porphycene

2-1. Preface

The π-conjugation system of porphyrin, a tetrapyrrolic 18π-conjugated macrocycle, is controlled by designing the framework structures, e.g., peripheral substitutions [1], changes in the arrangement of pyrrole units including ring expansion/contractions [2], and introducing non-pyrrolic units [2]. However, the structure-modified porphyrinoids, in many cases, also maintain aromaticity, i.e., the (4n + 2) π-conjugation system. In contrast, the preparation of porphyrinoids with 4n π-conjugation system, namely, "nonaromatic porphyrinoids", is a unique approach to dramatically alter the π-conjugation behaviors of a tetrapyrrolic macrocycle [3]. The nonaromatic porphyrinoid being most structurally close to porphyrin is isophlorin, a tetrapyrrole with a 20π-conjugated character, first reported by Woodward [4]. Generally, the isolations of 20π-conjugated porphyrinoids are rather difficult because of their tendency to be oxidized to the corresponding 18π-conjugated form, unless the nitrogens on the pyrrole rings are alkylated or replaced with oxygen or sulfur atoms [5]. However, a recent report of a 20π-conjugated Cu-porphyrin having four CF_3 and phenyl groups in the framework suggests the possibility of isolating 20π-conjugated porphyrinoids by well-considered electronic/structural modulations on the framework [3].

Porphycene, a structural isomer of porphyrin pioneered by Vogel [6], is normally synthesized by McMurry coupling of two 5,5'-formylbipyrroles (**10** or **13** in Scheme 2-1). During the coupling of **13** (R = Me), the presumed coupling product **14**, a 20π-conjugated form, is readily oxidized to **2** in air, whereas the formation of a CF_3-introduced porphycene **1** requires the addition of DDQ to the reaction mixture [7]. On the basis of this fact, it can be expected that the 20π-conjugated porphycene would be stabilized by controlling the electronic configurations of the porphycene framework. This is another strategy to prepare a structural isomer of isophlorin such as pyrrolophanediene-porphycene [8,9].

In this chapter, the author reports the chemistry of the 20π-conjugated porphycene with CF_3 groups at the β-pyrrolic positions, **15**, shown in Scheme 2-1 together with the 18π-conjugated form, **1**.

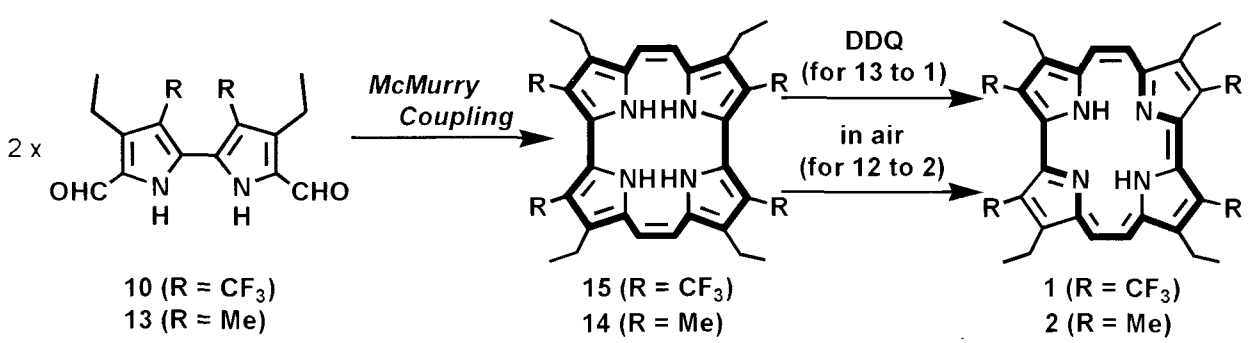

10 (R = CF_3)
13 (R = Me)

15 (R = CF_3)
14 (R = Me)

1 (R = CF_3)
2 (R = Me)

Scheme 2-1.

2-2. Materials and Methods

2-2-1. Instruments

NMR spectra were recorded on a Bruker DPX-400 spectrophotometer or a JEOL JNM-AL400 spectrophotometer. Chemical shifts in ^{1}H NMR and ^{13}C NMR spectra were reported relative to the residual protiated solvents (δ = 5.32 for $CDHCl_2$ or δ = 7.24 for $CHCl_3$) and to the carbon of the solvent (δ = 54.5 for $^{13}CD_2Cl_2$ or δ = 77.2 for $^{13}CDCl_3$), respectively. ^{19}F NMR chemical shifts were referenced to hexafluorobenzene (δ = −162). UV–vis spectra were measured using a Shimadzu UV-3150 double beam spectrophotometer equipped with a thermostated cell holder. FAB mass spectra were measured using a JEOL JMS-700 spectrophotometer with positive ion mode.

2-2-2. Materials

Commercially available reagents were used as received unless noted. Undeuterated solvents were distilled prior to use. Deuterated solvents were dried on CaH_2 under a nitrogen atmosphere, and purified by vacuum transfer technique. The dried solvents were kept in a dry box.

2-2-3. Reactions

Porphycenes (**1**, **2**) and H_2Por(EtioCF_3) (**12**) were reacted with some reducing reagents to yield 20π-conjugated products (Scheme 2-2).

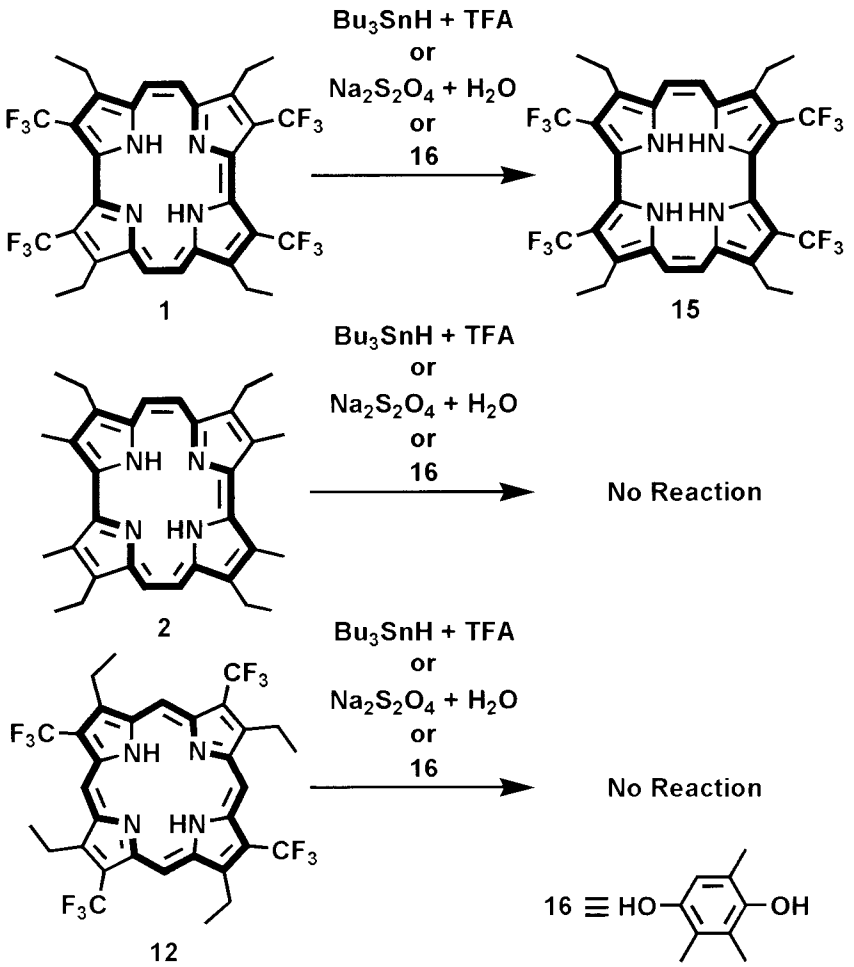

Scheme 2-2.

Reaction of 1 with tributyltin hydride (Bu_3SnH)/trifluoroacetic acid (TFA) (UV–vis and NMR experiment):

For following the UV–vis spectral changes, **1** was dissolved in dry CH_2Cl_2 (3 mL) under a nitrogen atmosphere. The solution was transferred to a quartz cell (L = 10mm) without air contact and sealed with a septum. After the UV–vis spectrum was recorded, Bu_3SnH and TFA were sequentially added to the solution with a micro syringe and the UV–vis spectrum was measured again 24 h after the addition of the reagents. The final concentrations of **1**, Bu_3SnH and TFA were 1.2×10^{-5} M, 2.4×10^{-5} M and 2.4×10^{-5} M, respectively. For the NMR experiments, **1** was dissolved to dry CD_2Cl_2 in a NMR tube equipped with a J-young cock. Bu_3SnH and TFA were sequentially added to the solution with avoiding air contact, and the NMR spectra were collected after 24 h. The final concentrations were 2.0×10^{-3} M for **1**, 4.0×10^{-3} M for Bu_3SnH and 4.0×10^{-3} M for TFA. ^{1}H NMR (CD_2Cl_2, 400 MHz) δ(ppm) = 9.47 (brs, 4H), 6.15 (s, 4H), 2.60 (q, J = 7.0 Hz, 8H), 1.17 (t, J = 7.0 Hz, 12H). ^{13}C NMR ($CDCl_3$, 100 MHz) δ(ppm) = 127.3, 126.5, 123.4 (q, $^1J_{CF}$ = 268.7 Hz), 120.6, 114.4 (q, $^2J_{CF}$ = 35.2 Hz), 113.0, 17.4, 15.6. ^{19}F NMR ($CDCl_3$, 376 Hz) δ(ppm) = −55.7 (CF_3 in **15**), −74.7 (TFA).

Reaction of 1 with sodium dithionite ($Na_2S_2O_4$) (UV–vis experiment):

For following the UV–vis spectral changes, **1** (1.2×10^{-5} M) was dissolved in THF (3 mL) under a nitrogen atmosphere. Excess amount of sodium dithionite in water (1 mL) was added to the solution and the UV–vis spectral changes were followed.

Reactions of 2 or 12 with Bu_3SnH/TFA:

The UV–vis spectral changes in the reactions of **2** or **12** with Bu_3SnH/TFA were followed in the same manner as the reaction of **15** as described above. The concentrations of **2** and **12** employed were 3.3×10^{-3} M and 8.6×10^{-3} M, respectively. The amounts of Bu_3SnH and TFA were 2.0 equiv. of the pophyrinoids.

Reactions of 1 with hydroquinones:

The isolated **1** (1.0×10^{-5} M) was dissolved in dry THF under a nitrogen atmosphere at a quartz cell (L = 10 mm). After the cell was sealed with a septum to keep the anaerobic conditions, huge excess amount of **16** (1.5×10^{-3} M) or **17** (3.0×10^{-2} M) in dry THF was added to the solution with a micro syringe and the UV–vis spectral changes were followed at 25 °C.

2-2-4. Syntheses.

Isolation of 15 by the reaction of 1 with $Na_2S_2O_4$:

1 was reacted with $Na_2S_2O_4$ in water/THF (1:3, v/v) for 10 min at 25 °C. The solvent was removed by azeotropy with toluene. After the residue was treated with CH_2Cl_2 and water and the water phase was discarded, the organic phase was concentrated in vacuo. The residue was purified by silica gel chromatography (ϕ 0.5 cm × 5 cm) with the elution of N_2-purged CH_2Cl_2. The yellow band was collected and the solvent was evaporated to give yellow powder of **15** (91% yield). The product was kept in dry box. ^{1}H NMR ($CDCl_3$, 400 MHz) δ(ppm) = 10.19 (brs, 4H), 6.01 (s, 4H), 3.61 (m, 16H), 2.54 (q, J = 7.0 Hz, 8H), 1.81 (m, 16H), 1.14 (t, J = 7.0 Hz, 12H). ^{13}C NMR ($CDCl_3$, 100 MHz) δ(ppm) = 128.1, 127.0, 123.4 (q, $^1J_{CF}$ = 268.7 Hz), 119.3, 115.2 (q, $^2J_{CF}$ = 36.2 Hz), 112.9, 68.1, 26.1, 17.7, 16.0. ^{19}F NMR ($CDCl_3$, 376 Hz) δ (ppm) = −56.5. MS (FAB) calculated for $[M]^+$ $C_{32}H_{30}N_4F_{12}^+$, 696.2122; found 696.2128. UV–vis λ_{max} (ε: $M^{-1}cm^{-1}$) in CH_2Cl_2; 282 (2.9×10^4), 319 (4.0×10^4), 381 (sh, 3.6×10^3), 596 (3.3×10^2), 640 (3.0×10^2), 680 (3.8×10^2) nm.

Hydrogenation of 15:

15 (1.7 mg, 2.4 μmol) was dissolved in 2 mL of ethyl acetate containing 1% acetic acid in a 25-mL round flask, and 10% Pd-C (1.5 mg) was added after introducing nitrogen. The reaction mixture was vigorously stirred under hydrogen atmosphere for 10 h at room temperature and filtered. The filtrate was concentrated, and the greenish yellow residue was obtained. The product was identified as the hydrogenated compound **18** (88% yield). ^{1}H NMR ($CDCl_3$, 400 MHz) δ(ppm) = 6.92 (brs, 4H), 3.08 (d, J = 9.6 Hz, 4H), 2.58 (m, 8H), 2.42 (d, J = 9.6 Hz, 4H), 1.19 (t, J = 7.4 Hz, 12H). ^{13}C NMR ($CDCl_3$, 100 MHz) δ(ppm) = 129.2, 124.4(q, $^1J_{CF}$ = 267.7 Hz), 121.1, 120.4, 110.73 (q, $^2J_{CF}$ = 34.2 Hz), 26.8, 17.9, 16.8. ^{19}F NMR ($CDCl_3$, 376 Hz) δ(ppm) = −53.6. MS (FAB) calculated for $[M]^+$ $C_{32}H_{32}N_4F_{12}^+$, 700.2435; found, 700.2432. UV–vis λ_{max} in CH_2Cl_2; 266 nm.

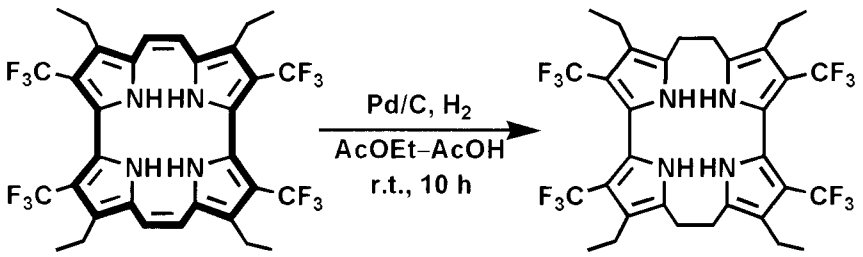

15 18

Scheme 2-3.

2-2-5. Measurement of Oxidative Stability of 15.

15 (8.2×10^{-6} M) was dissolved in THF at a quartz cell (L = 10 mm) under the air and the cell was sealed with septum with avoid solvent evaporation. The UV–vis spectroscopic measurements were carried out at the beginning of the reaction and 24 h after the sample preparation. Then, excess amount of DDQ were added to the solution and the UV–vis spectrum was recorded within 1 min again.

2-2-6. X-ray Crystallography

Crystal of **15** suitable for X-ray crystal structure analysis was grown by slow evaporation from water/THF mixed solvent. All measurements were made on a Rigaku RAXIS-RAPID Imaging Plate diffractometer with graphite monochromated Mo Kα radiation. An absorption correction was not applied. The data were corrected for Lorentz and polarization effects. The structure was solved by direct methods and expanded using Fourier techniques [10,11]. All calculations were performed using the teXsan crystallographic software package of Molecular Structure Corporation [12].

2-3. Results and Discussion

2-3-1 Reactions and Syntheses

The isolation of the 20π-conjugated porphycene **15** from the reaction mixture of McMurry coupling of **10** was impossible due to the difficulty in the separation of many kinds of byproducts. Therefore, the author attempted the reaction of **1** with some reducing reagents to yield the pure **15**. Upon the addition of 2.0 equiv. of tributyltin hydride (Bu_3SnH) and 2.0 equiv. of trifluoroacetic acid (TFA) to the solution of **1** in dry CH_2Cl_2 at 25 °C, the typical absorption bands of **1** around 380, 600 and 720 nm decreased over 24 h along with the growth of a new band around 300 nm (Figure 2-1). In the absence of TFA, no such spectral change was observed. This finding indicates that both two protons and two electrons are required for the reaction to proceed. Similar spectral changes were also observed in the reaction with sodium dithionite in water/THF (1:3, v/v) (Scheme 2-2), in which water would function as a proton donor. The disappearance of the absorption bands suggests a significant perturbation to the electronic states in the 18π-aromtic ring system. Similar spectral changes were also reported for the previous pyrrolphanediene-porphycne synthesis [8].

The ^{1}H NMR spectral changes are demonstrated in Figure 2-2. When Bu_3SnH and TFA were added to the solution of **1** in CD_2Cl_2, the peak of the protons on the ethylene bridges (C9–C10 and C19–C20 moieties) at 9.45 ppm disappeared along with the growth of new peaks at 6.15 and 9.47 ppm. The former peak is located in the range observed for typical olefinic protons [13]. The latter peak integrated as 4 protons is rather broad and exchangeable with D_2O, indicative of pyrrole-NH protons. A broad peak is observed in a field similar to that seen for the NH protons of bipyrrole **10**, although the NH protons in **1** are observed at 2.29 ppm due to the ring current effect in the 18π-conjugated system [7a]. The protons in the peripheral ethyl groups are observed in a more upfield region when compared to those in **1**. These spectroscopic characteristics indicate that the product structure coincides with the 20π-conjugated porphycene **15**. The lost of aromaticity in **15** is also indicated in the ^{13}C NMR spectrum. All peaks of the carbons on the pyrrole rings in **15** shifted to a more upfield region when compared with the spectrum for **1** (110–130 ppm for **15**, 110–150 ppm for **1**). The ^{19}F NMR spectrum of the reaction product shows the peak for the fluorine atom of the CF_3 group at −55.7 ppm, whereas the fluorine atoms in **1** are observed in the downfield region (−51.8 ppm). This finding also supports the nonaromaticity of **15**. The observation of peaks in the up-field region for 1H and 13C NMR, compared with the parent 18π-conjugated molecule, was also reported [8]. However, the tendency of the peak shifts is quite different, probably because of the differences in the orientations of the two bipyrrole moieties.

The reaction with Bu_3SnH/TFA or aqueous $Na_2S_2O_4$ was also examined for **2** and **12** (Scheme 2-2). However, no UV–vis spectroscopic change was observed for both compounds even upon the addition of the reducing reagents, suggesting that the reactivity of **1** toward the reducing reagents would mainly stem from the positive shift of the reduction potentials for **1**: E_{red} = −0.14 and −0.43 V in **1**, −0.92 and −1.21 V in **2**, −0.80 and −1.19V in **12** (vs. Ag/AgCl, in PhCN) (Table 1-2) [7a].

The conversion of **1** into **15** is supposed to proceed by the typical $2H^+$–$2e^-$ transfer mechanism, because no reaction was observed upon the addition of only a hydride donor (≡ $1H^-$ and $2e^-$) to **1**. Therefore, the injection of $2H^-$ and $2e^-$ by typical $2H^-$–$2e^-$ donors such as hydroquinones would be possible. When **1** was mixed with trimethylhydroquinone **16** in THF (Scheme 2-2), the UV–vis spectral changes during the reaction were similar to

that observed during the reaction of Bu_3SnH/TFA (Figure 2-3). The half-life time of **1** (1.0×10^{-5} M) in the presence of **16** (1.5×10^{-3} M) was calculated to be 122 sec at 25 °C. The reaction rate was found to be dependent on the oxidation potential of the employed hydroquinone, because monomethylhydroquinone **17** reacted with **1** more slowly with the same half-life time at the higher concentration of **17** (3.0×10^{-2} M).

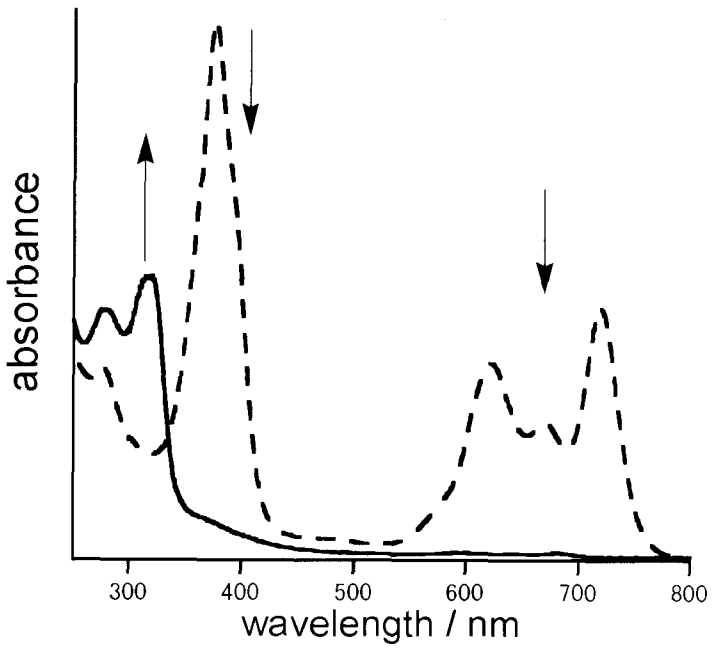

Figure 2-1. UV–vis spectral changes during the reaction of **1** (1.2×10^{-5} M) with Bu_3SnH (2.4×10^{-5} M) in the presence of TFA (2.4×10^{-5} M) in CH_2Cl_2 at 25 °C. Dashed blue line: the spectrum of **1**; Solid red line: the spectrum measured 24 h after the addition of Bu_3SnH and TFA.

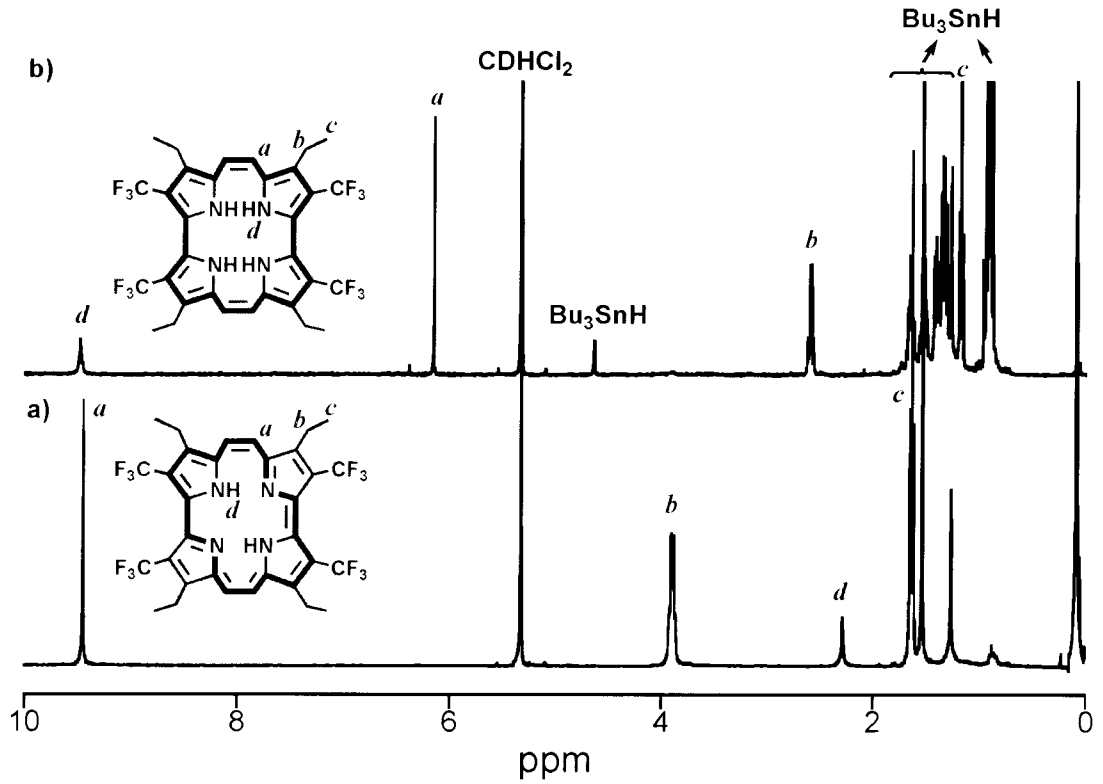

Figure 2-2. ^{1}H NMR spectra of **1** in the absence and presence of Bu_3SnH/TFA in CD_2Cl_2: a) in the absence of Bu_3SnH and TFA; b) 24 h after the addition of Bu_3SnH and TFA.

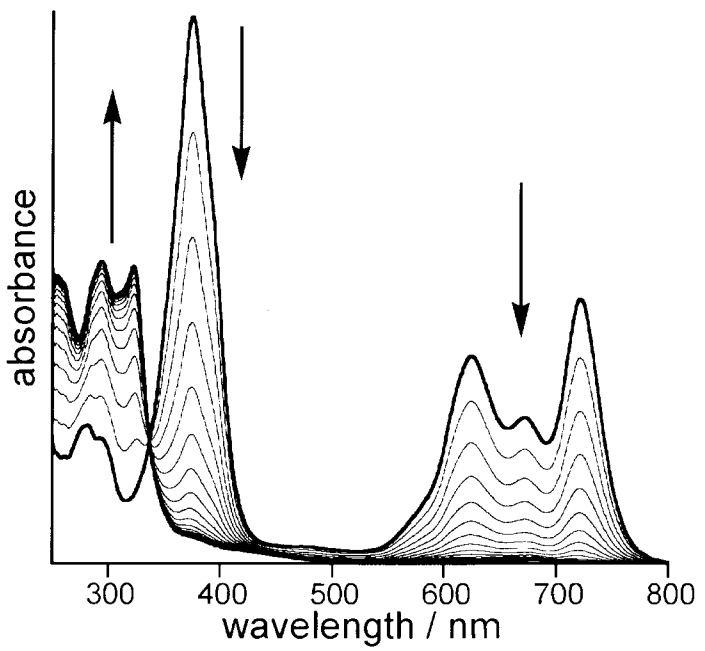

Figure 2-3. UV–vis spectral changes during the reaction of **1** (1.0×10^{-5} M) with **16** (1.5×10^{-5} M) in THF at 25 °C for 16 h. First line: the initial spectrum of the reaction (the spectrum for **1** + **16**); Last line: the spectrum measured 24 h after the addition of **16**.

2-3-2. Oxidative Stability

Compound **15** is expected to be relatively stable toward dioxygen because the parent compound, **1**, has a positively shifted redox potential when compared with that of the porphycene without CF_3 groups, **2**. To confirm this tendency, **15** was prepared by the reduction of **1** with sodium dithionite in water/THF. After being quickly purified by silica gel chromatography under aerobic conditions, **15** was isolated as a yellow powder in 91% yield. The product was dissolved in CH_2Cl_2 in air at 22 °C and then stored in air. Surprisingly, the UV–vis spectrum measured after 24 h indicates that more than 98% of **15** still remained as the 20π-form. Upon the addition of DDQ, **15** was returned to **1** (Figure 2-4).

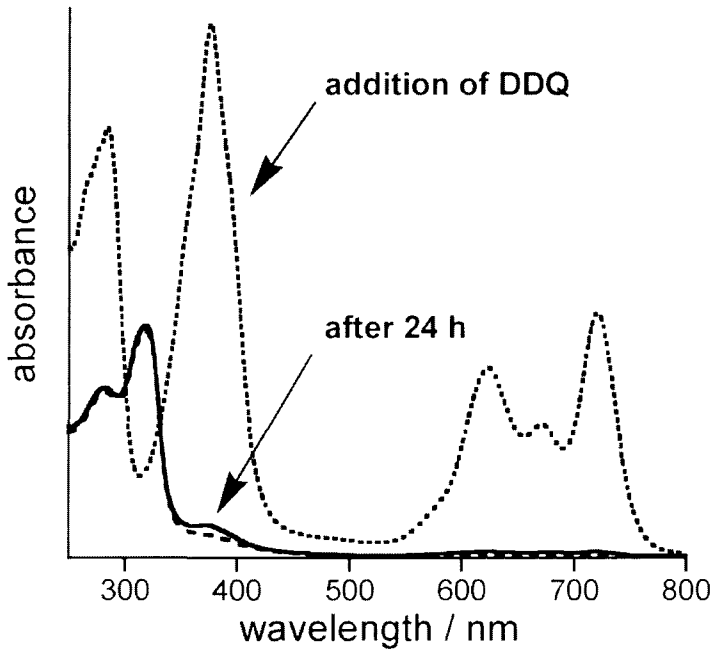

Figure 2-4. UV–vis spectra of **15** (and **1**) in CH_2Cl_2 under the air. Dashed line: before exposing to the air (the spectrum for **15**); Solid line: after 24 h; Dotted line: after the addition of DDQ (the spectrum for **1** + DDQ).

2-3-3. Crystal Structure

The author successfully obtained a yellow crystal of **15** with the orthorhombic crystal system from THF-water in the presence of sodium dithionite as **15·(THF)$_2$**, where two THF molecules are contained in one porphycene ring. The molecular structure of **15·(THF)$_2$** determined by X-ray crystallography is shown in Figure 2-5 and crystallographic data for **15·(THF)$_2$** are summarized in Table 2-1. Similar to the structure of **1** described above [7a], the porphycene framework of **15·(THF)$_2$** is strongly ruffled and each bipyrrole is twisted due to steric repulsion of the CF_3 groups. The dihedral angle of the two bipyrroles is 50.83°, much larger than that in **1** (23.13°). These structural features result from the lost of aromaticity in **15**. However, the bipyrrole moieties are not significantly twisted as the previously reported pyrrolophanediene porphycene (64.3°) [8]. The bond lengths between C8–C9, C9–C10 and C10–C11 in **15·(THF)$_2$** are 1.443, 1.348 and 1.468 Å, respectively. In the case of **1**, the lengths of the corresponding bonds are 1.407, 1.388 and 1.401 Å, respectively. The bond distance between C9–C10 in **15·(THF)$_2$** is significantly shorter than the other two bonds in this molecule, whereas the distances for the three bonds in **1** are almost similar. This tendency reflects that the ethylene bridge in **15** has a rather olefinic character, as suggested in the ^{1}H NMR spectroscopy. The oxygen atoms of two THF molecules are close to the NH protons with the distance of 2.968 Å of average, suggesting the formation of hydrogen bondings between the oxygen atoms in THF and the pyrrole-NHs in the crystal state. The hydrogen bondings are also suggested by the down-field shift of the pyrrole-NH proton in the ^{1}H NMR spectrum of **15** containing THF.

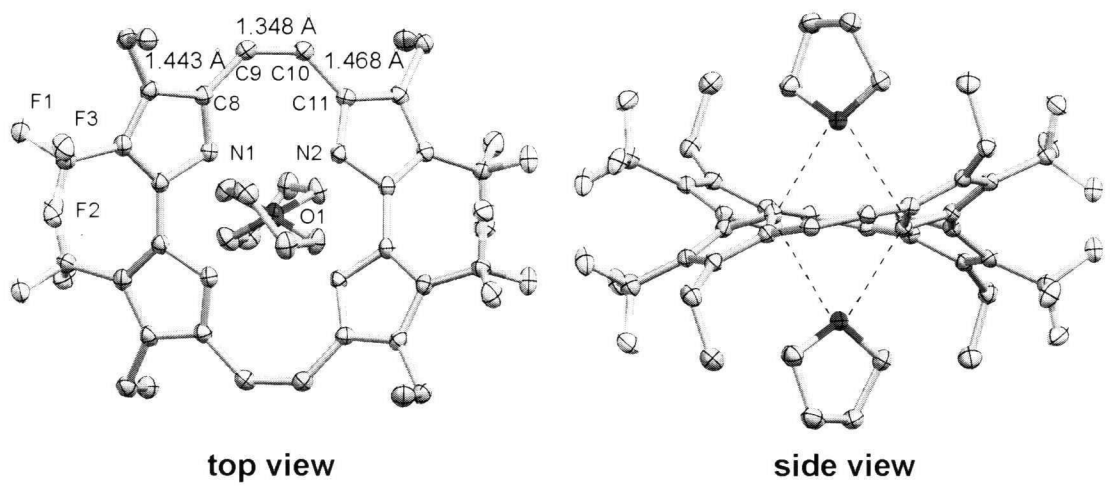

Figure 2-5. ORTEP diagram of **15** with 50% thermal probability elipsoilds. Hydrogen atoms are omitted for clarity. The dotted lines in the top figure represent the hydrogen bondings.

Table 2-1. Crystallographic Data for **15**·$(THF)_2$.

Empirical formula	$C_{40}H_{44}F_{12}N_4O_2$
Formula weight	840.79
Temperature, K	113(1)
Crystal color	yellow prism
Crystal size, mm^3	0.56 × 0.40 × 0.36
Crystal system	orthorhombic
Space group	*Pbcn*
a, Å	13.1247(4)
b, Å	17.5400(4)
c, Å	16.2721(4)
α, deg	90
β, deg	90
γ, deg	90
V, $Å^3$	3746.0(3)
Z	4
D_{calcd}, g cm^{-1}	1.491
F(000)	1744
μ(Mo, Kα), mm^{-1}	0.133
Theta range for data collection	3.05 to 27.45
Reflections collected	41740
Independent reflections	4267
Parameters	350
Goodness-of-fit on F^2	1.288
$R1^{a)}$, $wR2^{b)}$ [$I > 2\sigma(I)$]	0.041, 0.132
Largest diff. peak and hole	0.29 and −0.25

a) $R1 = \Sigma||F_o|-|F_c||/\Sigma|F_o|$. b) $wR2 = [\Sigma w(F_o^2-F_c^2)^2/\Sigma w(F_o^2)^2]^{1/2}$.

2-3-4. Hydrogenation of 15

The olefinic character of the ethylene bridge in **15** was revealed by the hydrogenation in the presence Pd/C at room temperature (Scheme 2-3). The reaction smoothly afforded the hydrogenated compound **18** as determined by NMR (Figure 2-6) and UV–vis spectra (Figure 2-7) and FAB mass. The 18π-conjugated porphycene **1** also gave the same product. Probably, **15** is transiently formed during the reaction. In contrast, the non-trifluoromethylated porphycene **2** showed the complicated reaction behavior to afford many unidentified products. The trifluoromethylated porphyrin **12** has poor reactivities under the same conditions due to its low solubility.

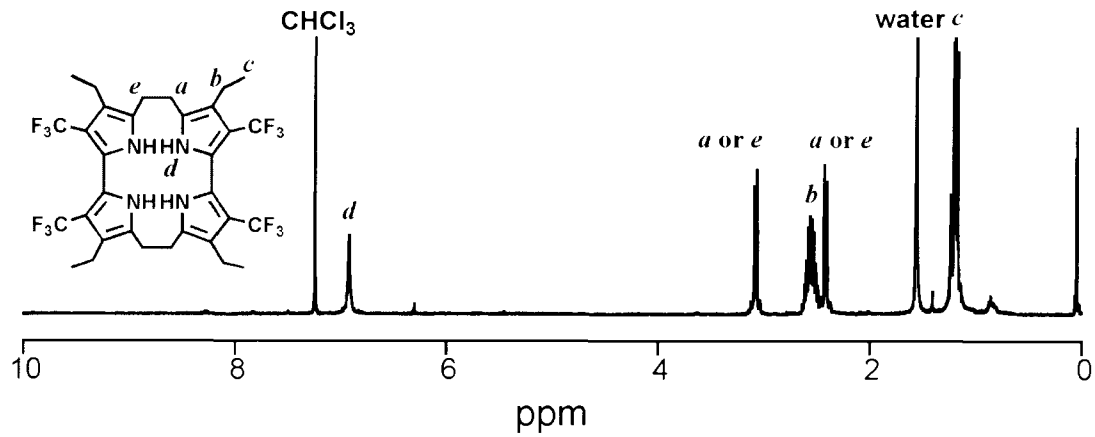

Figure 2-6. ^{1}H NMR spectra of **18** produced by hydrogenation of **15.**

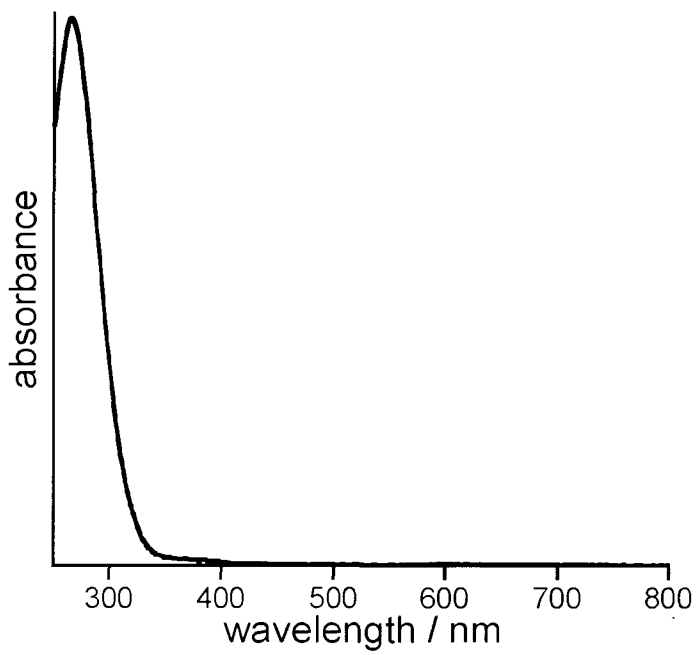

Figure 2-7. UV–vis spectra of **18** produced by hydrogenation of **15.**

2-4. Summary

$H_2Pc(EtioCF_3)$ (**1**) was easily converted to 20π-conjugated porphycene. The 20π-product was successfully characterized. All the reactions described here were carried out in homogenous reaction media, whereas the previous preparations of the 20π-conjugated porphyrins have been attained by metal reduction in a heterogeneous system. The 20π-conjugated porphycene was remarkably stable and the ethylene bridge has olefinic character.

Reference

1. In *The Porphyrin Handbook*; Kadish, K. M., Smith, K. M., Guilard, R., Eds.; Academic Press: San Diego, 2000; Vol. 1.
2. (a) Sessler, J. L.; Seidel, D. *Angew. Chem., Int. Ed. Engl.* **2003**, *42*, 5134-5175, and references therein. (b) In *The Porphyrin Handbook*; Kadish, K. M., Smith, K. M., Guilard, R., Eds.; Academic Press: San Diego, 2000; Vol. 2.
3. The selected papers for 4n π-conjugated porphyrins are listed in: Liu, C.; Shen, D.-M.; Chen, Q.-Y. *J. Am. Chem. Soc.* **2007**, *129*, 5814–5815, and references therein.
4. Woodward, R. B. *Angew. Chem.* **1960**, *72*, 651–652.
5. Pohl, M.; Schmickler, H.; Lex, J. *Angew. Chem., Int. Ed. Engl.* **1991**, *30*, 1693–1697.
6. Vogel, E.; Köcher, M.; Schmickler, H.; Lex, J. *Angew. Chem., Int. Ed. Engl.* **1986**, *25*, 257–259.
7. (a) Hayashi, T.; Nakashima, Y.; Ito, K.; Ikegami, T.; Aritome, I.; Suzuki, A.; Hisaeda, Y. *Org. Lett.* **2003**, *5*, 2845–2848. (b) Hayashi, T.; Nakashima, Y.; Ito, K.; Ikegami, T.; Aritome, I.; Aoyagi, K.; Ando, T.; Hisaeda, Y. *Inorg. Chem.* **2003**, *42*, 7345–7347.
8. Vogel, E.; Grigat, I.; Köcher, M.; Lex, J. *Angew. Chem., Int. Ed. Engl.* **1989**, *28*, 1655–1657.
9. Nonell, S.; Borrell, J. I.; Borrós, S.; Colominas, C.; Rey, O.; Rubio, N.; Sánchez-García, D.; Teixidó, J. *Eur. J. Org. Chem.* **2003**, 1635–1640.
10. SIR92: Altomare, A.; Burla, M. C.; Camalli, M., Cascarono, M., Giacovazzo, C., Guagliardi, A., Polidori, G.; *J. Appl. Cryst.* **1994**, *27*, 435.
11. DIRDIF94: Beurskens, P. T., Admiraal, G., Beurskens, G., Bosman, W. P., de Gelder, R., Israel, R.; Smits, J. M. M., **1994**. The DIRDIF-94 program system, Technical Report of the Crystallography Laboratory, University of Nijmegen, The Netherlands.
12. teXsan: Crystal Structure Analysis Package, Molecular Structure Corporation, **1985** and **1999**.
13. McMurry, J. In *Organic Chemistry*, 3rd ed.; Wadsworth: Belmont, CA, 1992; Chapter 13, pp 442–487.

Chapter 3.
Synthesis, Structure, and Autoreduction of Trifluoromethylated Iron Porphycene

3-1. Preface

Metalloporphycene [1,2], a structural isomer of metalloporphyrin, has attracted considerable interest not only as a powerful probe to understand the physicochemical properties of a series of pyrrolic macrocycles [3] but also as a useful reactant such as a catalyst [4,5]. One of the important characteristics of the porphycene system is that the LUMO energy level of the ring is clearly stabilized due to the decrease in the symmetry of the macrocycle [6,7]. Therefore, it is expected that a porphycene with strong electron-withdrawing substituents will show a unique nature compared with porphyrins. However, the variety of peripheral groups substituted on the porphycene framework is limited and almost all known porphycenes have only peripheral alkyl substituents on the framework [3]. To further explore the striking features of metalloporphycenes, the author is investigating the synthesis of a new type of porphycene and its metal complex [8].

In this chapter, trifluoromethylated iron porphycenes, μ-oxo-bis{2,7,12,17-tetraethyl-3,6,13,16-tetramethylporphycenatoiron(III)}, [{$Fe^{III}Pc(EtioCF_3)$}$_2$(μ-O)] (**17**), and Chloro-2,7,12,17-tetraethyl-3,6,13,16-tetra(trifluoromethyl)porphycenatoiron(III), [$Fe^{III}ClPc(EtioCF_3)$] (**18-Cl**), were synthesized as described in Scheme 3-1 and their properties were investigated by ^{1}H NMR and UV–vis spectra, X-ray structure and electrochemical analysis. In addition, it was found that the μ-oxo dimer (**17**) was easily converted into the monomeric iron(II) complex via the Fe–O bond cleavage in pyridine. To discuss the mechanisms of the unusual fast Fe–O bond cleavage and the following autoreduction of **17**, iron porphycenes without any electron-withdrawing groups, [{$Fe^{III}Pc(EtioCH_3)$}$_2$(μ-O)] (**19**) and [$Fe^{III}ClPc(EtioCH_3)$] (**20-Cl**), and the corresponding iron porphyrins, [$Fe^{III}ClPor(EtioCF_3)$] (**21-Cl**) and [{$Fe^{III}Por(EtioCF_3)$}$_2$(μ-O)] (**22**) were prepared and their physicochemical properties were explored (Chart 3-1) [9,10]. Furthermore, the author describes the first example of the crystal structure of the 6-coordinated iron(II) porphycene complex.

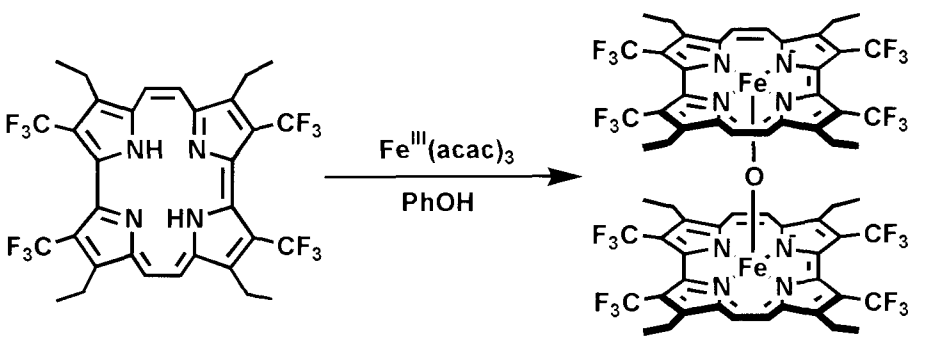

1

[{Fe^{III}Pc(EtioCF$_3$)}$_2$(μ-O)] (**17**)

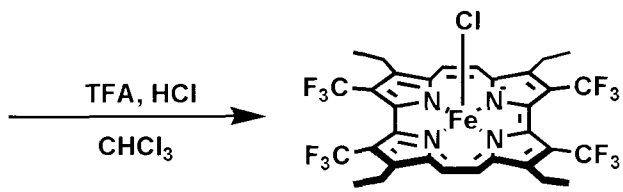

[Fe^{III}ClPc(EtioCF$_3$)] (**18-Cl**)

Scheme 3-1.

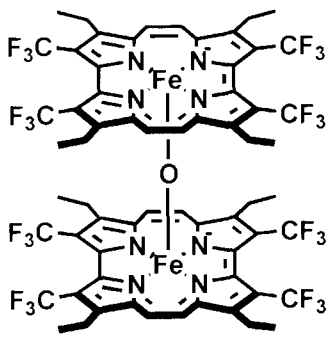

[{$Fe^{III}Pc(EtioCF_3)$}$_2$(μ-O)] (**17**)

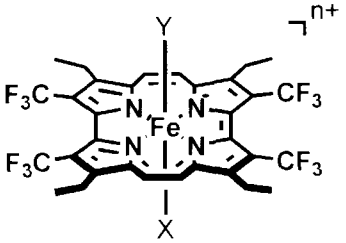

X = Cl, Y = (none), n = 0:
[$Fe^{III}ClPc(EtioCF_3)$] (**18-Cl**)
X = Y = Py, n = 1:
[$Fe^{III}Pc(EtioCF_3)(Py)_2]^+$ (**18-Py$_2$**)
X = Y = Py, n = 0:
[$Fe^{II}Pc(EtioCF_3)(Py)_2$] (**23-Py$_2$**)

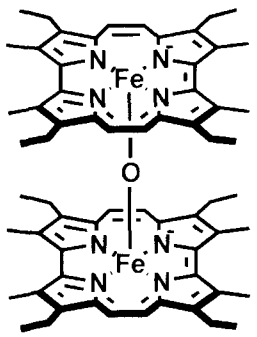

[{$Fe^{III}Pc(EtioCH_3)$}$_2$(μ-O)] (**19**)

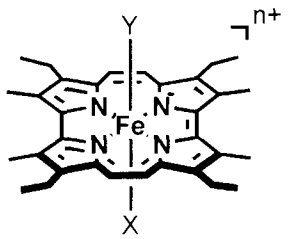

X = Cl, Y = (none), n = 0:
[$Fe^{III}ClPc(EtioCH_3)$] (**20-Cl**)
X = Y = Py, n = 1:
[$Fe^{III}Pc(EtioCH_3)(Py)_2]^+$ (**20-Py$_2$**)

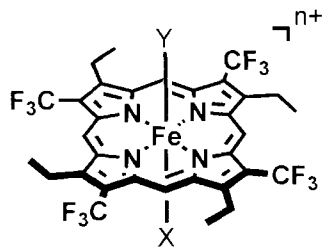

X = Cl, Y = (none), n = 0:
[$Fe^{III}ClPor(EtioCF_3)$] (**21-Cl**)
X = Y = Py, n = 1:
[$Fe^{III}Por(EtioCF_3)(Py)_2]^+$ (**21-Py$_2$**)

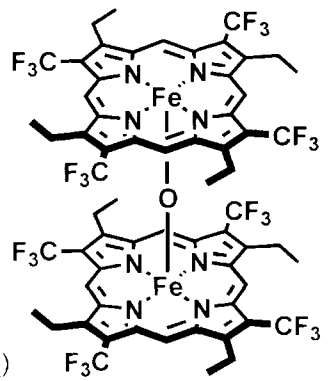

[{$Fe^{III}Por(EtioCF_3)$}$_2$(μ-O)] (**22**)

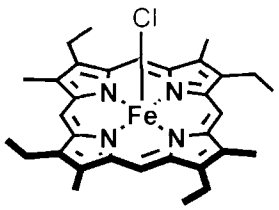

[$Fe^{III}ClPor(EtioCH_3)$] (**24-Cl**)

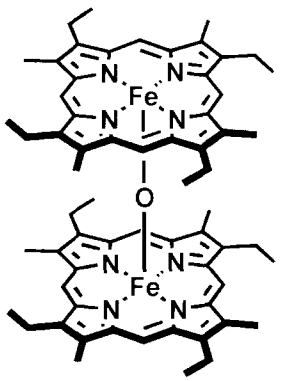

[{$Fe^{III}Por(EtioCH_3)$}$_2$(μ-O)] (**25**)

Chart 3-1.

3-2. Materials and Methods

3-2-1. Instruments

All NMR spectra were recorded on Bruker Avance 500 instruments in $CDCl_3$ solvent at 25 °C; ^1H and ^{19}F NMR chemical shifts were reported relative to residual $CHCl_3$ (7.24 ppm) and $CFCl_3$ (0 ppm), respectively. UV–vis spectra were measured on a Shimadzu U-3500 double beam spectrophotometer equipped with a thermostat cell holder. FAB positive ion mass spectra were obtained from NBA matrix on a JEOL JMS-SX10A high resolution mass spectrometer. MALDI-TOF mass spectra were performed on an Applied Biosystems Voyager Biospectrometry Workstation with a dithranol matrix. ESI-TOF and APCI-TOF mass spectra were performed on an Applied Biosystems Mariner Workstation. Electrochemical studies were performed on Bioanalytical Systems CV-50W electrochemical workstations.

3-2-2. Materials

All reagents and chemicals were obtained from commercial sources and used as received unless otherwise noted. For all the measurements, dichloromethane was distilled over calcium hydride prior to use. Pyridine was carefully distilled over potassium hydroxide prior to use. The kinetic studies were carried out in pyridine and $CHCl_3$ (1:1 v/v). The dehydrated $CHCl_3$ with amylene added was obtained from Wako Pure Chemical Industries, Ltd. Tetrabutylammonium perchlorate (TBAP) was recrystallized from ethanol and then dried under reduced pressure prior to use.

3-2-3. Syntheses

Compounds **17** and **18-Cl** were prepared as described in Scheme 3-1 [11]. The compounds **19** and **20-Cl** were prepared as described in the literature [12]. Compound **21-Cl** was prepared by a modified method [9,10].

μ-oxo-bis{2,7,12,17-tetraethyl-3,6,13,16-tetra(trifluoromethyl)porphycenatoiron(III)}, [{Fe^{III}Pc(EtioCF$_3$)}$_2$(μ-O)] (17):

To a solution of H_2Pc(EtioCF$_3$) (**1**) (6.0 mg, 8.6 μmol) in phenol (3 mL), was added acetylacetonatoiron (III) (20 mg, 57 μmol) and the mixture was stirred at 110 °C for 10 min. After cooling to room temperature, CH_2Cl_2 was added to the reaction mixture and the solution was washed with 1% NaOH (4 × 20 mL) and H_2O (20 mL). The organic layers were then dried over anhydrous $MgSO_4$ and evaporated under reduced pressure to afford the crude solid. The product was purified by silica gel chromatography to yield dark green [{Fe^{III}Pc(EtioCF$_3$)}$_2$(μ-O)] (**17**) (2.5 mg, 46%). ^1H NMR (500 MHz, $CDCl_3$): δ (ppm) = 6.99 (br, 8H), 6.51 (br, 8H), 4.63 (br, 16H), 1.43 (br, 24H). ^{19}F NMR (470 MHz, $CDCl_3$): δ (ppm) = −45.4 (s). MS (FAB) calculated for $[M]^+$ $C_{64}H_{48}N_8OF_{24}^+$, 1512.2267; found 1512.2273. UV–vis λ_{max} (ε, $M^{-1}cm^{-1}$) in CH_2Cl_2: 366 (6.2×10^4), 687 (5.4×10^4) nm.

Chloro-2,7,12,17-tetraethyl-3,6,13,16-tetra(trifluoromethyl)porphycenatoiron(III), [Fe^{III}ClPc(EtioCF_3)] (18-Cl)

To a solution of [{Fe^{III}Pc(EtioCF_3)}$_2$(μ-O)] (**17**) (2.4 mg, 1.6 μmol) in $CHCl_3$ (10 mL) was added trifluoroacetic acid (0.2 mL, 2.6 mmol). The mixture was stirred at room temperature for 30 min and poured into 0.1 M aqueous HCl (10 mL) and extracted with $CHCl_3$. The combined organic layers were dried over anhydrous $MgSO_4$ and evaporated under reduced pressure to afford crude black-green solid. Purification of the product by gel permission chromatography gave green powder, [Fe^{III}ClPc(EtioCF_3)] **(18-Cl)**, (quant.). ^{1}H NMR (500 MHz, $CDCl_3$): δ (ppm) = 39.98 (br, 4H), 31.41 (br, 4H), 6.04 (br, 12H), −21.1 (br, 4H), ^{19}F NMR (470 MHz, $CDCl_3$): δ (ppm) = 67.4 (br), MS (MALDI-TOF) calculated for [M − Cl]$^+$ $C_{32}H_{24}N_4F_{12}^+$, 748.12; found 748.98. UV–vis λ_{max} (ε, $M^{-1}cm^{-1}$) in CH_2Cl_2; 365 (4.9×10^4), 687 (2.8×10^4) nm.

Chloro-1,3,5,7-tetra(trifluoromethyl)-2,4,6,8-tetraethyl-porphyrinatoiron(III), [Fe^{III}ClPor(EtioCF_3)] (21-Cl):

To a solution of H_2Por(EtioCF_3) (**12**) (10 mg, 1.4 μmol) in acetic acid (15 mL) was dropwise added a mixture of iron(II) sulfate (80 mg, 0.53 mmol) and sodium chloride (80 mg, 1.4 mmol) in water (0.2 mL) and pyridine (0.4 mL). The mixture was stirred at 130 °C for 40 min. After cooling to room temperature, 50 mL of $CHCl_3$ was added and the solution was washed with 3 M HCl. The organic layer was separated and washed with water twice. The solvent was evaporated and the residue was purified with $CHCl_3$ on TLC to yield [Fe^{III}ClPor(EtioCF_3)] **(21-Cl)** (4.8 mg, 44%). ^{1}H NMR (500 MHz, $CDCl_3$): δ (ppm) = 33.3 (brs, 8H), 6.3 (brs, 12H), −68.5 (brs, 4H). ^{19}F NMR (470 MHz, $CDCl_3$): δ (ppm) = 8.79 (brs). MS (MALDI-TOF) calculated for [M − Cl]$^+$ 748.1; found 748.4. UV–vis λ_{max} (ε, $M^{-1}cm^{-1}$) in $CHCl_3$; 369 (2.7×10^4), 409 (7.6×10^4), 507 (7.6×10^3), 535 (5.3×10^3), 634 (1.1×10^3) nm.

μ-oxo-bis{1,3,5,7-tetra(trifluoromethyl)-2,4,6,8-tetraethyl-porphyrinatoiron (III)}, [{Fe^{III}Por(EtioCF_3)}$_2$(μ-O)] (22):

Compound **22** was obtained by treating **21-Cl** (12 mg, 15 μmol) with 1M NaOH in CH_2Cl_2 and then purified by chromatography (Silica, CH_2Cl_2) to give a brown solid, [{Fe^{III}Por(EtioCF_3)}$_2$(μ-O)] (**22**) (4.2 mg, 37 %). ^{1}H NMR (500 MHz, $CDCl_3$): δ (ppm) = 6.97 (brs, 4H), 6.03 (brs, 4H), 4.88 (brs, 4H), 1.80 and 1.74 (brs, 12H, regioisomer). ^{19}F NMR (470 MHz, $CDCl_3$): δ (ppm) = −47.3 and −47.5 (brs, regioisomer); MS (FAB) contains only a signal of the fragment ion produced by the cleavage of Fe–O bond; calculated for [M − $C_{32}H_{24}F_{12}N_4FeO$]$^+$ 748.1169; found 748.1159. UV–vis λ_{max} (ε, $M^{-1}cm^{-1}$) in $CHCl_3$; 326 (3.3×10^4), 404 (1.0×10^5), 569 (9.4×10^3) nm.

3-2-4. X-ray Crystallography

Crystal of **17** and **23-Py$_2$** suitable for X-ray crystal structure analysis was grown by slow evaporation from a $CHCl_3$/2-propanol mixture for **17** and $CDCl_3$/d_5-pyridine/H_2O mixture for **23-Py$_2$**, respectively. X-ray diffusion data were measured on a Bruker SMART APEX CCD diffractometer with graphite monochromated Mo Kα radiation (λ = 0.71073 Å). Frames collected by a combination of ω and ϕ scans with frame widths of 0.30°. Data collection and cell refinement were handled with Bruker SMART 5.629 software. Frame integration were

carried out using the SADABS program [13]. The structure was solved by direct methods and refined using all data (based on F^2) with Bruker SHELXTL 6.14 and local programs therein [14].

3-2-5. Kinetic Measurements.

All the kinetic measurements were carried out in mixed solvents of $CHCl_3$ and pyridine (1:1, v/v) at 20 °C. Autoreduction of the porphycenes and porphyrins was followed by the ^{19}F NMR and/or UV–vis spectroscopies. The rate constants of the autoreductions for **17**, **18-Cl** and **22** were determined by analyzing the peak integrations for the iron(III) species and the iron(II) species in the ^{19}F NMR spectra according to first-order kinetics law. Furthermore, the rate constants for **17** and **21-Cl** were measured by UV–vis spectroscopy, where the absorbance changes at 367 nm for **17**, and at 415 nm for **21-Cl** during the reactions, were analyzed by the single-exponential kinetics.

3-2-6. Cyclic Voltammetry

Cyclic voltammetry was carried out with a three-electrode system consist of a platinum button electrode as working, a platinum wire electrode as counter, and an Ag/AgCl electrode as reference. The reference electrode was separated from the bulk solution by a fritted-glass bridge filled with a 0.1 M KCl aqueous solution.

3-3. Results and Discussion

3-3-1. Syntheses

As shown Scheme 3-1, synthesis of [{$Fe^{III}Pc(EtioCF_3)$}$_2$(μ-O)] (**17**) was accomplished by heating 110 °C in phenol. But, the corresponding monomeric complex, [$Fe^{III}ClPc(EtioCF_3)$] (**18-Cl**), was not available because the formation of the μ-oxo dimer was preferable even under the neutral conditions. After the treatment of CF_3COOH/aqueous HCl for over 30 min at room temperature, the monomeric **18-Cl** was obtained. However, further purification of the monomeric complex was difficult, because **18-Cl** was easily converted into the μ-oxo dimer **17** again in the solution.

These iron complexes, **17** and **18-Cl**, were characterized by UV–vis, ^1H and ^{19}F NMR, and mass spectroscopies. The UV–vis spectra of **17** and **18-Cl** are shown in Figure 3-1 together with those of the corresponding reference iron porphycenes, **19** and **20-Cl**. The Q-band absorptions of **17** and **18-Cl** exhibited significant red shifts compared to those of **19** and **20-Cl** in CH_2Cl_2. For example, the characteristic Q-band of **18-Cl** is located at 687 nm, which is 69 nm red-shifted from that of **20-Cl**. These significant red shifts are similar in behavior to a series of perhaloganoporphyrin iron complexes [15], indicating that the four trifluoromethyl groups at the β-pyrrolic carbons effectively regulate the electronic properties of the iron porphycene complexes.

The ^{19}F NMR spectrum of **18-Cl** in $CDCl_3$ shows a broad peak at 67.4 ppm due to the high-spin iron center, and the resonance is shifted by more than 50 ppm downfield from that of the corresponding iron porphyrin [16,17]. In the case of **17**, the ^{19}F resonance shifted upfield at −45.4 ppm due to antiferromagnetic coupling.

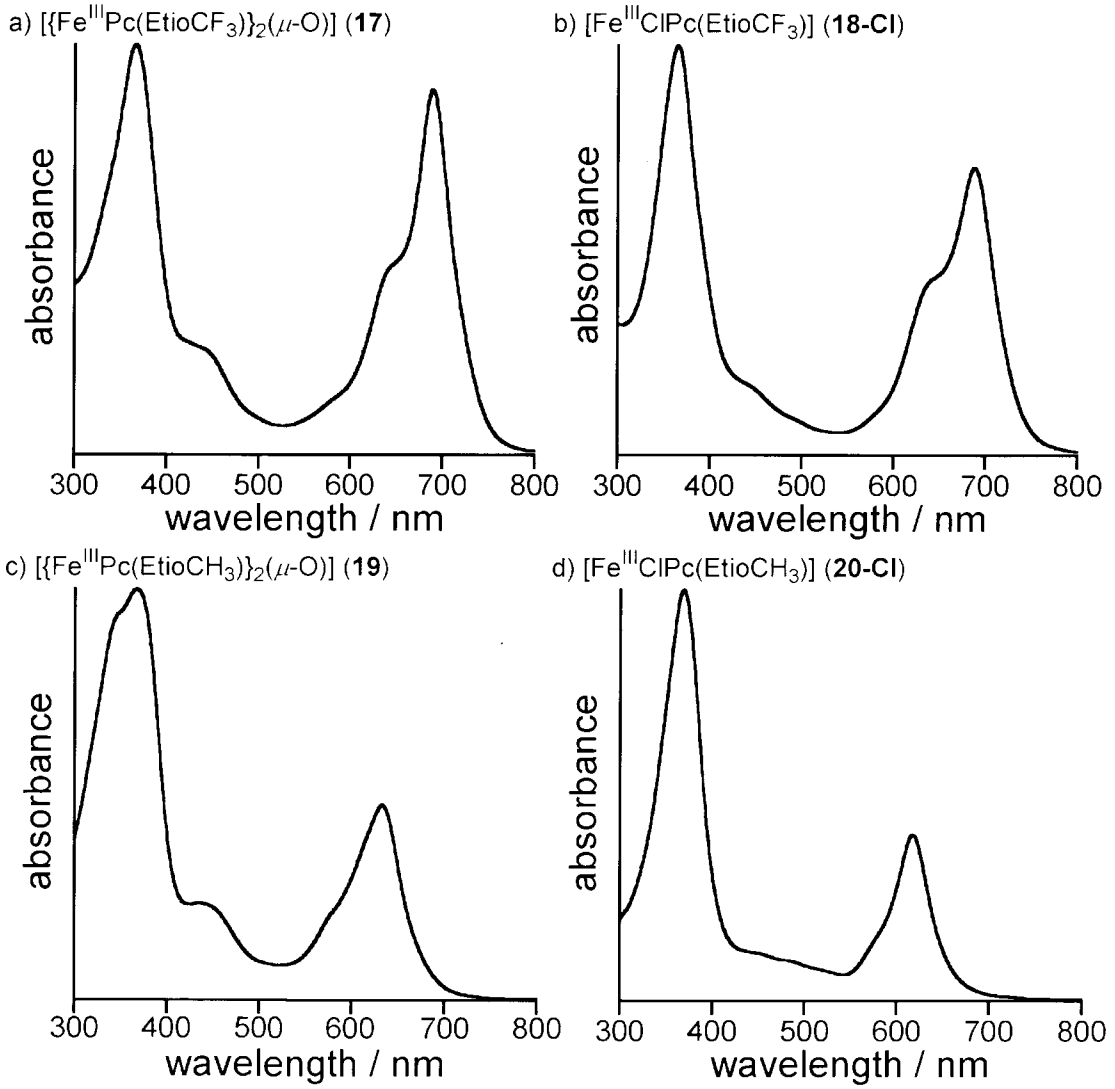

Figure 3-1. UV–vis spectra of iron porphycenes in CH_2Cl_2: a) [{Fe^{III}Pc(EtioCF$_3$)}$_2$(μ-O)] (**17**); b) [Fe^{III}ClPc(EtioCF$_3$)] (**18-Cl**); c) [{Fe^{III}Pc(EtioCH$_3$)}$_2$(μ-O)] (**19**); d) [Fe^{III}ClPc(EtioCH$_3$)] (**20-Cl**). Each absorption maximum is normalized by setting the highest absorbance (Soret band) equal to unity.

3-3-2. Crystal Structure of 17

The crystal structure of **17** had already been reported in previous studies [8]. Figure 3-2 shows the molecular structure of **17** recrystallized from $CHCl_3$ and 2-propanol and Figure 3-3 shows the molecular structure of reference compound **20-Cl**. Crystallographic data for **17** and **20-Cl** are summarized in Table 3-1. The complex exists in the crystal as a molecule with C_2 symmetry, and two iron porphycenes show the highly distorted square-pyramidal coordination with the saddle-shape configuration. The μ-oxo dimer was found to possess a completely linear Fe–O–Fe angle due to the steric bulky CF_3 substituents between the two porphycene rings. The two Fe–O bond lengths in **17** are 1.753(4) and 1.755(4) Å, and the two iron atoms are displaced by 0.630 and 0.541 Å from the least-squares plane in **17** through the four porphyrin nitrogen atoms. These values are almost comparable with those observed in the reported μ-oxo dimers of the iron porphycenes and porphyrins [18]. In contrast, the displacements of the β-pyrrolic carbon atoms from the N4 mean planes vary from −0.836 to 0.339 Å, which are significantly larger values than those observed in the reference compound of **20-Cl** (−0.451 to 0.092 Å). The average of the four pyrrole–pyrrole dihedral angles in **17** is 23.13°, which is significantly larger than that observed in a series of the μ-oxo dimers [18] or **20-Cl** with a 4.80° dihedral angle. These findings indicate that the substitution of the four electron-withdrawing CF_3 groups produces the severe saddle-shaped deformation of the aromatic framework.

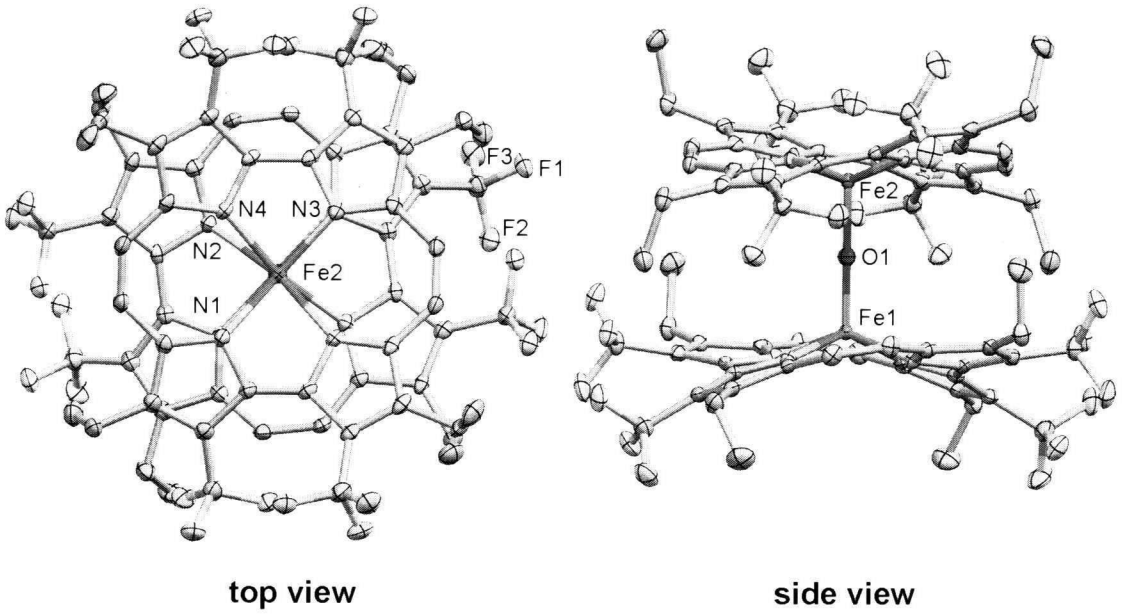

Figure 3-2. ORTEP diagram of **17** with 50% thermal probability elipsoilds. Hydrogen atoms are omitted for clarity.

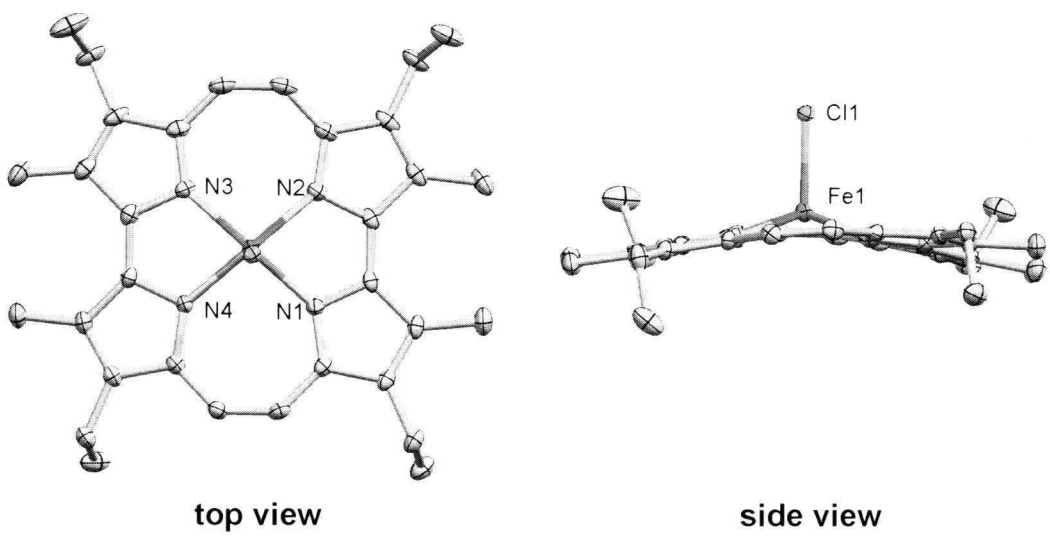

Figure 3-3. ORTEP diagram of **20-Cl** with 50% thermal probability elipsoilds. Hydrogen atoms are omitted for clarity.

Table 3-1. Crystallographic Data for **17** and **20-Cl**.

Complexes	**17**	**20-Cl**
Empirical formula	$C_{65}H_{49}Cl_3F_{24}Fe_2N_8O$	$C_{32}H_{36}ClFeN_4$
Formula weight	1632.17	567.95
Temperature, K	100(2)	100(2)
Crystal color	purple plate	purple prism
Crystal size, mm^3	0.18 × 0.14 × 0.07	0.18 × 0.10 × 0.09
Crystal system	orthorhombic	triclinic
Space group	*Aba2*	*P*−1
a, Å	14.568(1)	9.9804(6)
b, Å	21.610(2)	11.1226(6)
c, Å	21.023(2)	13.8062(8)
α, deg	90	104.441(1)
β, deg	90	109.790(1)
γ, deg	90	93.900(1)
V, $Å^3$	6618(1)	1376.8(1)
Z	4	2
D_{calcd}, g cm^{-1}	1.638	1.370
F(000)	3288	598
μ(Mo, Kα), mm^{-1}	0.678	0.674
Theta range for data collection	1.88 to 26.41	1.64 to 26.37
Reflections collected	20487	9001
Independent reflections	5619	5609
Parameters	488	351
Goodness-of-fit on F^2	1.015	1.051
$R1^{a)}$, $wR2^{b)}$ [$I > 2\sigma(I)$]	0.0372, 0.0831	0.0417, 0.1013
Largest diff. peak and hole	0.544 and −0.293	0.569 and −0.467

a) $R1 = \Sigma||F_o|-|F_c||/\Sigma|F_o|$. b) $wR2 = [\Sigma w(F_o^2-F_c^2)^2/\Sigma w(F_o^2)^2]^{1/2}$.

3-3-3. Redox Behavior

Electrochemistry of **17** clearly reveals the significant effect on the substitution of the electron-withdrawing groups on the porphycene framework as shown in Figure 3-4 [8]. First, the oxidation process of **17** was not observed by conventional analysis in CH_2Cl_2, since the oxidation could occur outside the solvent/electrolyte potential window. This result suggests that the first oxidation potential could be higher than +1.3 V (vs Ag/AgCl), although **19** undergoes four one-electron oxidations in the range 0.69–1.22 V. Second, the four reductions of **17** occurred at $E_{1/2}$ = −0.29, −0.45, −0.71, and −0.86 V, which are approximately 800 mV more positive than those observed in **19** (Table 3-2) [7,19]. These results emphasize the fact that the drastic shifts in the oxidation and reduction potentials are derived from the combination of the characteristics of the porphycene framework and the substitution of the strong electron-withdrawing CF_3 groups at the β-pyrrolic carbons.

The same tendency is also detected in the redox potentials of the monomeric iron complex, **18-Cl**. The Fe^{II}/Fe^{III} redox couple of **18-Cl** displayed in Figure 3-5 is observed at the potential of −0.02 V (vs. Ag/AgCl) in CH_2Cl_2. As shown in Table 3-3, this potential is anodically shifted by more than 250 mV from that of **20-Cl** due to the introduction of the four electron-withdrawing trifluoromethyl groups, whereas the corresponding trifluoromethylated iron porphyrin, **21-Cl**, exhibited the same potential. It is not surprising that the redox potential of **18-Cl** is comparable to that of **21-Cl** [19]. This is the same behavior for the Fe^{II}/Fe^{III} redox couple that is moderately different between **20-Cl** and [Fe^{III}ClPor(EtioCH$_3$)] (**24-Cl**). Therefore, the symmetry of the macrocycle does not have any significant influence on the redox potential. In any event, the introduction of four trifluoromethyl groups into the β-pyrrolic carbons of the porphycene ring may stabilize the iron(II) oxidation state.

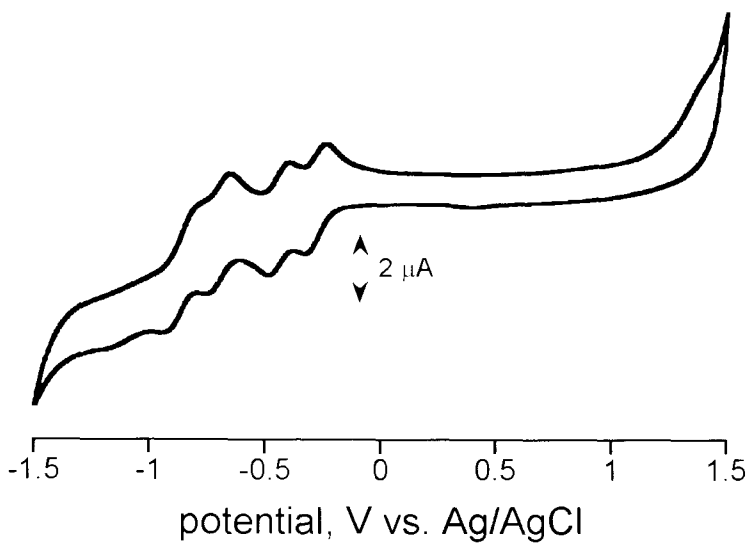

Figure 3-4. Cyclic voltammogram of **17** in CH_2Cl_2, 0.1 M TBAP. Scan rate = 0.1 V/s. Reference electrode: Ag/AgCl.

Table 3-2. Comparative Oxidation and Reduction Potentials (V vs. Ag/AgCl) for Iron μ-oxo dimers.[a)]

	Reduction				Oxidation			
Compounds	4th	3rd	2nd	1st	1st	2nd	3rd	4th
17	–0.87	–0.70	–0.44	–0.29	>1.3	——	——	——
19	——	——	–1.14	–1.10	0.69	0.94	1.18	——

a) 0.1 M TABP at 25 °C. Scan rate = 0.1 V/s.

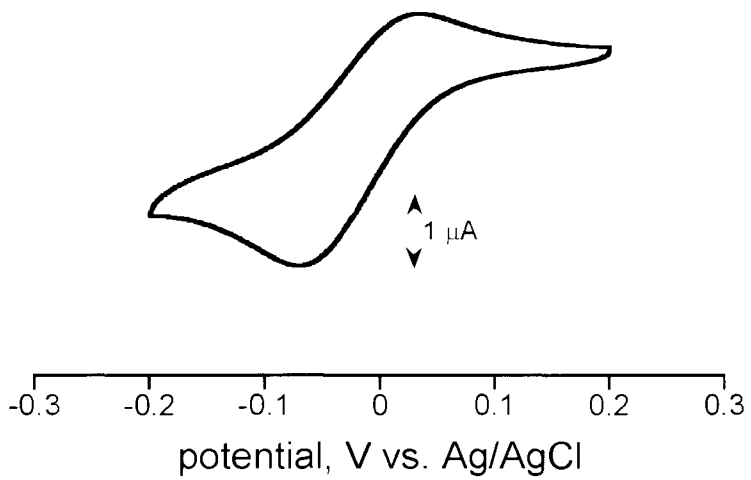

Figure 3-5. Cyclic voltammogram of **18-Cl** in CH_2Cl_2, 0.1 M TBAP. Scan rate = 0.1 V/s. Reference electrode: Ag/AgCl.

Table 3-3. Half-Wave Potantials (V vs. Ag/AgCl) for Metal Reduction and Oxidation of Iron Complexes in CH_2Cl_2.[a)]

	$E_{1/2}$ (V vs. Ag/AgCl)
Iron complexes	Fe^{II}/Fe^{III}
18-Cl	–0.02
20-Cl	$(-0.48)E_{pc}$ $(-0.09)E_{pa}$
21-Cl	0.00
24-Cl	–0.57

a) 0.1 M TABP at 25 °C. Scan rate = 0.1 V/s.

3-3-4. Autoreduction of μ-Oxo Dimer of Iron Porphycenes and Porphyrins in Pyridine

To evaluate the Lewis acidity and redox property of the porphycene iron atom, the reaction of the complexes with pyridine was monitored. The UV–vis spectrum of **17** in pyridine under anaerobic conditions produced significant changes over 40 h via clear isosbestic points. The UV–vis spectroscopic studies demonstrated the conversion from the iron(III) **17** to the iron(II) form without any intermediate, such as the monomeric iron(III) complex. Furthermore, the author has monitored the autoreduction of **17** by ^{19}F NMR spectroscopy, showing that the signal of **17** at –44.7 ppm assigned to the C^{19}F$_3$ groups disappeared after 1 day along with the increasing intensity at –53.2 ppm due to the iron(II) species. In contrast, no monomeric [Fe^{III}Pc(EtioCF$_3$)(Py)$_2$]$^+$ (**18-Py$_2$**) was detected during the conversion of **17** to the iron(II) species. The autoreduction product, the iron(II) complex, was also characterized by UV–vis and ^{1}H NMR spectroscopies and an X-ray structural analysis (see 3-3-6). Based on these findings, the author proposes the mechanism of the autoreduction in Scheme 3-2. It was concluded that the autoreduction of **17** smoothly proceeded after the Fe–O bond cleavage of the μ-oxo dimer.

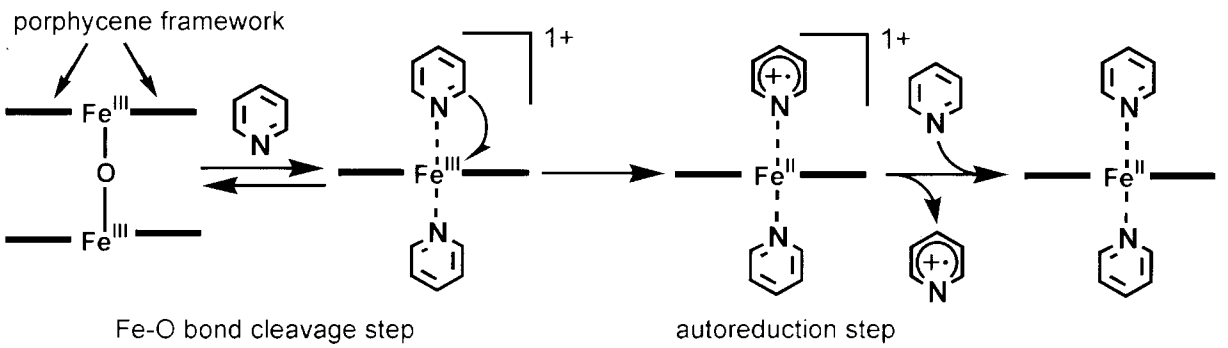

Scheme 3-2.

3-3-5. Crystal Structure of the Reaction Product.

Figure 3-6 presents the molecular structure of the autoreduction product recrystallized from chloroform including pyridine (1:1, v/v). Crystallographic data for **26** are summarized in Table 3-4. The iron porphycene in the monoclinic system with the space group *C2/m* has both a crystallographically required 2-fold axis and a mirror plane of symmetry, with the iron atom at a symmetry center. Two pyridine molecules coordinated to the iron atom were found in the complex with an eclipsed conformation. The porphycene framework is slightly distorted, whereas the iron atom is located inside the plane; the displacements of the C_{β} carbon atoms from the least-squares plane defined by the four central nitrogen atoms are determined to be ±0.224 Å and ±0.313Å, and those of C_{α} and $C_{ethylene}$ are ±0.085 Å and ±0.045 Å, respectively.

Table 3-5 displays an informative comparison with the series of low-spin bispyridine iron(II) complexes. The magnitudes of the perpendicular displacements of these carbon atoms from the plane of the four pyrrolyl nitrogen atoms for $[Fe^{II}Pc(EtioCF_3)(Py)_2]$ (**23-Py$_2$**) are clearly smaller than those of the iron porphyrin bispyridine complexes with electron-withdrawing substitutes [17,20]. However, as seen in Table 3-5, the Fe–$N_{pyridyl}$ (2.007 Å) and Fe–$N_{pyrrolyl}$ (1.958 Å) bonds in **23-Py$_2$** reveal remarkably short distances among the bis-pyridine coordinated iron(II) porphyrins [20–22]. Particularly, the short Fe–$N_{pyridyl}$ bond lengths in **23-Py$_2$** suggest that the electron deficient iron atom in the porphycene ring having the four strong electron-withdrawing CF_3 groups tightly interacts with the pyridine molecule with a strong Lewis basicity. Moreover, the relative orientation of the two axial pyridine planes of **23-Py$_2$** is quite different from those of the other low spin iron(II) complexes having electron-withdrawing groups [17,20], whereas it is known that the bispyridine iron(II) complex of the tetraphenylporphyrin $[Fe^{II}Por(C_6H_5)_4(Py)_2]$ without any electron-withdrawing groups exhibit a similar eclipsed configuration of two pyridine planes as **23-Py$_2$** [21]. It is likely that the four trifluoromethyl substituents in **23-Py$_2$** produce no serious strain on the porphycene framework, and the two axial ligands are consequently eclipsed in the complex, which features a relatively planar porphyrin macrocycle [21].

In addition, surprisingly, the crystal of the bispyridine–iron(II) porphycene complex was not oxidized even under aerobic conditions for over a month, suggesting that the bispyridine complex of the iron(II) porphycene is extremely stable.

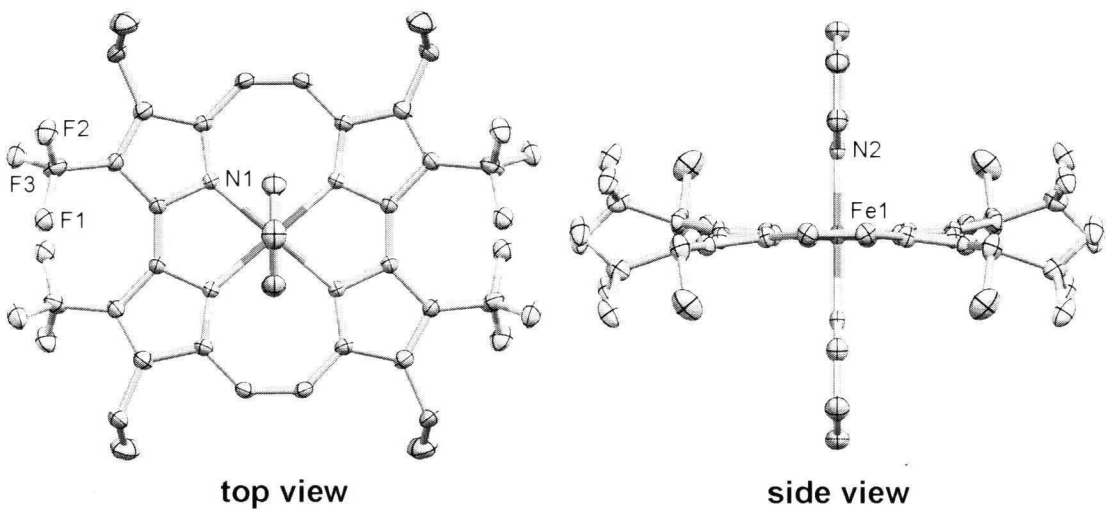

Figure 3-6. ORTEP diagram of **23-Py$_2$** with 50% thermal probability elipsoilds. Hydrogen atoms are omitted for clarity.

Table 3-4. Crystallographic Data for **23-Py$_2$**.

Empirical formula	$C_{42}H_{34}F_{12}FeN_6$
Formula weight	906.60
Temperature, K	100(2)
Crystal color	purple needle
Crystal size, mm^3	0.20 × 0.05 × 0.03
Crystal system	monoclinic
Space group	*C*2/*m*
a, Å	14.101(2)
b, Å	14.804 (2)
c, Å	10.070(1)
α, deg	90
β, deg	114.858(2)
γ, deg	90
V, Å^3	1907.4(4)
Z	2
D_{calcd}, g cm^{-1}	1.579
F(000)	924
μ(Mo, Kα), mm^{-1}	0.496
Theta range for data collection	2.10 to 26.37
Reflections collected	6177
Independent reflections	2028
Parameters	150
Goodness-of-fit on F^2	1.039
$R1^{a)}$, $wR2^{b)}$ [$I > 2\sigma(I)$]	0.0459, 0.1056
Largest diff. peak and hole	0.509 and −0.238

a) $R1 = \Sigma||F_0|-|F_c||/\Sigma|F_0|$. b) $wR2 = [\Sigma w(F_0^2-F_c^2)^2/\Sigma w(F_0^2)^2]^{1/2}$.

Table 3-5. Selected Bond Distances and Angles for Bispyridine Coordinated Iron(II) Complexes.

Iron complexes	$Fe\text{-}N_{pyridine}$ distance (Å)	$Fe\text{-}N_{pyrrole}$ distance (Å)	$bis(Py)_2$ relative orientation (°)[d]
23-Py_2	2.007	1.958	0.0
$[Fe^{II}Por(C_3F_7)_4(Py)_2]$[a]	2.002	1.958	87.5
$[Fe^{II}Por\{Br_8(C_6F_5)_4\}(Py)_2]$[b]	2.012	1.963	68.3
$[Fe^{II}Por(C_6H_5)_4(Py)_2]$[c]	2.037	2.001	4.8

Iron complexes	$C_{(methylene\ or\ meso)}$ deviation (Å)[e]	C_β deviation (Å)[f]	reference
23-Py_2	0.07	0.27	this work
$[Fe^{II}Por(C_3F_7)_4(Py)_2]$	0.62	0.24	ref. 17
$[Fe^{II}Por\{Br_8(C_6F_5)_4\}(Py)_2]$	0.11	0.97	ref. 20
$[Fe^{II}Por(C_6H_5)_4(Py)_2]$	0.10	0.25	ref. 21

a) $[Fe^{II}Por(C_3F_7)_4(Py)_2]$ = bispyridine-5,10,15,20-tetrakis(heptafluoropropyl)porphyrinatoiron(II). b) $[Fe^{II}Por\{Br_8(C_6F_5)_4\}(Py)_2]$ = bispyridine-2,3,7,8,12,13,17,18-octabromo-5,10,15,20-tetrakis(pentafluorophenyl)-porphyrinatoiron(II). c) $[Fe^{II}Por(C_6H_5)_4(Py)_2]$ = bispyridine-5,10,15,20-tetraphenylporphyrinatoiron(II). d) Defined as the torsional angle between two planar pyridines. e) Defined as the average value of methylene or *meso*-carbon atom deviation from the N4 mean plane. f) Defined as the average value of β-carbon atom deviation from the N4 mean plane.

3-3-6. Kinetic Study of the Autoreduction from Iron(III) μ-Oxo Dimer Complexes.

To evaluate the influence of the CF_3 substituents and framework structure on the autoreduction from the iron(III) μ-oxo dimers via the Fe–O bond cleavage, the author compared the reactivities of **17** in pyridine with the reference iron porphycene and porphyrins. Scheme 3-3 summarizes the rates of the sequential two-step reactions of the iron porphycene and porphyrin compounds. The rate constants depicted in Scheme 3-3 were determined by the ^1H or ^{19}F NMR and/or UV–vis spectroscopic analyses shown in Figure 3-7. First of all, it is clear that the Fe–O bond cleavages of the μ-oxo dimers of the iron porphycenes occurred at the initial stage of the reactions are faster than those of the iron porphyrins, regardless of whether or not there are electron-withdrawing groups at the peripheral positions of the porphycene framework. It is known that the equilibrium between the two iron species is shifted to the μ-oxo dimer in the iron porphyrin chemistry. Therefore, the unusual equilibrium shifted to the monomeric species, i.e., from **17** and **19** to **18-Py$_2$** and $[Fe^{III}Pc(EtioCH_3)(Py)_2]^+$ (**20-Py$_2$**) respectively, in pyridine supports the facts that the pyridine-ligated monomeric iron porphycenes are thermodynamically more stable than the corresponding μ-oxo dimers. As shown in Table 3-6, this finding can be explained by the increase in the Lewis acidity of the central iron atom in the porphycene frameworks [23]; the strong binding of pyridine promotes the Fe–O bond cleavage. In addition, it is known that the Fe–O bond cleavage of the μ-oxo dimer in pyridine is also observed for the iron dioxoporphodimethene complex [24].

Second, the autoreduction reactivities between **17** and **19** are quite different. As described above, the Fe–O bond cleavage and the following autoreduction of **17** smoothly proceeded with the overall rate constant of 4.3×10^{-2} h^{-1} in $CHCl_3$/pyridine (1:1, v/v) at 20 °C, whereas the reaction of **19** stopped at the formation of the monomeric iron(III) porphycene, and the diamagnetic iron(II) complex was not detected in $CDCl_3/d_5$-pyridine (1:1, v/v) by ^1H NMR spectroscopy. The monomeric iron porphycene with CF_3 groups, **18-Cl**, was also converted into the iron(II) complex with the rate constant of $\sim 2 \times 10^{-1}$ h^{-1} [25], while **20-Cl** as the starting material was not reduced in $CHCl_3$/pyridine (1:1, v/v). On the other hand, both **21-Cl** and **22** allowed the autoreduction upon dissolution in $CHCl_3$/pyridine (1:1, v/v) at room temperature. The reaction from the monomeric species, **5-Cl**, is much slower by 2-fold than that observed for **18-Cl**, and the overall reaction from the corresponding μ-oxo dimer, **22**, took over one month: Labinger, Gray et al. prepared iron(II) porphyrin with multiple electron-withdrawing groups upon dissolution in pyridine for 1 h, although they did not comment on the details [20]. Moreover, neither **24-Cl** nor its μ-oxo dimmer (**25**) showed any reactions in $CHCl_3$/pyridine (1:1, v/v). These findings suggest that the autoreduction of the tetrapyrrole iron complexes mainly depend on the Fe^{II}/Fe^{III} redox potential in spite of the structure of the macrocyclic ligands, i.e., more positive the redox potential, more readily the autoreduction proceeds.

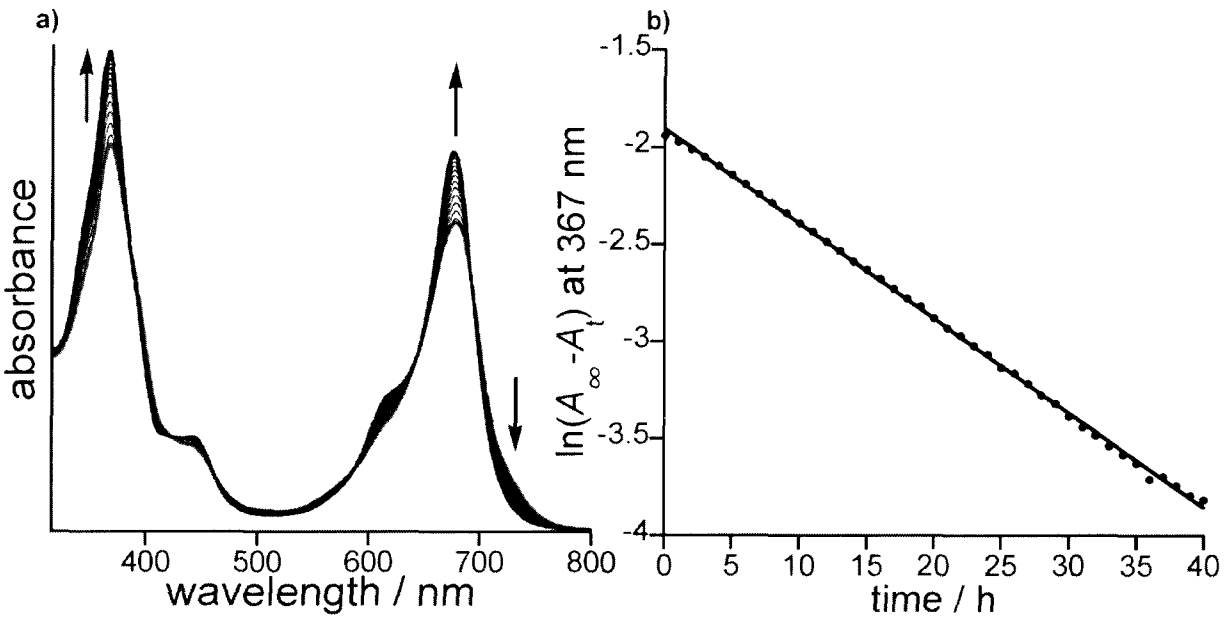

Figure 3-7. a) UV–vis spectral changes in the autoreduction from **17** (red line) to **23-Py$_2$** (blue line) in $CHCl_3$/pyridine (1:1, v/v) at 20 °C for 45 h; b) A plot of $\ln(A_\infty - A_t)$ at 367 nm vs. time, where A_∞ and A_t stand for the absorbances at the completion of the reaction and at certain time, respectively.

Table 3-6. Pyridine Association Constants for the Monomeric Iron Complexes.[a)]

Iron complexes	K_1 (M^{-1})
18-Cl	23
20-Cl	76
21-Cl	1.4
24-Cl	0.41

a) The association constants were determined by UV–vis titrimetirc measurements in CH_2Cl_2 at 25 °C.

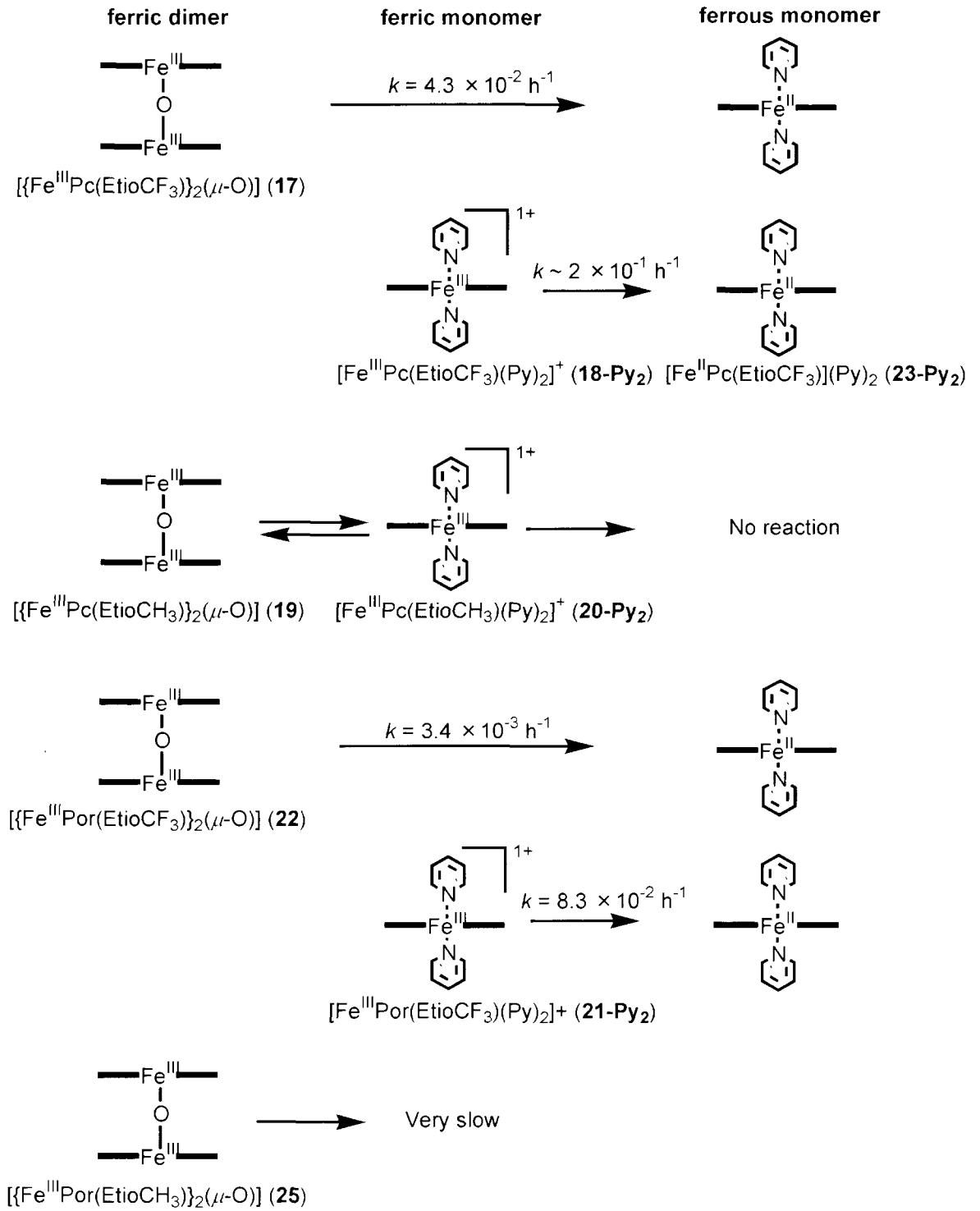
ferric dimer
ferric monomer
ferrous monomer
k = 4.3 × 10-2 h-1
[{FeIIIPc(EtioCF3)}2(μ-O)] (17)
k ~ 2 × 10-1 h-1
[FeIIIPc(EtioCF3)(Py)2]+ (18-Py2)
[FeIIPc(EtioCF3)](Py)2 (23-Py2)
No reaction
[{FeIIIPc(EtioCH3)}2(μ-O)] (19)
[FeIIIPc(EtioCH3)(Py)2]+ (20-Py2)
k = 3.4 × 10-3 h-1
[{FeIIIPor(EtioCF3)}2(μ-O)] (22)
k = 8.3 × 10-2 h-1
[FeIIIPor(EtioCF3)(Py)2]+ (21-Py2)
Very slow
[{FeIIIPor(EtioCH3)}2(μ-O)] (25)

Scheme 3-3.

3-4. Summary

The author has demonstrated the first example of fluorine-containing iron porphycene which demonstrates unusual structure, redox potentials. Furthermore, the author successfully obtained the clearly stable iron(II) porphycene complex linked by four strong electron-withdrawing groups, CF_3 substituents, upon dissolution of the corresponding iron(III) μ-oxo dimer in pyridine. The Fe–O bond cleavage and the following autoreduction was also reported by iron dioxoporphodimethene complex for over one week at room temperature [23], whereas the present μ-oxo dimer of the iron porphycene is more readily cleaved and reduced in pyridine after one day at room temperature [26]. Moreover, to the best of my knowledge, the crystal structure of $[Fe^{II}Pc(EtioCF_3)(Py)_2]$ (**23-Py$_2$**) is the first example of a 6-coordinate low spin iron(II) porphycene complex, although there is only one report describing the 4-coordinated iron(II)porphycene without any axial ligands [27]. The Fe–$N_{pyridyl}$ and Fe–$N_{pyrrolyl}$ bond lengths of **23-Py$_2$** are remarkably shortened as seen in the special iron porphyrin with C_3F_7 groups at each *meso*-position [17], whereas the structure of the macrocycle and the two axial ligand configurations are relatively similar to those of $[Fe^{II}Por(C_6H_5)_4(Py)_2]$. It is concluded that the attractive physicochemical property of the present iron porphycene with four CF_3 groups is due to the strong Lewis acidity of iron atom and highly positive Fe^{II}/Fe^{III} redox potential.

Reference

1. Vogel, E. *Pure Appl. Chem.* **1990**, *62*, 557–564.
2. Gisselbrecht, J. P.; Gross, M.; Köcher, M.; Laumsmann, M.; Vogel, M. *Angew. Chem., Int. Ed. Engl.* **1990**, *112*, 8618–8620.
3. Sessler, J. L.; Gebauer, A.; Vogel, E. In *The Porphyrin Handbook*; Kadish, K. M., Smith, K. M., Guilard, R., Eds.; Academic Press: San Diego, 2000; Vol. 2, Chapter 8 and references therein.
4. (a) Hayashi, T.; Okazaki, K.; Urakawa, N.; Shimakoshi, H.; Sessler, J. L.; Vogel, E.; Hisaeda, Y. *Organometallics* **2001**, *20*, 3074–3078. (b) Hayashi, T.; Dejima, H.; Matsuo, T.; Sato, H.; Murata, D.; Hisaeda, Y. *J. Am. Chem. Soc.* **2002**, *124*, 11226–11227.
5. Rachlewicz, K.; Latos-Grażyński, L.; Vogel, E. *Inorg. Chem.* **2000**, *39*, 3247–3251.
6. Renner, M. W.; Forman, A.; Wu, W.; Chang, C. K.; Fajer, J. *J. Am. Chem. Soc.* **1989**, *111*, 8618–8621.
7. Bernard, C.; Gisselbrecht, J. P.; Gross, M.; Vogel, E.; Lausmann, M. *Inorg. Chem.* **1994**, *33*, 2393–2401.
8. Hayashi, T.; Nakashima, Y.; Ito, K.; Ikegami, T.; Aritome, I.; Suzuki, A.; Hisaeda, Y. *Org. Lett.* **2003**, *5*, 2845–2848.
9. Ono, N.; Kawamura, H.; Maruyama, K. *Bull. Chem. Soc. Jpn.* **1989**, *62*, 3386–3388.
10. Yoshimura, T.; Toi, H.; Inaba, S.; Ogishi, H. *Inorg. Chem.* **1991**, *30*, 4315–4321.
11. Hayashi, T.; Nakashima, Y.; Ito, K.; Ikegami, T.; Aritome, I.; Aoyagi, K.; Ando, T.; Hisaeda, Y. *Inorg. Chem.* **2003**, *42*, 7345–7347.
12. Sessler, J. L.; Gebauer, A.; Vogel, E. In *The Porphyrin Handbook*; Kadish, K. M., Smith, K. M., Guilard, R., Eds.; Academic Press: San Diego, 2000; Vol. 2, pp. 3–14.
13. Sheldrick, G. *SADABS Software*; University of Gottingen: **1996**.
14. *SHELXS-97 and SHELXL-97 Software Packages*, Bruker AXS, Inc., Madison, WI, 5371–5373, USA, **1997**.
15. Senge, M. O. In *The Porphyrin Handbook*; Kadish, K. M., Smith, K. M. Guilard, R., Eds.; Academic Press: San Diego, 2000; Vol. 1, pp. 333.
16. Toi, H.; Homma, M.; Suzuki, A.; Ogoshi, H. *J. Chem. Soc., Chem. Commun.* **1985**, 1971–1972.
17. Moore, K. T.; Fletcher, J. T.; Therien, M. J. *J. Am. Chem. Soc.* **1999**, *121*, 5196–5209.
18. Lausmann, M.; Zimmer, I.; Lex, J.; Lueken, H.; Wieghardt, K.; Vogel, E. *Angew. Chem., Int. Ed. Engl.* **1994**, *33*, 736–739.
19. D'Souza, F.; Boulas, P.; Aukauloo, A. M.; Guilard, R.; Kisters, M.; Vogel, E.; Kadish, K. M. *J. Phys. Chem.* **1994**, *98*, 11885–11891.
20. Grinstaff, M. W.; Hill, M. G.; Birnbaum, E. R.; Schaefer, W. P.; Labinger, J. A.; Gray, H. B. *Inorg. Chem.* **1995**, *34*, 4896–4902.
21. Li, N.; Coppens, P.; Landrum, J. *Inorg. Chem.* **1988**, *27*, 482–488.
22. Although the refinement of the crystal structure of $[Fe^{II}Por(EtioCF_3)(Py)_2]$ has never been completed, the $Fe-N_{pyridyl}$ and $Fe-N_{pyrrole}$ bond distances were preliminary determined as 2.02 Å and 2.00 Å, respectively.
23. Bernard, C.; Le Mest, Y.; Gisselbrecht, J. P. *Inorg. Chem.* **1998**, *37*, 181–190.
24. Balch, A. L.; Noll, B. C.; Olmstead, M. M.; Phillips, S. L. *Inorg. Chem.* **1996**, *35*, 6495–6506.
25. It was confirmed that the reaction was completed after 28 h.
26. Labinger, Gray and their co-workers prepared iron(II) porphyrin with multiple electron-withdrawing groups

upon dissolution in pyridine for 1 h, although they did not comment on the details. See ref. 20.

27. Rachlewicz, K.; Latos-Grażyński, L.; Vogel, E.; Ciunik, Z.; Jerzykiewicz, L. B. *Inorg. Chem.* **2002**, *41*, 1979–1988.

Chapter 4.
Ligand Binding Behavior of Myoglobin Reconstituted with an Iron Porphycene Having Trifluoromethyl Groups

4-1. Preface

The kinetic studies on O_2 and/or CO bindings of myoglobin (Mb), an O_2-storage hemoprotein, have been one of the fundamental and important research targets to understand the physiological properties in a series of O_2-storage/transport and hemoproteins [1–4]. The affinities of the ligands are mainly determined by the following two factors: (i) the environment of the heme pocket constructed by the amino acid residues, and (ii) the electronic properties of the porphyrin prosthetic group. Over the last two decades, various myoglobin mutants have been prepared to discuss the ligand binding mechanisms [2–4]. In contrast, the replacement of the native heme (protoheme IX, **26**) with an artificially created prosthetic group is another way to understand the relationship between the ligand binding and the chemical properties of the heme in a protein [5]. Considering the molecular design of an artificial heme, the next three points will be important: (i) the electronic and structural properties of the peripheral alkyl groups, (ii) the position of the two heme-propionate side chains, and (iii) the structure of the heme framework. It is known that the replacement of the peripheral methyl groups with electron-withdrawing groups such as formyl and trifluoromethyl group have an influence on the ligand binding events [6–10]. Furthermore, it has been proposed that the two heme-propionates also play significant roles in regulating the stability of the O_2-bound complex [11,12]. On the other hand, it has recently been reported that several structural isomers of iron porphyrin as an artificial prosthetic group produce drastic changes in the ligand binding events in the heme pocket. Thus, these porphyrin isomers have been interesting not only for understanding the physiological properties but also for regulating the hemoprotein function [13–18]. Recently the author found that, among iron porphyrin isomers, iron porphycene is one of the most attractive complexes as an artificial prosthetic group to enhance the O_2 affinity of myoglobin. The reconstituted myoglobin with the iron porphycene having two propionates **27**, rMb(**27**), shows 2600-fold O_2 affinity and interesting O_2/CO selectivity [19–21],because of the lower symmetry of the porphycene ring. Furthermore, it was disclosed that the positions of the propionates also contribute to a high O_2 affinity of the reconstituted myoglobin [22]. The recent X-ray crystallographic study suggests that the porphycene **27** is properly accommodated in the heme pocket [23]. Next, our attention has been on how the peripheral groups in the porphycene ring affect the ligand binding of the myoglobin with an iron porphycene. The introduction of electronic perturbations to the porphycene ring is supposed to bring about the characteristic effects on the ligand binding properties of the reconstituted myoglobin, because the ligand field around an iron atom in porphycene is remarkably different from that in porphyrin due to the low symmetry in the ring framework of porphycene. Especially, one of the unique characteristics of porphycene is its higher redox potential of the ring, comparing with the corresponding porphyrin [24]. This suggests that the introduction of electron-withdrawing groups into a porphycene framework would bring about more drastic effects on the electronic state of the porphycene character, enabling us to observe attractive reactivities of the metalloporphycene. Therefore, in this chapter, the author focuses on the electron-withdrawing effects on porphycene and wishes to report the preparation of the myoglobin reconstituted with the

trifluoromethylated iron porphycene **28** (Chart 4-1) and its ligand binding properties.

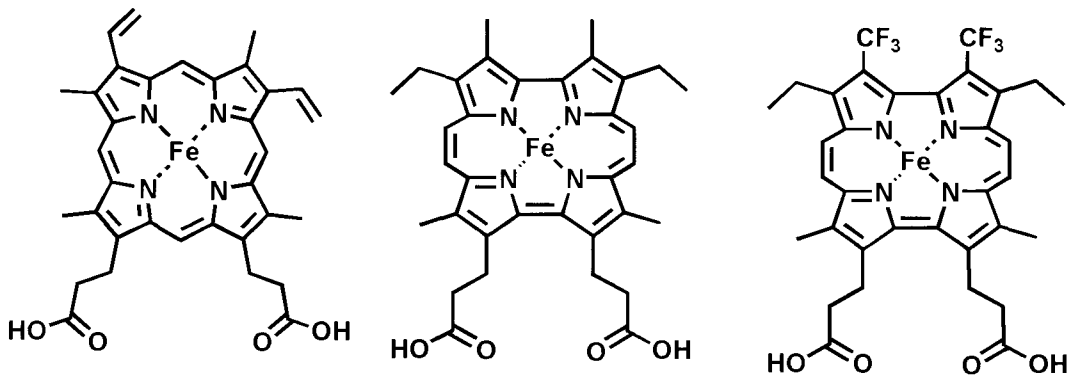

Chart 4-1.

4-2. Materials and Methods

4-2-1. Instruments

The UV–vis spectra were recorded on a Shimadzu UV-3150 double beam spectrometer with a thermostated cell holder with a 0.1 °C deviation or an Agilent 8453 diodearray UV–visible spectrometer. The ESI-TOF mass and FAB mass were carried out by using the mass spectrometer equipped with electrospray ionization on as Applied Biosystems Mariner API-TOF workstation and a JEOL JMS-700 mass spectrometer, respectively. The circular dichroism (CD) spectra were collected using a JASCO J-720S spectrometer. The pH values were monitored by a HORIBA F-52 pH meter. The spectroelectrochemical measurement was performed by regulating the potentials using a Hokuto Denko HA-305 potentiostat/galvanostat. The IR spectra of the CO-ligated Mbs were measured using a Perkin–Elmer Spectrum One IR spectrometer. Kinetic measurements for the O_2 and CO binding were carried out with a stopped-flow/laser flash photolysis system constructed by Unisoku Co., Ltd. (Osaka, Japan). A Xe Arc lamp was employed as a source of the probe light to follow the spectral changes. For laser flash photolysis, a sample was excited with 5 ns pulses (355 or 532 nm) from a Q-switched Nd:YAG laser (Surelite I, Continuum).

4-2-2. Materials

All regents and chemicals were obtained from commercial sources and used as received unless other wise noted. Distilled water was demineralized by a Barnstread NANOpure DiamondTM. The native sperm whale Mb (Biozyme Laboratories Ltd.) was purified by column chromatography through CM-52 (Whatman). First, the protein was washed with 10 mM potassium phosphate buffer (KPi) (pH 6.0) on the column and was eluted with linear gradient from 10 mM KPi (pH 6.0) to 100 mM KPi (pH 7.0).

4-2-3. Syntheses

The precursors of the porphycene (**28**), 3,3'-dimethyl-4,4'-bis[(2-methylcarbonyl)ethyl]-5,5'-diformyl-2,2'-bipyrrole, is synthesized as describes in the previous report [18]. As shown in Scheme 4-1, the freebase porphycene was prepared by McMurry coupling of the two bipyrroles in the same manner as the previous reports [18,25], except for the ring oxidization by DDQ. After the iron insertion, the product was hydrolyzed to yield **28**.

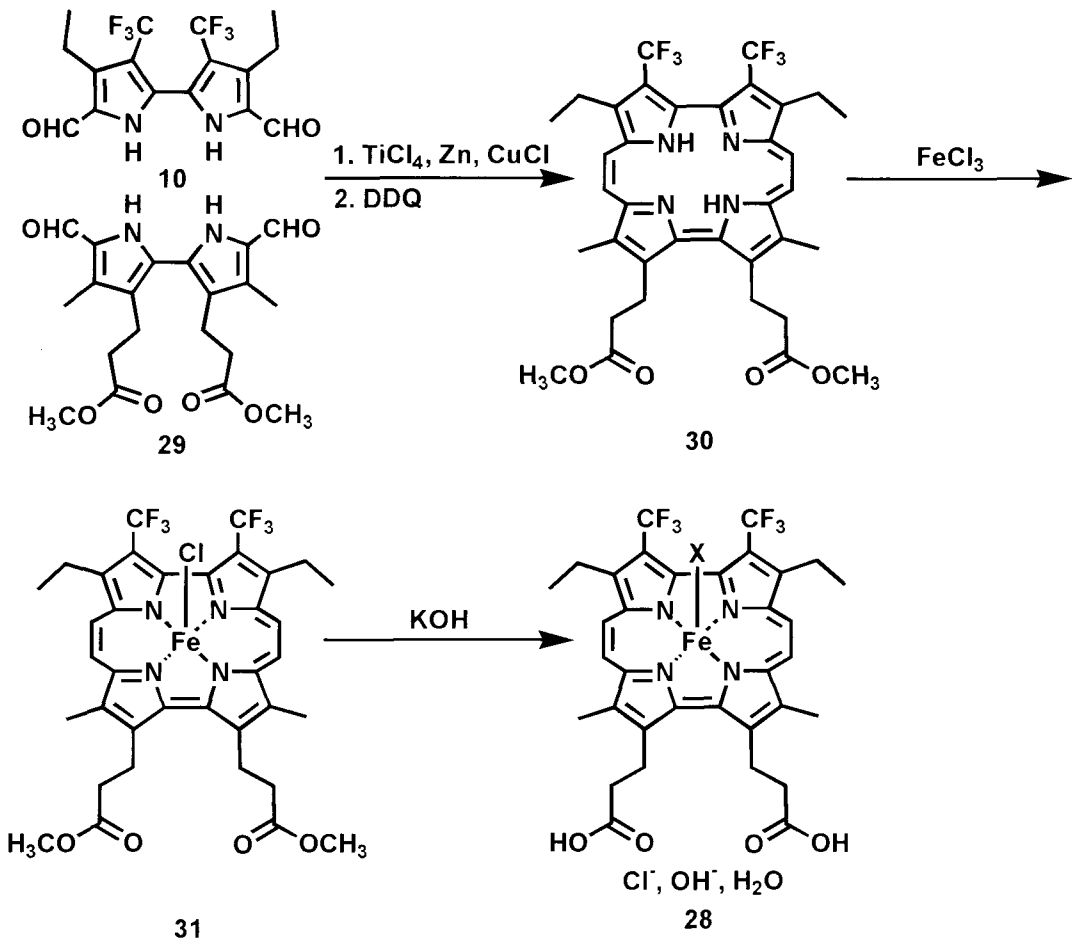

Scheme 4-1.

2,7-Diethyl-3,6-bis(trifluoromethyl)-12,17-dimethyl-13,16-bis(2-methoxycarbonylethyl)porphycene (30):

To a dry THF solution (220 mL) containing activated Zn (5.3 g, 80 mmol), of CuCl (0.80 g, 8 mmol) was added 4.4 g of $TiCl_4$ at 0 °C over 2 h and then refluxed for 3 h. To the mixture was added dropwise 360 mL of a dry THF solution containing **10** (210 mg, 0.54 mmol) and 3,3'-dimethyl-4,4'-bis[(2-methylcarbonyl)ethyl]-5,5'-diformyl-2,2'-bipyrrole (**29**) (210 mg, 0.54 mmol) at room temperature over 10 h. The reaction mixture was refluxed for 30 h. After cooling to 10 °C, 10% aqueous Na_2CO_3 (72 mL) was added over 1 h. After the filtration of the precipitates, the filtrate was extracted with CH_2Cl_2 and washed with water and dried over $MgSO_4$. The solvent was removed and dissolved with $CHCl_3$. To the solution was added about DDQ (250 mg, 1.1 mmol) and stirred for 10 min. The solvent was removed to yield crude products. The crude porphycenes were

collected by column chromatography (neutral alumina active III, CH_2Cl_2 as eluent), the resulting porphycenes were separated by column chromatography (Silica gel, CH_2Cl_2 as eluent). The solvent was removed to yield porphycene (**30**) (29.3 mg, 8%). ^{1}H-NMR ($CDCl_3$, 500 MHz): δ (ppm) 9.46 (ABq, J = 11.3Hz, 2H), 9.21 (ABq, J = 11.3 Hz, 2H), 4.20 (t, 4H), 3.91 (q, 4H) 3.53 (s, 6H), 3.31(s, 6H), 2.92 (t, 4H), 2.01 (brs, 2H), 1.60 (s, 6H). MS (ESI-TOF) calculated for $[M + 2H]^+$ $C_{36}F_6H_{38}N_4O_4^+$, 704.3; found 704.4. UV–vis λ_{max} in CH_2Cl_2; 376, 605, 652, 689 nm.

Chloro-2,7-diethyl-3,6-bis(trifluoromethyl)-12,17-dimethyl-13,16-bis(2-methoxycarbonylethyl)porphycen-atoiron (31):

To a CH_3COOH solution (5.0 mL) containing porphycene (**30**) (4.0 mg, 4.9 μmol) was added anhydrous $FeCl_3$ (5.8 mg, 35 μmol) and CH_3COONa (0.90 mg, 11 μmol) and the mixture was refluxed for 1 h. After cooling to room temperature, the solution was diluted with CH_2Cl_2, treated with 2 M HCl, washed with water, and dried over anhydrous $MgSO_4$. The solvent was removed to yield crude iron porphycene. Silica gel chromatography (CH_2Cl_2/CH_3OH) afforded a green fraction. The solvent was then removed and the residue was dried in vacuo to yield pure iron porphycene **31** (2.0 mg, 52%). MS (ESI-TOF) calculated for $[M + H - Cl]^+$ $C_{36}F_6H_{35}N_4O_4{}^{56}Fe^+$, 757.2; found 757.1. UV–vis λ_{max} in CH_2Cl_2; 388, 655 nm.

Porphycene (28):

To a CH_3OH/THF (1:1, v/v) solution (8 mL) containing 0.2 M aqueous NaOH (4 mL) was added iron porphycene (**31**) (2.5 mg, 0.0032 mmol) and the mixture was stirred at room temperature for 3 h. After neutralization by 0.1 M HCl to pH 6, the solution was extracted with CH_2Cl_2 and washed with water. The solvent was then dried over anhydrous $MgSO_4$ and removed to yield a dark green powder **28** (1.0 mg, 41%). MS (FAB) calculated for $[M - X]^+$ $C_{34}F_6H_{30}N_4O_4{}^{56}Fe^+$, 728.1524; found 728.1521. UV–vis λ_{max} in CH_2Cl_2; 363, 655 nm.

4-2-4. Preparation of Myoglobins Reconstituted with Porphycene

The sperm whale apomyoglobin was prepared from met-Mb by Teale's 2-butanone method. To a solution of apo-Mb was added a pyridine solution of porphycene (**28**) and slowly shook at 4 °C. The solution was then dialyzed against a 100-fold volume of 100 mM phosphate buffer (pH 7.0, 3 h × 3 at 4 °C). After the mixture was concentrated, the solution was passed through a Sephadex G-25 column. The solution of a purified rMb was concentrated and maintained at 4 °C. The extinction coefficient of rMb(**28**) was determined to be 50200 $M^{-1}cm^{-1}$ (at 653 nm) by the pyridine-hemochrome method [26].

4-2-5. Ligand Replacement Examination

To a Mb solution (1 mL, nMb: 11 μM, rMb(**27**): 9.3 μM) in 100 mM phosphate buffer (pH 7.0) was added pyridine solution (4 μL) containing **28** (1.4 eq for nMb, 1.1 eq for rMb(**27**)). After 6 h at 25 °C, the UV–vis spectrum was measured to obtain the observed spectrum. To calculate the simulated spectrum, the same solution except for the absence of Mb in the solution was prepared and the UV–vis spectrum was measured.

4-2-6. Acid Titration

To 100 mM aqueous KCl (2 mL) was added a concentrated Mb solution (20 μL) in 100 mM phosphate buffer (pH 7.0). UV–vis spectra of the solution were monitored at 25 °C under various pH conditions adjusted by incremental additions of aqueous solutions of 0.1 or 1 M HCl. The pH values of the solution were recorded before measurements of the UV–vis spectra. The $pK_{1/2}$ value, the pH corresponding to a 50% loss of a prosthetic group, was determined by fitting to the modified Henderson–Hasselbach equation for one proton process [27].

4-2-7. Fe^{II}/Fe^{III} Redox Properties of a Porphycene Cofactor and Reconstituted Myoglobins

The reduction potential (E_{pc}) for ferric Cl-coordinated form of **28** in CH_2Cl_2 was measured by cyclic voltammetry at 25 °C under a N_2 atmosphere in the presence of tetrabutylammonium tetrafluoroborate as a supporting electlyte, using Pt electrodes. The measurement of Fe^{II}/Fe^{III} redox potential for rMb(**28**) was carried out at 25 °C under a N_2 atmosphere using an SEC-C thin layer quartz glass cell (L = 1 mm, ALS Co., Ltd.). Pt mesh working electrode and Pt counter electrode were employed along with an Ag/AgCl reference electrode. Anthraquinone-2-sulfonate (E = −230 mV vs. SHE) and $Ru(NH_3)_6Cl_3$ (E = +51 mV vs. SHE) were employed as electron mediators. An oxygen-scavenging system composed of 60 mM glucose, 0.1 mg/mL glucose oxidase and 3000 units/mL catalase was applied to ensure the anaerobiosis [28]. A typical increment of 25 mV was applied to the system, and at each applied potential, the UV–vis spectra were monitored until no change was detected due to establishment of equilibrium. The data obtained were fitted to a Nernst equation, and the resulting midpoint of the Fe^{II}/Fe^{III} redox potential was corrected to the value referenced to SHE.

4-2-8. Preparation of Deoxy, O_2, CO–ligated rMb(28)

For preparing the O_2-bound Mb, met-Mb was reduced by sodium dithionite to give deoxy-Mb and separated from excess sodium dithionite by Sephadex G-25 gel filtration with 100 mM phosphate buffer (pH 7.0). During the elution, the deoxy-Mb species smoothly changed to the O_2-bound form by dissolving O_2 in buffer. The CO form of Mbs was observed upon reduction of met-Mbs by adding $Na_2S_2O_4$ under a CO atmosphere. For the measurement of CO dissociation from Mbs, excess sodium dithionite was removed by Sephadex G-25 gel filtration with elution of CO-saturated 100 mM phosphate buffer (pH 7.0).

4-2-9. Kinetic Measurements

The kinetic measurements were carried out in 100 mM phosphate buffer (pH 7.0) at 25 °C, except for monitoring the autoxidation rate at 37 °C. The ligand associations for rMb(**28**) were observed by following the spectral changes at 645 nm after laser flash photolysis (λ_{ex} = 355 nm, 5 ns pulse) under atmospheric pressure in air (for O_2 association). The first-order rate constant was determined by fitting the reaction curve by a nonlinear least-squares method. Dividing the rate constants by the concentration of O_2 ($[O_2] = 2.67 \times 10^{-4}$ M) afforded the rate constants of the O_2 associations. The probe light used to follow the kinetics was passed through a monochromator. The O_2 dissociations for rMb(**28**) were measured by displacement with ferricyanide method by

a stopped-flow apparatus. Under $[K_3Fe(CN)_6] >> [Mb]$, the decay of the absorbance at 638 nm was analyzed by a first-order rate law. The probe light at the shorter wavelength (<480 nm) was cut off. The dependency of the observed rate constants on $[K_3Fe(CN)_6]$ was analyzed by the Michaelis–Menten type equation shown below to yield the dissociation rate constants:

$$k_{obs} = k^{L}_{off}[K_3Fe(CN)_6]/(C + [K_3Fe(CN)_6]) \quad (L = O_2 \text{ or CO}),$$

where k_{obs} is the observed pseudo first-order rate constant, k^{L}_{off} is the dissociation rate constant of ligand L (L = O_2 or CO), and C is the constant.

Autoxidation measurements for rMb(**28**) were carried out by following the spectral changes in the range of 500 – 800 nm every 30 min at 37 °C under 1 atm of the air. The time course of absorbance at 638 nm was analyzed by first-order kinetics to afford the autoxidation rate.

The CO associations for rMb(**28**) were measured by monitoring the changes in the absorbance at 640 nm after laser flash photolysis (λ_{ex} = 532 nm, 5 ns pulse) under 1 atm of CO. The first-order rate constant was determined by fitting the reaction curve by a nonlinear least-squares method. Dividing the rate constants by the concentration of CO ([CO] = 9.85×10^{-4} M) afforded the rate constants of the CO associations. For the measurements, the probe light used to follow the kinetics was passed through a monochromator.

The CO dissociations for rMb(**28**) were measured by displacement with ferricyanide method by a stopped-flow apparatus. Under $[K_3Fe(CN)_6] >> [Mb]$, the decay of the absorbance at 635 nm was analyzed by a first-order rate law. The probe light at the shorter wavelength (<480 nm) was cut off. The dissociation rate constant was obtained by the analysis using the equation shown above.

4-2-10. IR Measurements

The C–O stretching modes, ν(C–O), in the CO-ligated Mbs were measured in a cell (L = 1 mm) with CaF_2 windows. The measurement was carried out at room temperature, and the background spectrum was collected for the corresponding deoxy-Mb. The observed spectra were deconvoluted into 2–5 components with the half-width of 7 cm^{-1}.

4-3 Results and Discussion

4-3-1. Preparation and Characterization of Trifluoromethylated Iron Porphycene

The trifluoromethylated iron porphycene **28** was synthesized from two formyl bipyrroles by McMurry coupling as shown in Scheme 4-1, and obtained as ferric Cl-coordinated form. The syntheses of the bipyrroles were followed by a method described in the previous reports [19,25]. The addition of DDQ was required for the formation of the porphycene ring after the coupling, probably due to the electron-withdrawing trifluoromethyl groups interfering with the autoxidation to give the 18π-conjugated product. The prepared porphycene **28** shows the absorption bands at 362 and 649 nm in CH_2Cl_2, whereas the parent porphycene **27** has the bands at 368 and 622 nm (Figure 4-1). In porphycene **28**, the low-energy-band corresponding to the Q-band for porphyrin is located in the longer wavelength regions than that for **27**. The reduction potential (E_{pc}) of ferric Cl-coordinated **28** in CH_2Cl_2 was determined to be +6 mV vs. SHE by cyclic voltammetry. This value is more positive by 311 mV than that for ferric Cl-coordinated **27**. These physicochemical properties of **28** are indicative of electron-withdrawing effect of the trifluoromethyl groups in the framework of **28**.

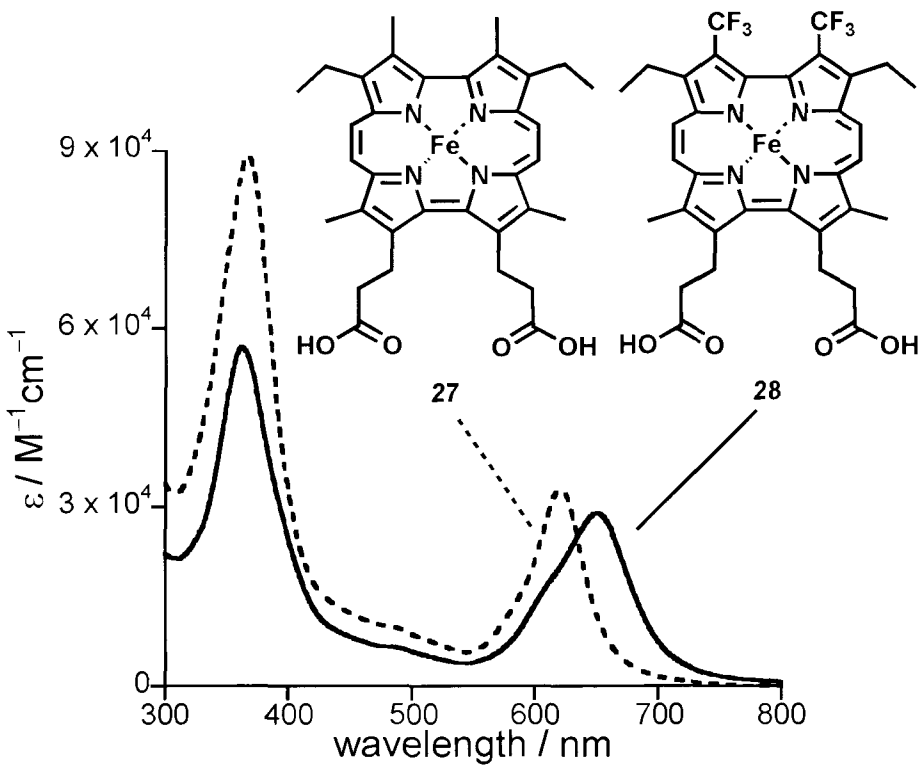

Figure 4-1. UV–vis Spectra of **27** and **28** in CH_2Cl_2.

4-3-2. Properties of Ferric Reconstituted Myoglobin

The reconstitution of myoglobin with the trifluoromethylated iron porphycene **28** was carried out by adding **28** in pyridine into a buffer solution of sperm whale apomyoglobin (Figure 4-2). The complexation of **28** and apomyoglobin was confirmed by ESI-TOF mass spectroscopy, showing some multiple charged species of the protein: 2242 (8+), 1993 (9+) and 1794 (10+) (Figure 4-3a). The deconvolution of the raw data gave the mass number of 17,929, which corresponds to the mass number of the reconstituted myoglobin with **28**, rMb(**28**) (Figure 4-3b). The UV–vis spectrum of ferric rMb(**28**) shown in Figure 4-4 has the characteristic bands at 386, 592 and 653 nm. These bands show a typical red-shift with respect to those observed for the reconstituted myoglobin with a non-trifluoromethylated iron porphycene [19,20]. This finding clearly results from the electron-withdrawing effect of the trifluoromethyl groups on the π-system of the porphycene ring.

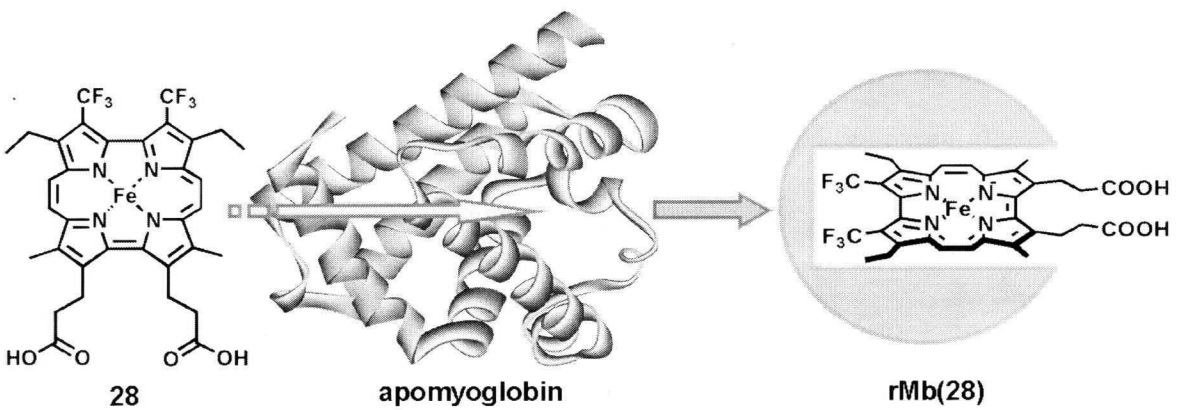

Figure 4-2. Reconstitution of myoglobin with the iron porphycene (**28**).

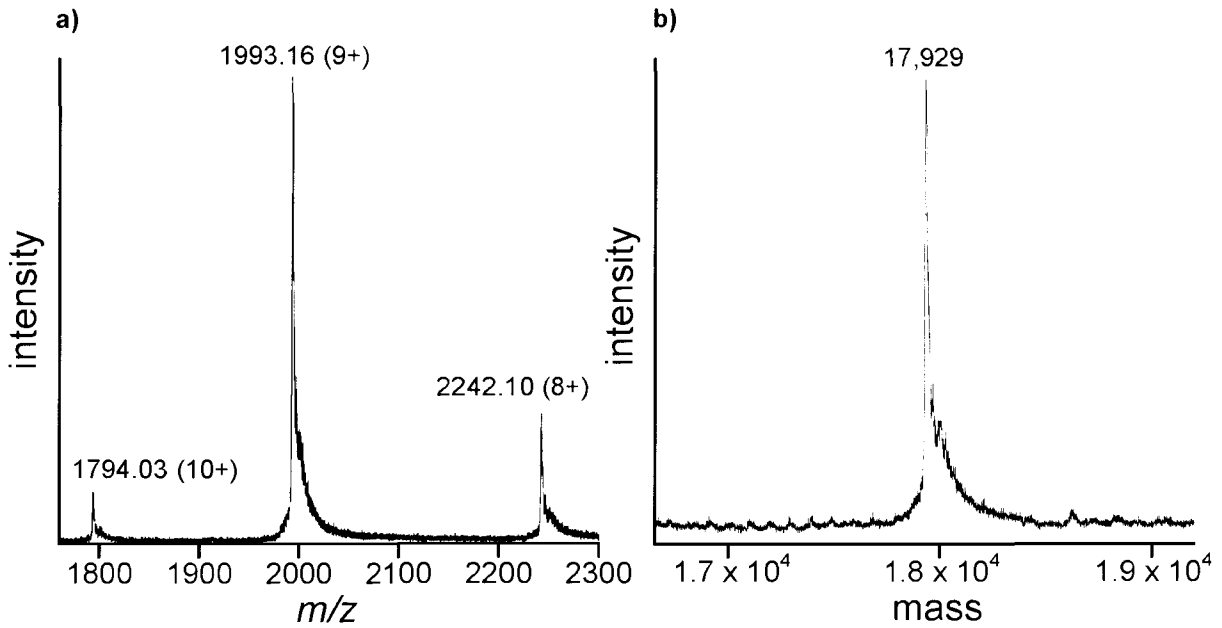

Figure 4-3. ESI-TOF mass spectra of rMb(28): a) Observed spectrum; b) Deconvoluted spectrum.

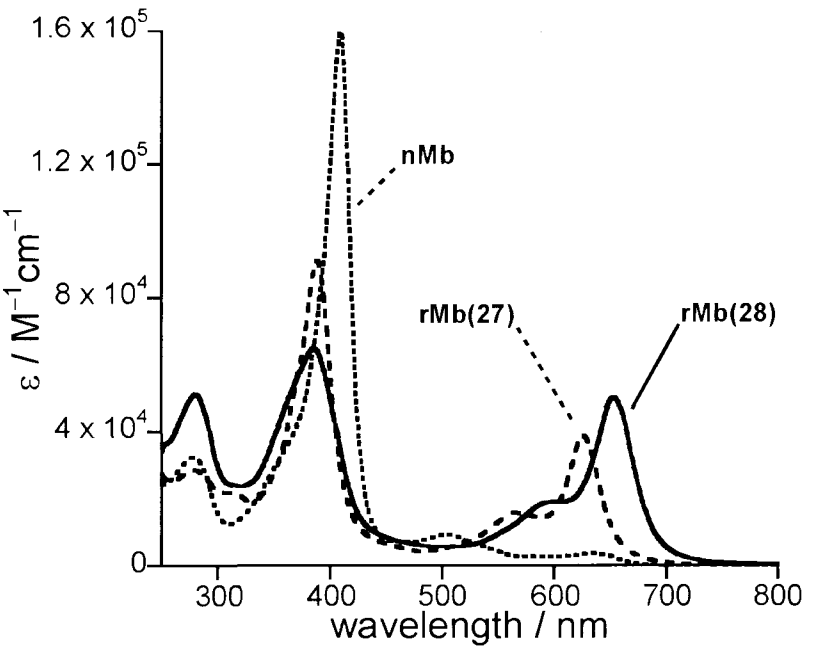

Figure 4-4. UV–vis spectra of nMb, rMb(**27**) and rMb(**28**) in 100 mM KPi buffer (pH 7.0) at 25 °C.

4-3-3. Structural Information of the Reconstituted Myoglobin

27 is accommodated in the same fashion as the native myoglobin, which is clarified by X-ray crystallography (Ref. [23] in the revised manuscript). To confirm that **28** is in the same manner in the native myoglobin, the ligand replacement experiment between nMb and **28** was carried out to observe the spectral changes in the visible region. As shown in Figure 4-5, the band at 646 nm has been shifting to 653 nm and the small band at 500 nm (mainly contributed to by the Q-band of the native myoglobin) disappearing over 6 h. This suggests that the heme in the native myoglobin was clearly replaced with **28**. The same experiment was carried out in the case of rMb(**27**) and **28** (Figure 4-6). This suggests that **27** in the reconstituted myoglobin is clearly replaced with **28**. The band at 627 nm (mainly contributed to by the Q-band of rMb(**27**)) has been shifting to 650 nm (mainly contributed to by the Q-band of rMb(**28**), λ_{max} = 653 nm). These findings indicate that the porphycene with CF_3 groups also binds to the heme pocket in the same manner as the native cofactor or the porphycene without CF_3 group (**27**). Furthermore, the author checked the CD spectra for the reconstituted myoglobins having porphycene with/without CF_3 groups (Figure 4-7). These spectra show the close CD pattern in 200–230 nm because of α-helix, suggesting that the secondary structures of them are almost same.

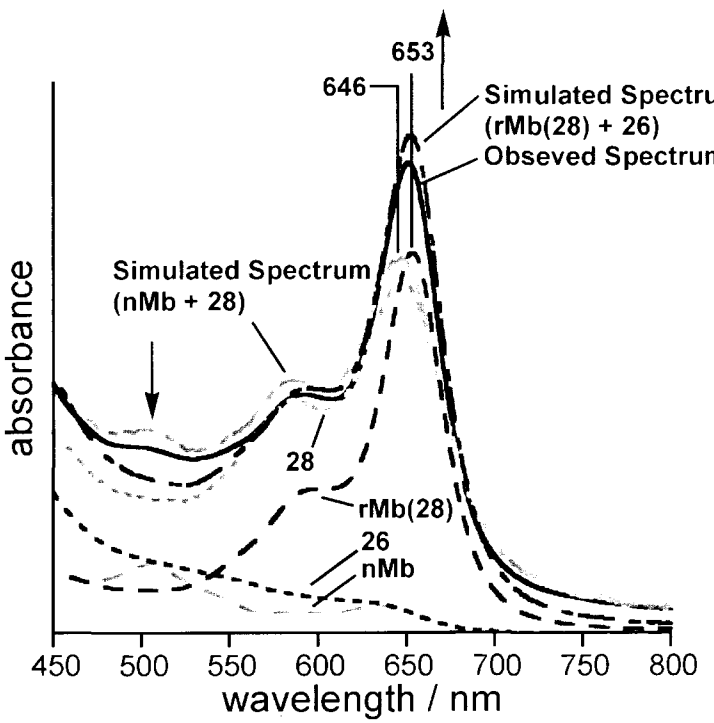

Figure 4-5. UV–vis spectra of the ligand replacement experiment between nMb and **28** in 100 mM KPi buffer (pH 7.0) at 25 °C: Observed spectrum, UV–vis spectrum of the mixture of nMb and **28** after the equilibrium at 25 °C for 6 h. Simulated spectrum (nMb + **28**) is the simulated spectrum of before replacement. The spectrum was obtained from the overlap of the spectra of nMb and **28**. Simulated spectrum (rMb(**28**) + **26**) is the simulated spectrum of after replacement. The spectrum was obtained from the overlap of the spectra of **26** and rMb(**28**).

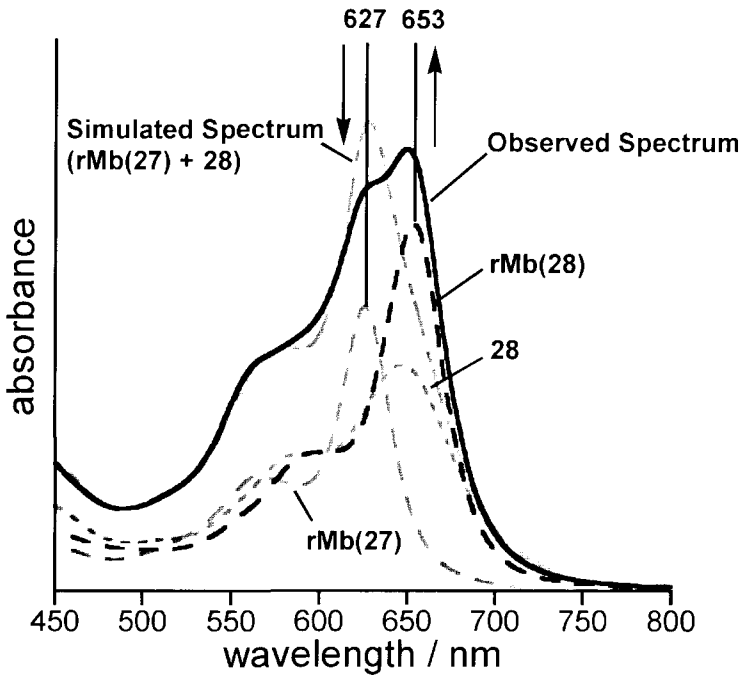

Figure 4-6. UV–vis spectra of the ligand replacement experiment between rMb(**27**) and **28** in 100 mM KPi buffer (pH 7.0) at 25 °C: Observed spectrum, UV–vis spectrum of the mixture of rMb(**27**) and **28** after the equilibrium at 25 °C for 6 h. Simulated spectrum (rMb(**27**) + **28**) is the simulated spectrum of before replacement. The spectrum was obtained from the overlap of the spectra of rMb(**27**) and **28**.

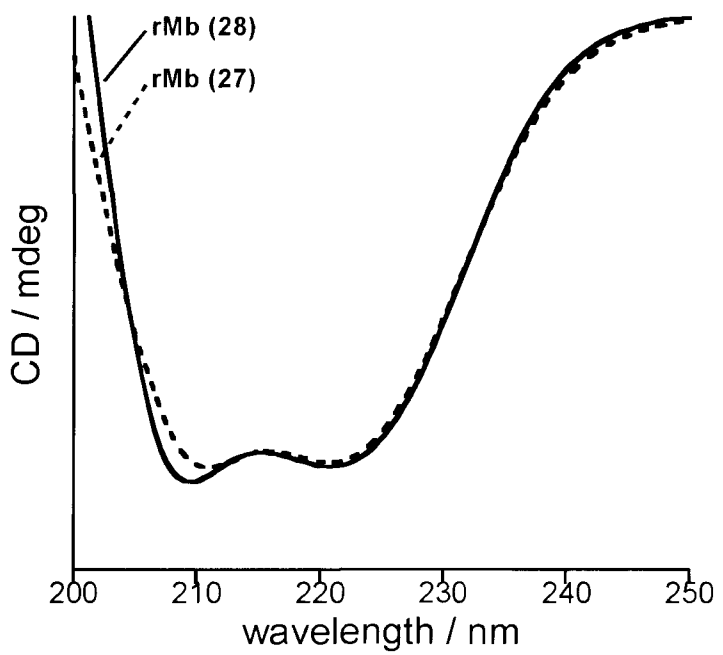

Figure 4-7. CD spectra of rMb(**27**) and rMb(**28**) in 100 mM phosphate buffer (pH 7.0) at 25 °C.

4-3-4. Strength of a Proximal His93 Imidasol–Iron Bond

The $pK_{1/2}$, that is, the pH value corresponding to a 50% loss of a prosthetic group, was estimated to be 2.7 for rMb(**28**), whereas the value is 3.1 for rMb(**27**) and 4.1 for the native myoglobin, nMb (Figure 4-8), respectively. The lower $pK_{1/2}$ values for the rMbs than that for nMb suggests that the strong coordination of His93 to the iron atom occurs due to the enhanced Lewis acidity of the porphycene ring caused by its ring symmetry.

The redox potential of rMb(**28**) was found to be −41 mV (vs. SHE) by spectroelectrochemical measurement (Figure 4-9). The previous reports show us the value of −195 mV for rMb(**27**) and +52 mV for nMb [19,20], respectively. The strong coordination of the imidazole in His93 to the porphycene iron brings about the lower redox potentials for rMbs. The positively shifted redox potential in rMb(**28**), comparing with rMb(**27**), stems from the introduction of the electron-withdrawing trifluoromethyl groups into the porphycene ring as indicated in the red-shift of the Q-band in the UV–vis spectra [29].

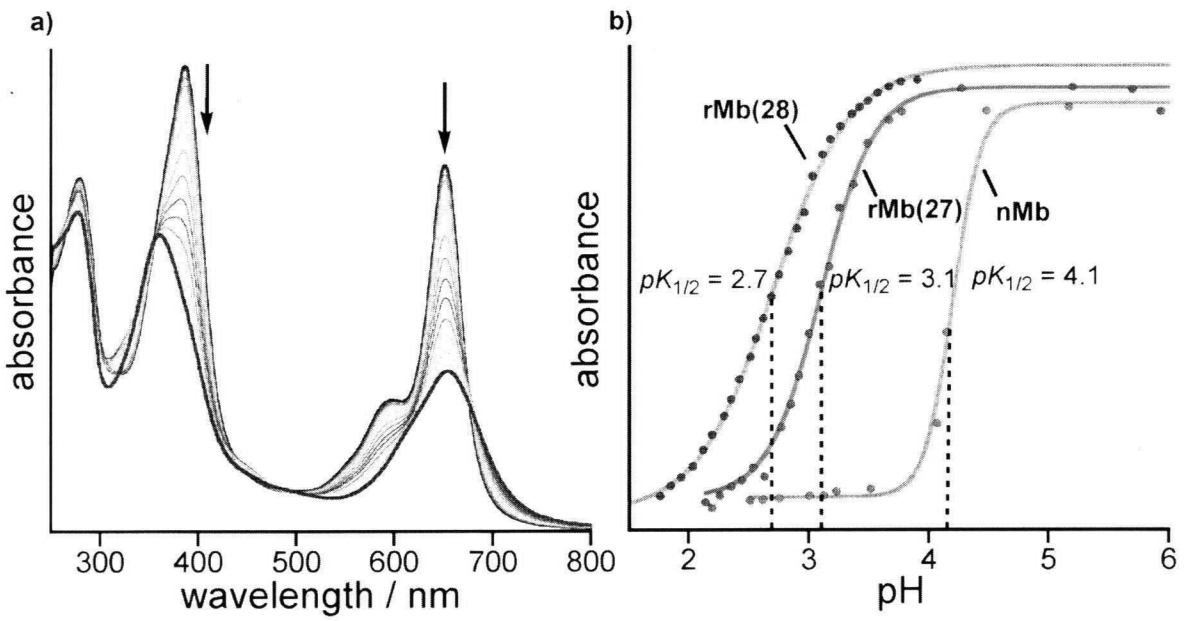

Figure 4-8. a) UV–vis spectral changes in the acid titration for rMb(**28**) in 100 mM aqueous KCl at 25 °C; b) Acid titration for nMb, rMb(**27**) and rMb(**28**) at 409, 387, and 385 nm, respectively. The solid lines are the fitting curve for the modified Henderson-Hasselbach equation.

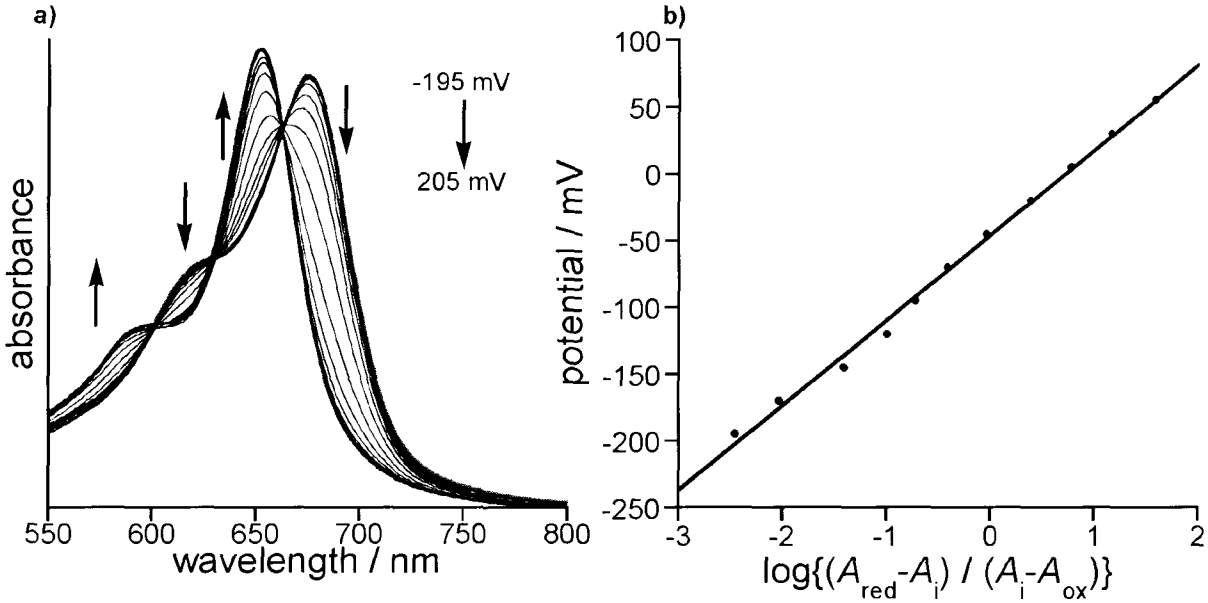

Figure 4-9. UV–vis spectra of rMb(**28**) in the spectroelectrochemical measurements: a) Observed spectra (first line = −195 mV, last line = 205 mV vs. SHE); b) Nernst plot (vs. SHE) obtained from the absorbance change at 675 nm in 100 mM KPi buffer (pH 7.0) at 25 °C.

4-3-5. UV–vis spectra of O_2- and CO-bound rMb(28)

The O_2-bound and CO-bound forms of ferrous rMb(**28**) were identified by the UV–vis spectra shown in Figure 4-10. The UV–vis data for these species are summarized in Figure 4-11and Table 4-1 along with those of the previously reported ferrous rMb(**27**) [20]. The visible band was observed at 647 nm in the O_2-bound form and at 643 nm in the CO-bound form, both of which appeared in the range of the longer wavelength. This finding suggests that the UV–vis spectra of the ferrous rMbs are also affected by the electron density of the ring framework.

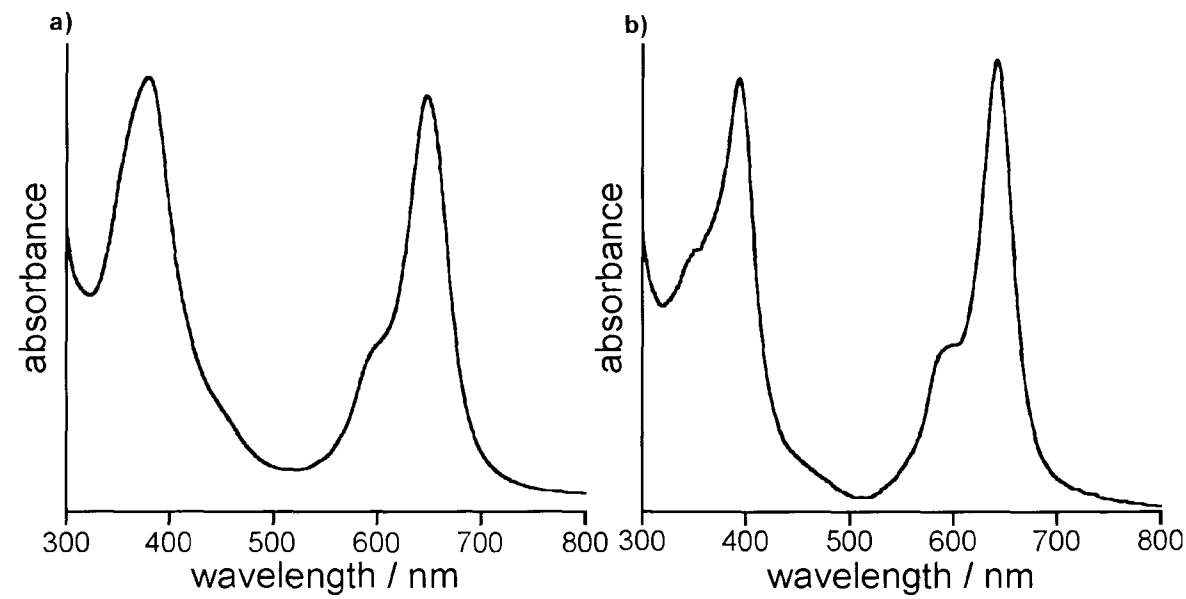

Figure 4-10. UV–vis spectra of ligand-bound ferrous rMb(**28**)s in 100 mM KPi buffer (pH 7.0) at 25 °C: a) O_2-bound form; b) CO-bound form.

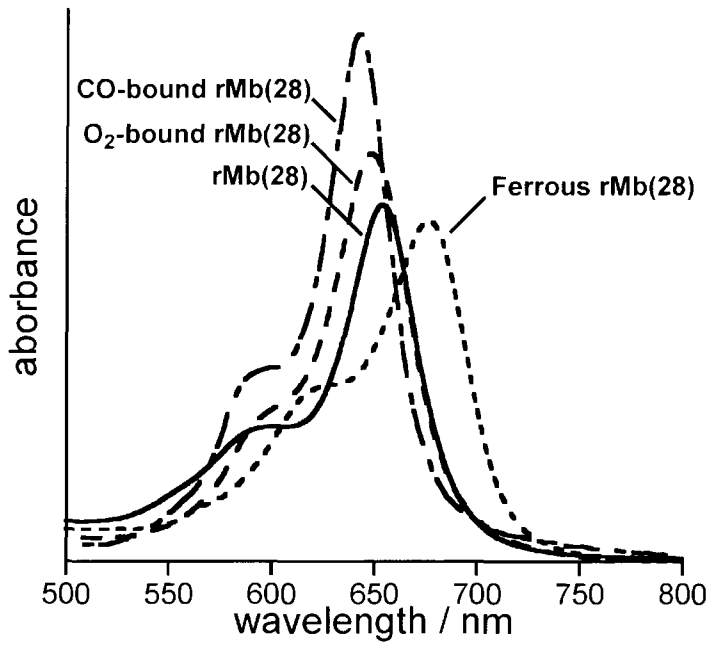

Figure 4-11. UV–vis spectra of various form rMb(**28**) in the range of wavelength from 500 to 800 nm.

Table 4-1. Absorption Maximam (nm), λ_{max}, for rMbs.[a)]

rMbs	rMb(**28**)	rMb(**27**)[b)]
Ferric	386, 592 (sh), 653	387, 563 (sh), 624
Ferrous	369, 626 (sh), 676	352 (sh), 375, 584 (sh), 615
O_2-bound	380, 598 (sh), 647	387, 562 (sh), 619
CO-bound	393, 592 (sh), 643	391, 567 (sh), 613

a) 100 mM KPi buffer (pH 7.0) at 25 °C. b) Quoted from ref. 20.

4-3-6. O_2 binding properties for reconstituted myoglobins

The kinetic parameters for the O_2 bindings are summarized in Table 4-2. The O_2 association for rMb(**28**) was measured by laser flash photolysis of the O_2-bound form. The single-phase first-order kinetics affords the O_2 association rate, $k^{O_2}_{on}$, of 38 s^{-1} based upon the apparent rate constant and the O_2 concentration at 25 °C. This value is interpolated between those for rMb(**27**) and nMb as shown in Table 4-2. The O_2 dissociation was followed by rapidly mixing O_2-bound rMb(**28**) with excess $K_3Fe(CN)_6$ at 25 °C. The dependency of the apparent pseudo first-order rate constant is given as a saturation profile against $[K_3Fe(CN)_6]$ (Figure 4-12), and the level-off value determined by a Michaelis–Menten type equation (see 4-3-7) was attributed to the $k^{O_2}_{off}$ of 0.82 s^{-1}. The ratio of $k^{O_2}_{on}$ and $k^{O_2}_{off}$, which represents the O_2 affinity for rMb(**28**), is calculated to be 4.7×10^7 M^{-1}. This value is about two orders of magnitude lower than that of rMb(**28**). The lower O_2 affinity of rMb(**28**) than that of rMb(**27**) is mainly caused by the enhancement of the O_2 dissociation rate. In other words, the O_2-bound form was destabilized by the attachment of the electron-withdrawing groups in the ring framework. A similar tendency has been reported in previous studies using the myoglobin having iron porphyrins with electron-withdrawing and electron-donating peripheral groups [8,9]. According to previous reports, the O_2 affinities of the myoglobins are getting lower as the electron density of the porphyrin ring decreases. Normally, the bond configuration of the O_2-bound form of myoglobin is expressed as Fe^{III}–$O_2^{\cdot -}$ [30]. The electron-withdrawing effect of the introduced trifluoromethyl groups would interfere with the Fe^{III}–$O_2^{\cdot -}$ bond configuration because of the decrease in the electron density of the porphycene iron. However, the O_2 dissociation of rMb(**28**) is still slower, leading to the higher O_2 affinity, in comparison to the native myoglobin. This is because the energy level of the d_{z^2} orbital decreases due to the lower symmetric framework, forming a relatively stable Fe–O_2 σ-bonding [20]. The observed O_2 dissociation rate for rMb(**28**) results from a delicate balance of the intrinsic characteristics in a porphycene ring and the electronic effect of the peripheral group.

Autoxidation measurement was carried out at 37 °C. The UV–vis spectral changes in the Q band region during stages of autoxidation reaction for O_2-bound rMb(**28**) every 2 h are shown in Figure 4-13a. The autoxidation rate was obtained by a liner fitting as shown Figure 4-13b. It was found that the autoxidation rate of rMb(**28**) was almost identical to that of rMb(**27**) (0.021 h^{-1} and 0.024 h^{-1}, respectively). It has been reported that, in a series of mutant myoglobins, the autoxidation is more accelerated with decreasing in the oxygen affinity [3]. With respect to this point, the slow autoxidation rate of rMb(**28**) is an interesting character, because the oxygen affinity of rMb(**28**) is lower by two orders of magnitude than that of rMb(**27**). One of the reasons for the slow autoxidation of rMb(**28**) would be due to the higher Fe^{II}/Fe^{III} redox potential of rMb(**28**) than that of rMb(**27**), leading to the suppression of the oxidation into the ferric form.

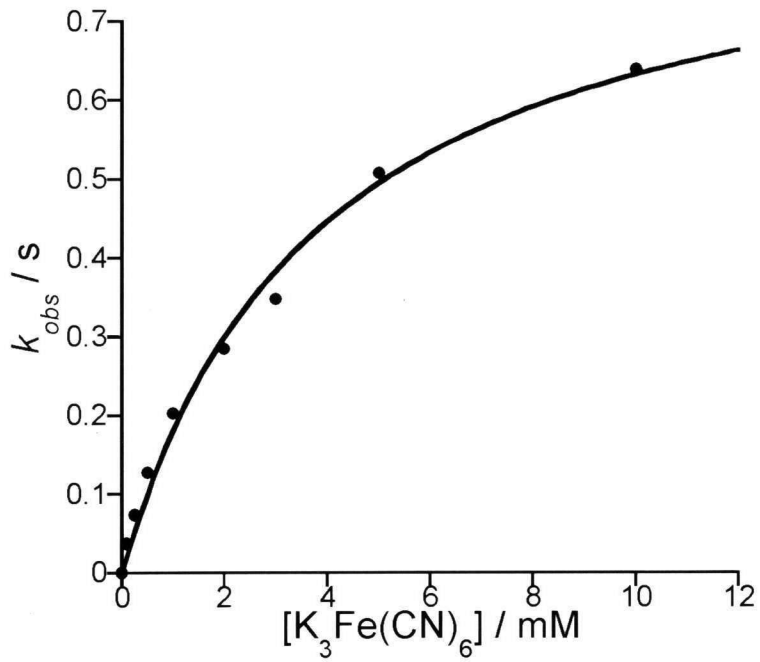

Figure 4-12. Plots of observed pseudo-first-order rate constant, k_{obs}, versus $[K_3Fe(CN)_6]$ for the reaction of O_2-bound rMb(**28**) ([rMb(**28**)] ~10 μM) with $K_3Fe(CN)_6$ in 100 mM KPi buffer (pH 7.0) at 25 °C.

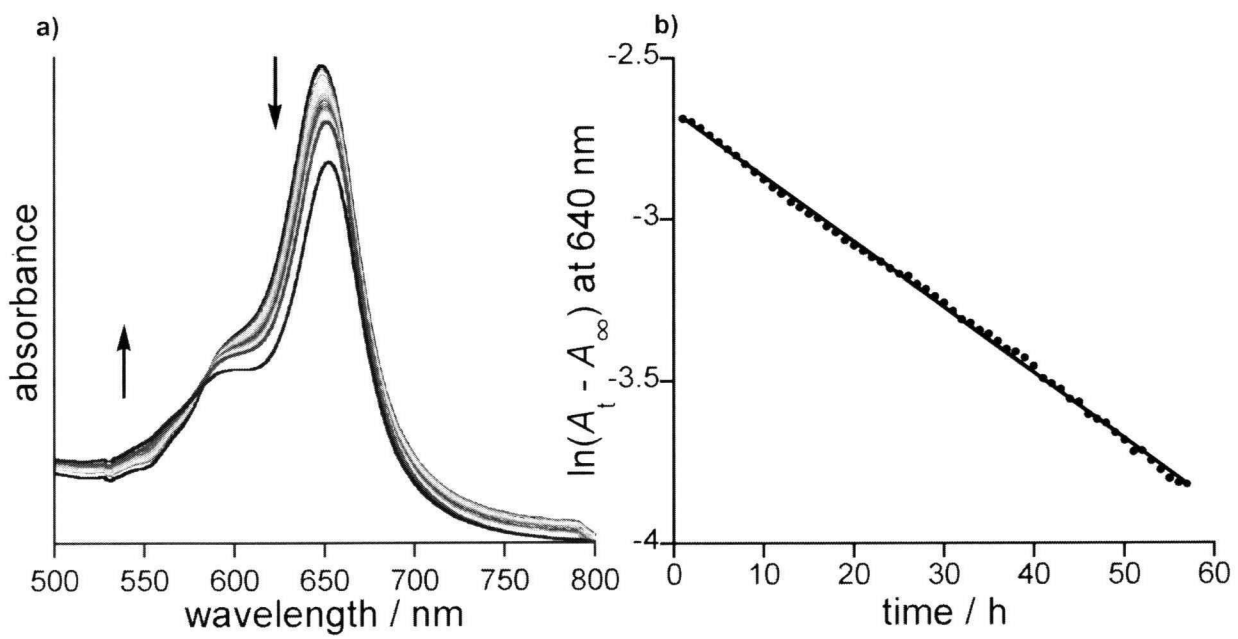

Figure 4-13. a) UV–vis spectral changes in the autoxidation for O_2-bound rMb(**28**) in 100 mM KPi buffer (pH 7.0) at 37 °C; b) A plot of $\ln(A_t - A_\infty)$ at 640 nm vs. time, where A_∞ and A_t stand for the absorbances at the completion of the reaction and at certain time, respectively.

Table 4-2. O_2 binding parameters for myglobins.[a)]

Mbs	$k^{O_2}_{on}$ ($(\mu M)^{-1}$ s^{-1})[b)]	$k^{O_2}_{off}$ (s^{-1})[c)]	K_{O_2} (M^{-1})[d)]	k_{auto} (h^{-1})[e)]
rMb(**28**)	38 ± 2	0.82 ± 0.05	4.7×10^7	0.021 ± 0.001
rMb(**27**)[f)]	91 ± 10	0.057 ± 0.005	1.6×10^9	0.024 ± 0.001
nMb[f)]	17 ± 1	28 ± 2	6.1×10^5	0.1 ± 0.01

a) 100 mM KPi buffer (pH 7.0) at 25 °C. b) Association rate constant. c) Dissociation rate constant. d) $K_{O_2} = k^{O_2}_{on}/k^{O_2}_{off}$. e) Autoxidation rate constant. f) Quoted from ref. 20.

4-3-7. CO binding properties for reconstituted myoglobins

The CO binding was also monitored by the same method as the O_2 binding. The kinetic parameters for the CO binding are summarized in Table 4-3. The CO association rate constant, k^{CO}_{on}, for rMb(**28**) was yielded as 8.4×10^6 M^{-1} s^{-1}. A similar CO association rate constant was found in rMb(**27**), and both of them are much larger than that for nMb. The acceleration of the CO association in the reconstituted myoglobins with iron porphycenes is explained by the in-plane location of the porphycene iron so that the CO can readily bind to the porphycene iron. This is also due to the lower symmetry of the porphycene ring, in comparison to the iron porphyrin [20]. The reaction of the CO-bound rMb(**28**) with excess $K_3Fe(CN)_6$ provided the CO dissociation rate constant, k^{CO}_{off}, of 0.04 s^{-1} (Figure 4-14). Therefore, the CO affinity of rMb(**28**) was calculated to be 2.0×10^8 M^{-1}. No significant difference in the CO bindings between two myoglobins having iron porphycenes with and without trifluoromethyl groups was found, although a remarkable difference was revealed in the C–O stretching modes observed by the Fouriertransform infrared resonance (FT-IR) measurements. The spectra are shown in Figure 4-15. The C–O stretching band for the CO-ligated nMb is observed around 1945 cm^{-1} as the dominant component (70%) with a small population at 1934 cm^{-1} (Figure 4-15a). On the other hands, the C–O stretching modes for the CO-bound rMbs were observed in relatively higher energy regions: the CO-bound rMb(**27**) has widely distributed bands with similar populations from 1920 cm^{-1} to 1970 cm^{-1} (1927 cm^{-1} (24%), 1940 cm^{-1} (32%), 1953 cm^{-1} (23%) and 1963 cm^{-1} (21%)), whereas rMb(**28**) shows the corresponding band around 1970 cm^{-1} together with a broad component of small population in the lower energy region (1937 cm^{-1} (6%), 1948 cm^{-1} (7%), 1959 cm^{-1} (10%), 1968 cm^{-1} (50%) and 1979 cm^{-1} (27%)), where each component for rMb(**28**) is located in the larger wavenumbers than that for rMb(**27**). The observation of several components in the C–O stretching mode suggests the existence of several structural and/or electronic Fe–C–O bond characteristics. Generally, a low C–O stretching frequency is brought about by the back donation from the iron to the π^* orbital of the C–O bond [31]. The CO dissociation rates for these three proteins are clearly similar. Therefore, the differences in the IR spectra, at first glance, look inconsistent. However, the observed CO dissociation rate constant is, according to the previous works, an average value for each conformer in the CO-bound forms, and the existence of several Fe–C–O configurations is not necessarily related to the CO dissociation kinetics [31]. Furthermore, the CO dissociation rates from native and mutant myoglobins are not sensitive to their C–O stretching frequencies. Therefore, it seems to be difficult to relate the CO dissociation rate with the C–O stretching frequency in this case. The significant distributions in the higher frequencies in rMb(**28**) suggest a poor π-back donation from the iron ion, which would cause the accumulation of the electron density in the iron in the process of the CO association. However, the electron-withdrawing group in the porphycene ring

can help to cancel the excess electron density on the iron ion, resulting in the formation of stable CO-bound form. A similar tendency was reported by Kitagawa et al. for the myoglobin reconstituted with 2,4-diformylporphyrin iron complex, where the C–O stretching band for the reconstituted myoglobin was observed at a higher wavenumber than that for the native protein [10]. Furthermore, Caughey et al. proposed that an electron-withdrawing group attached at the heme framework decreases the π-donation ability of the porphyrin iron, based upon the dependency of the C–O stretching band on the electronic effect of the peripheral group [7].

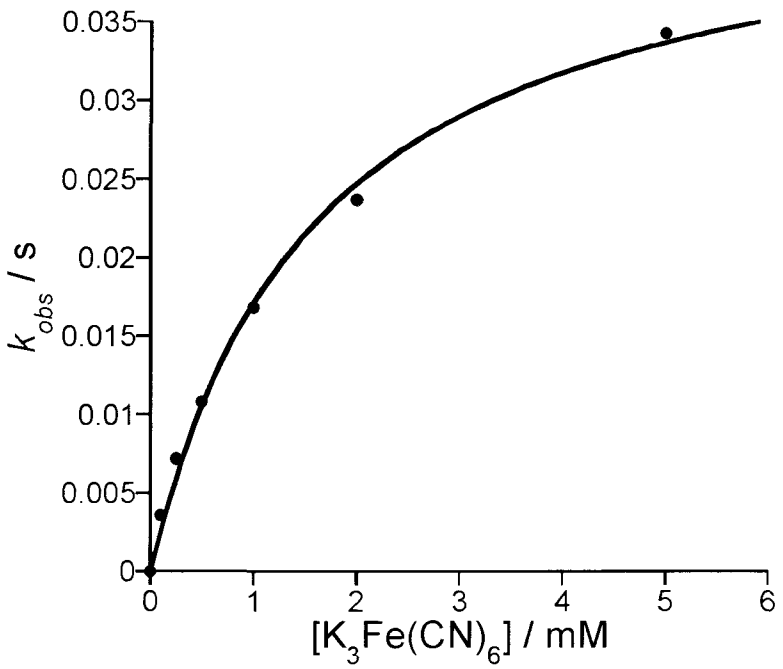

Figure 4-14. Plots of observed pseudo-first-order rate constant, k_{obs}, versus $[K_3Fe(CN)_6]$ for the reaction of CO-bound rMb(**28**) ([rMb(**28**)] ~10 μM) with $K_3Fe(CN)_6$ in 100 mM KPi buffer (pH 7.0) at 25 °C.

Table 4-3. CO binding parameters for myglobins[a)]

Mbs	k^{CO}_{on} ($(\mu M)^{-1}$ s^{-1})[b)]	k^{CO}_{off} (s^{-1})[c)]	K_{CO} (M^{-1})[d)]
rMb(**28**)	8.4 ± 0.6	0.043 ± 0.001	2.0×10^8
rMb(**27**)[e)]	11 ± 1	0.070 ± 0.008	1.6×10^8
nMb[e)]	0.51 ± 0.01	0.050 ± 0.006	1.0×10^7

a) 100 mM KPi buffer (pH 7.0) at 25 °C. b) Association rate constant. c) Dissociation rate constant. d) $K_{CO} = k^{CO}_{on}/k^{CO}_{off}$. e) Quoted from ref. 20.

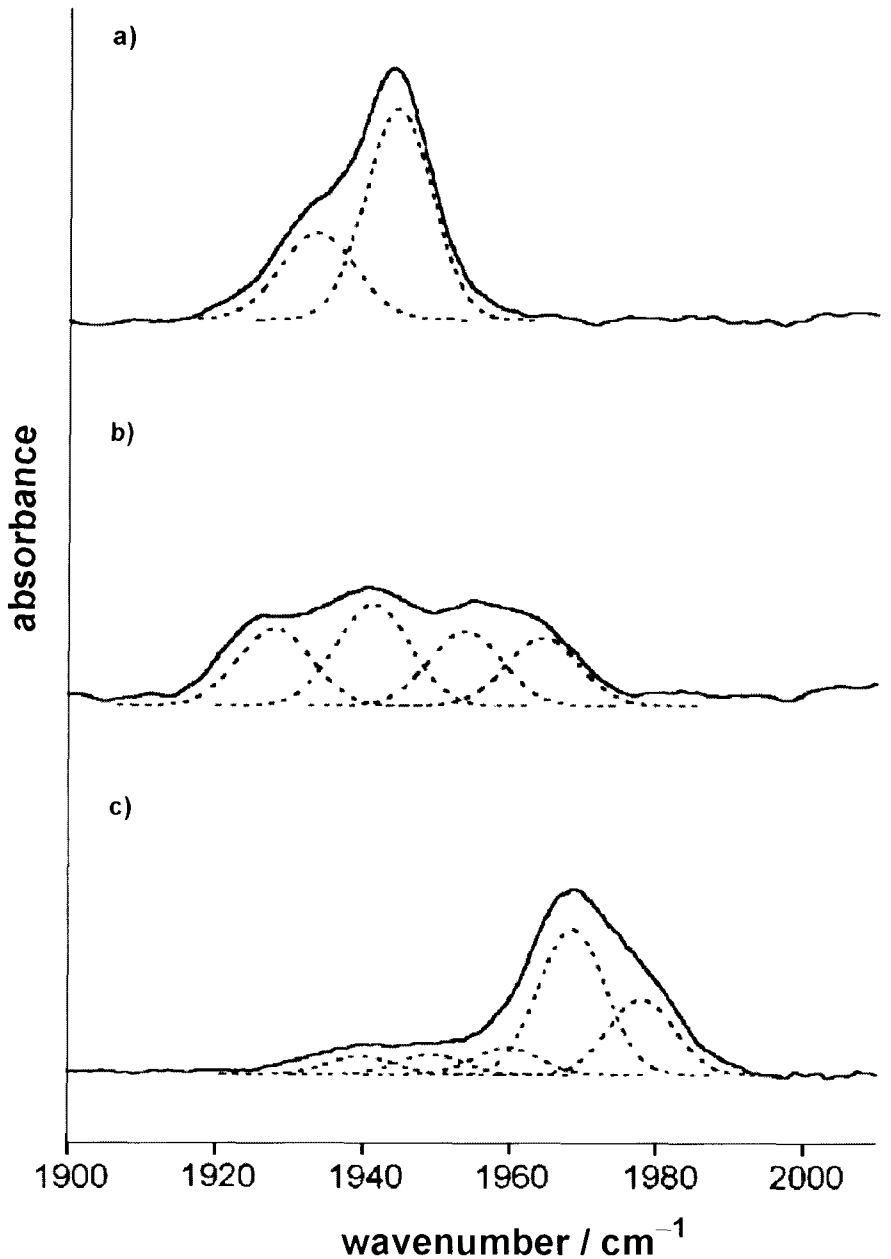

Figure 4-15. IR spectra of CO-bound myoglobins in 100 mM KPi buffer (pH 7.0). Solid line: observed spectrum; dotted line: deconvoluted spectrum: a) nMb; b) rMb(**27**); c) rMb(**28**)

4-4. Summary

In this chapter, the author investigated the electronic effect of the peripheral groups on the ligand binding properties of the reconstituted myoglobin with the iron porphycene attached trifluromethyl groups into the porphycene ring. The O_2 affinity clearly decreases in the newly prepared myoglobin, mainly caused by the acceleration of the O_2 dissociation. However, the autoxidation rate is relatively slow in spite of the low O_2 affinity. The slow autoxidation would be due to the stabilization of ferrous state by introducing the trifluoromethyl groups. On the other hand, the CO binding properties were not significantly affected by introducing a trifluromethylated iron porphycene into apomyoglobins in comparison to the myoglobin reconstituted with iron porphycene without trifluoromethyl groups, but a remarkable effect was observed in the C–O stretching frequencies. It was found, also in the reconstituted myoglobin with an iron porphycene, that the peripheral electronic perturbation affected the ligand binding kinetics and the structures of the proteins.

Reference

1. In *Hemoglobin and Myoglobin in Their Reactions with Ligands*; Antonini, E., Brunori, M., Eds., North-Holland, Amsterdamn, 1971, pp. 223.
2. Draghi, F.; Miele, A. E.; Travaglini-Allocatelli, C.; Vallone, B.; Brunori, M.; Gibson, Q. H.; Olson, J. S. *J. Bio. Chem.* **2002**, *277*, 7509–7519.
3. Springer, B. A.; Sligar, S. G.; Olson, J. S.; Phillips G. N., Jr. *Chem. Rev.* **1994**, *94*, 699–714.
4. In *Encyclopedia of Inogranic Chemistry*; Hayashi, T., Ed., Wiley, J., second ed., Chichester, 2005, pp. 2167–2180.
5. Hayashi, T.; Hisaeda, Y. *Acc. Chem. Res.* **2002**, *35*, 35–43.
6. Nagao, S.; Hirai, Y.; Suzuki, A.; Yamamoto, Y. *J. Am. Chem. Soc.* **2005**, *127*, 4146–4147.
7. Alben, J. O.; Caughey, W. S. *Biochemistry* **1968**, *7*, 175–183.
8. Sono, M.; Asakura, T. *J. Biol. Chem.* **1975**, *250*, 5227–5232.
9. Sono, M.; Smith, P. D.; McCray, J. A.; Asakura, T. *J. Biol. Chem.* **1976**, *251*, 1418–1426.
10. Tsubaki, M.; Nagai, K.; Kitagawa, T. *Biochemistry* **1980**, *19*, 379–385.
11. Hayashi, T.; Matsuo, T.; Hitomi, Y.; Okawa, K.; Suzuki, A.; Shiro, Y.; Iizuka, T.; Hisaeda, Y.; Ogoshi, H. *J. Inorg. Biochem.* **2002**, *91*, 94–100.
12. Harada, K.; Makino, M.; Sugimoto, H.; Hirota, S.; Matsuo, T.; Shiro, Y.; Hisaeda, Y.; Hayashi, T. *Biochemistry* **2007**, *46*, 9406–9416.
13. Stynes, D. V.; Liu, S.; Marcus, H. *Inorg. Chem.* **1985**, *24*, 4335–4338.
14. Neya, S.; Hori, H.; Imai, K. Kawamura-Konishi, Y.; Suzuki, H.; Shiro, Y.; Iizuka, T.; Funasaki, N. *J. Biochem.* **1997**, *121*, 654–660.
15. Sotiriou-Leventis, C.; Chang, C. K. *Inorg. Chim. Acta* **2000**, *311*, 113–118.
16. Neya, S.; Nakamura, M.; Imai, K.; Funasaki, N. *Chem. Pharm. Bull.* **2001**, *49*, 345–346.
17. Neya, S.; Imai, K.; Hori, H.; Ishikawa, H.; Ishimori. K.; Okuno, D.; Nagatomo, S.; Hoshino, T.; Hata, M.; Funasaki, N. *Inorg. Chem.* **2003**, *42*, 1456–1461.
18. Neya, S.; Imai, K.; Hiramatsu, Y.; Kitagawa, T.; Hoshino, T.; Hata, M.; Funasaki, N. *Inorg. Chem.* **2006**, *45*, 4238–4242.
19. Hayashi, T.; Dejima, H.; Matsuo, T.; Sato, H.; Murata, D.; Hisaeda, Y. *J. Am. Chem. Soc.* **2002**, *124*, 11226–11227.
20. Matsuo, T.; Dejima, H.; Hirota, S.; Murata, D.; Sato, H.; Ikegami, T.; Hori, H.; Hisaeda, Y.; Hayashi, T. *J. Am. Chem. Soc.* **2004**, *126*, 16007–16017.
21. Matsuo, T.; Tsuruta, T.; Maehara, K.; Sato, H.; Hisaeda, Y.; Hayashi, T. *Ionrg. Chem.* **2005**, *44*, 9391–9396.
22. Matsuo, T.; Ikegami, T.; Sato, H.; Hisaeda, Y.; Hayashi, T. *J. Inorg. Biochem.* **2006**, *100*, 1265–1271.
23. Hayashi, T.; Murata, D.; Makino, M.; Sugimoto, H.; Matsuo, T.; Sato, H.; Shiro, Y.; Hisaeda, Y. *Inorg. Chem.* **2006**, *45*, 10530–10536.
24. Sessler, J. L.; Gebauer, A.; Vogel, E. In *The Porphyrin Handbook*; Kadish, K. M., Smith, K. M., Guilard, R., Eds.; Academic Press: San Diego, 2000; Vol. 2, pp. 1–54.
25. Vogel, E.; Köcher, M.; Schmickler, H.; Lex, J. *Angew. Chem., Int. Ed. Engl.* **1986**, *25*, 257–259.
26. Paul, K.-G.; Thetorell, H.; Åkeson, Å. *Acta. Chem. Scand.* **1953**, *7*, 1284–1287.

27. Lloyd, E.; Bruk, D. L.; Ferrer, J. C.; Maurus, R.; Doran, J.; Carey, P. R.; Brayer, G. D.; Mauk, A. G. *Biochemistry* **1996**, *35*, 11901–11912.

28. Tosha, T.; Yoshioka, S.; Hori, H.; Takahashi, S.; Ishimori, K.; Morishiama, I. *Biochemistry* **2002**, *41*, 13883–13893.

29. D'Souza, F.; Boulas, P. L.; Kisters, M.; Sambrotta, L.; Aukauloo, A. M.; Guilard, R.; Kadhish, K. M. *Inorg. Chem.* **1996**, *35*, 5743–5746.

30. In *Iron Porphyrins*; Spiro, T. G., Ed., Addison Wesley Reading, MA, 1983, pp. 89–159, Part II.

31. Li, T.; Quillin, M. L.; Phillips, G. N., Jr.; Olson, J. S. *Biochemistry* **1994**, *33*, 1433–1446.

Conclusions

It is well known that a LUMO energy level of porphycene is stabilized due to the decrease of the framework symmetry as compared to porphyrin. The author expected that the LUMO energy level of the porphycene was further stabilized by introducing strong electron-withdrawing groups onto the porphycene framework. Thus, the author designed a novel trifluoromethylated porphycene, 2,7,12,17-tetraethyl-3,6,13,16-tetra(trifluoromethyl)porphycene. From the electrochemical studies, it was revealed that trifluoromethylation of the porphycene caused a large positive shift in the reduction potentials. This result indicates that the porphycene has a highly electron-deficient framework. In fact, the author has successfully isolated the unusually stable nonaromatic 20π-conjugated porphycene which is prepared by reduction of 18π-conjugated porphycene having trifluoromethyl groups.

Furthermore, the present work shows that the chemical properties of the porphycene endow its corresponding iron porphycene complex with unique properties. The μ-oxodimer of trifluoromethylated iron porphycene, μ-oxo-bis{2,7,12,17-tetraethyl-3,6,13,16-tetra(trifluoromethyl)porphycenatoiron(III)}, was easily converted to the ferrous complex via the cleavage of the Fe–O bond in pyridine. From the kinetic studies, the Fe–O bond cleavage step is controlled by the strength of the Lewis acidity of the central iron atom, and then the autoreduction step mainly depends on the Fe^{II}/Fe^{III} redox potential in spite of the structure of the macrocyclic ligands. Hence, it can be concluded that the attractive physicochemical property of the iron porphycene with four CF_3 groups as a peripheral substituents is derived from the strong Lewis acidity of iron atom and highly positive Fe^{II}/Fe^{III} redox potential.

In addition, a myoglobin reconstituted with an iron porphycene having two trifluoromethyl groups was prepared by conventional method. It is interesting to note that the reconstituted myoglobin has a slightly lower rate of autoxidation than a myoglobin reconstituted with an iron porphycene without electron-withdrawing groups. One of the reasons for the slow autoxidation would be due to the stabilization of ferrous form by introducing the trifluoromethyl groups, leading to the suppression of the oxidation into the ferric form.

In conclusion, of particular importance is the finding that the porphycene with trifluoromethyl groups can stabilize the reduced species, e.g., 20π-conjugated state of macrocycle, ferrous porphycene complex and ferrous Mb. It is considered that the combination of the porphycene framework and the strong electron-withdrawing trifluoromethyl substituents at the β-pyrrolic carbon plays a very important role in these stabilizations. On the basis of these results, the author suggests that the combination is proved to be an effective method for modulating the chemical properties of tetrapyrroles. The highly electron-deficient metalloporphycene will give us an attractive catalyst using a low valent metal species.

List of Publications

1) A Structural Isomer of Nonaromatic Porphyrin: Preparation of 20π-Conjugated Porphycene Based on Electronic Perturbation
Takashi Matsuo, Kazuyuki Ito, Nobuko Kanchisa, and Takashi Hayashi
Org. Lett. **2007**, *9*, 5303–5306.

2) Isolable Iron(II)-Porphycene Derivative Stabilized by Introduction of Trifluoromethyl Groups on the Ligand Framework
Kazuyuki Ito, Takashi Matsuo, Isao Aritome, Yoshio Hisaeda, and Takashi Hayashi
Bull. Chem. Soc. Jpn. **2008**, *81*, 76–83.

3) Effect of Peripheral Trifluoromethyl Groups in Artificial Iron Porphycene Cofactor on Ligand Binding Properties of Myoglobin
Takashi Matsuo, Kazuyuki Ito, Yuji Nakashima, Yoshio Hisaeda, and Takashi Hayashi
J. Inorg. Biochem. **2008**, *102*, 166–173.

List of Other Publications

1. Synthesis, Structure, and Chemical Property of the First Florine-Containg Porphycene
Takashi Hayashi, Yuji Nakashima, Kazuyuki Ito, Takahiro Ikegami, Isao Aritome, Akihiro Suzuki, and Yoshio Hisaeda.
Org. Lett. **2003**, *5*, 2845–2848.

2. Synthesis, Characterization, and Autoreduction of a Highly Electron-Deficient Porphycene(III) with Trifluoromethyl Substitutions
Takashi Hayashi, Yuji Nakashima, Kazuyuki Ito, Takahiro Ikegami, Isao Aritome, Katsuhiro Aoyagi, Tsutomu Ando, and Yoshio Hisaeda.
Inorg. Chem. **2003**, *42*, 7345–7347.

3. Autoreduction of Trifluoromethylated Porphycene Iron(III) Complex in Pyridine
Kazuyuki Ito, and Takashi Hayashi
J. Porphyrins Phthalocyanines **2006**, *10*, 684.

Acknowledgements

The study presented in this thesis has been carried out from April 2003 to March 2005 at the Department of Chemistry and Biochemistry, Graduate School of Engineering, Kyushu University and from April 2005 to December 2007 at the Department of Applied Chemistry, Graduated School of Engineering, Osaka University. The author would like to express sincerest gratitude to Professor Takashi Hayashi, Department of Applied Chemistry, Graduated School of Engineering, Osaka University, for his appropriate guidance, valuable discussions and warm encouragement throughout this thesis. The author would like to express great gratitude to Professor Yoshio Hisaeda, Department of Chemistry and Biochemistry, Graduate School of Engineering, Kyushu University, for his kind guidance, helpful suggestions, and warm encouragement throughout this research. The author would like to express my deep gratitude to Dr. Takashi Matsuo, Department of Applied Chemistry, Graduated School of Engineering, Osaka University, for his valuable suggestions, constant discussions.

The author acknowledges to Professor Takumi Oshima and Professor Toshikazu Hirao for reviewing this thesis and valuable discussions.

The author expresses great gratitude to Dr. Nobuko Kanehisa, Department of Applied Chemistry, Graduated School of Engineering, Osaka University, for analysis of the crystal structure and valuable discussions.

The author would like to thank Professor Araki Masuyama, Osaka Institute of Technology, Professor Manabu Abe, Department of Chemistry, Graduate School of Science, Hiroshima University, and Dr. Hisashi Shimakoshi, Department of Chemistry and Biochemistry, Graduate School of Engineering, Kyushu University, for their helpful discussion from various points of view.

The author would like to thank Dr. Hideaki Sato, Department of Medical Biochemistry, Kurume University, and Dr. Hiroaki Kitagishi, Department of Applied Chemistry, Graduated School of Engineering, Osaka University, for their valuable discussions.

The author would like to thank Dr. Tsutomu Ando, Dr. Isao Aritome, Dr. Takaaki Matsuda, and Dr. Dai Murata for their helpful discussions and warm encouragements.

Acknowledgement is also made to all members of Professor Takashi Hayashi's group and Professor Yoshio Hisaeda's group for encouragements and friendship in the laboratory.

The author would like to express great gratitude to his family for their constant assistance and warm encouragement.

Finally, the author is grateful for the financial support by the Japan Society for the Promotion of Science (JSPS) for 3 years.

Kazuyuki Ito

January 2008